

**A FINITE ELEMENT STUDY OF  
FOUR-POINT BENDING CREEP TESTS**

A FINITE ELEMENT STUDY OF  
FOUR-POINT BENDING CREEP TESTS

By

YOUNG SUK KIM, B.SC.

A Thesis

Submitted to the School of Graduate Studies

In Partial Fulfillment of the Requirements

For the Degree

Master of Applied Science

McMaster University

© Copyright by Young Suk KIM, May 2002

MASTER OF APPLIED SCIENCE (2002)  
(Mechanical Engineering)

McMaster University  
Hamilton, Ontario

TITLE: A FINITE ELEMENT STUDY OF  
FOUR-POINT BENDING CREEP TESTS

AUTHOR: Young Suk KIM, B. Sc.  
(Korea University, Seoul, Korea)

SUPERVISOR: Dr. Don Metzger, Associate Professor  
Department of Mechanical Engineering

NUMBER OF PAGES: xiv, 115

## ABSTRACT

Due to the cost and difficulty of conducting direct tensile and compression creep testing on engineering ceramics, four-point bending creep test methods are often used as an alternative. Stress distribution in the bending specimen is nonlinear, so a proper interpretation method is needed to get creep properties from data produced by four-point bending creep tests. The method of Hollenberg et al. and the method of Chuang are among the methods to predict the creep parameters from bending creep test data. However, bending creep test methods are often doubted for quantitative creep analysis with reasons like uncertainties from contact point shift or frictional effects in four-point bending creep tests.

Finite element simulations of the four-point bending creep tests were performed to evaluate the limitations and abilities of four-point bending creep tests and the methods to predict creep parameters from bend test data. Material model for asymmetric creep behavior (different creep rate in tension and in compression) of ceramics material were developed by modifying the existing symmetric creep model and implemented in the in-house non-linear finite element code. Explicit finite element method (dynamic relaxation) was successfully used to consider both, the frictional effects between loading rollers and specimen, and asymmetric creep properties of ceramics material. The developed asymmetric creep material model was verified by the simulation of C-ring compression creep test and comparison with published experimental data.

It was found that when friction between loading rollers and specimen was not applied in the simulations, both Hollenberg's and Chuang's methods well predicted creep parameters from bend creep simulation data. But, when friction was high as in normal bend creep tests, the pre-exponent ( $A$ ) was highly underestimated. Prediction of stress exponent ( $n$ ) was not affected much by friction.

Bend test set-up with rolling-pins in ASTM C 1211 was recommended to reduce the frictional effects in bend creep tests and a proof simulation was performed. The simulation showed that the test set-up in ASTM C 1211 effectively removed the frictional effect of the frequently used creep test set-up and the effect of bending moment increase due to the rolling of loading pin was minor.

## ACKNOWLEDGEMENTS

I would like to express my sincere gratitude to my supervisor, Dr. Don Metzger, for his knowledgeable supervision and patient encouragement throughout this research. I would also like to thank Dr. David Wilkinson for his useful comments and suggestions which gave me an insight to this research.

I would like to thank Tony Quan for the practical conversations we had in his lab while his ceramic specimens were creeping inside the furnaces. I wish to express my appreciation to my sister-in-law, Yenjin Kim, and her husband, Changwhan Baek, for their helps to visualize my research results in this thesis.

I would like to thank pastor Hae Taik Kim and, brothers and sisters in Hamilton Korean Presbyterian Church for their continual prayers which make me see the world and my way to run beyond this research.

I would like to express my gratitude to my dear wife, Yensen, my son, Samuel, and my daughter, Dahee, for all the support they gave as they always trusted me even at the moment when I was lost without purpose in the research.

Finally, I would like to express my deep gratitude towards my parents for their prayers, encouragement and love.

**To the One who is the beginning of knowledge**

## TABLE OF CONTENTS

ABSTRACT	iii
ACKNOWLEDGEMENT	v
TABLE OF CONTENTS	vii
LIST OF TABLES	xi
LIST OF FIGURES	xii
CHAPTER 1 INTRODUCTION	1
1.1 Creep in Engineering Ceramics	1
1.2 Four-Point Bending Creep Test vs. Direct Tensile & compressive Creep Test	2
1.3 Validity of the Methods to Extract Creep Parameters from Bend Test Data	3
1.4 Finite Element Analysis for Verification of Hollenberg's and Chuang's Methods	5
1.5 Explicit Finite Element Method for Ceramics Creep Test Simulation	6
1.6 Objectives of This Thesis	7
1.7 Outline of Methodology	8
CHAPTER 2 METHODS TO EXTRACT CREEP PARAMETERS FROM CREEP TEST DATA	10
2.1 Direct Tension and Compression Creep Test	10
2.2 Four-Point Bending Creep Test (Hollenberg's Method)	13
2.2.1 Stress Equations	14

2.2.2	Strain Equations with Curvature Rate	16
2.2.3	Strain Equations with Load-Point Displacement Rate	17
2.2.4	Example (Hollengerg's Method)	19
2.3	Four-Point Bending Creep Test (Chuang's Method)	21
2.3.1	Analysis	21
2.3.2	Example (Chuang's Method)	24
2.4	Summary	26
CHAPTER 3	A FINITE ELEMENT MODELING OF ASYMMETRIC CREEP BEHAVIOR OF CERAMICS	27
3.1	Explicit Finite Element Method	28
3.1.1	Dynamic Relaxation Algorithm	28
3.1.2	Stability of Dynamic Relaxation Algorithm	33
3.2	Finite Element Modeling for Asymmetric Creep Behavior of Ceramics	33
3.2.1	Material Model for Symmetric Creep	33
3.2.2	Stability of Dynamic Relaxation for Creep Calculation	36
3.2.3	Material Model for Asymmetric Creep	38
3.2.4	Stability of Dynamic Relaxation for Asymmetric Creep Calculation	40
3.2.5	Stable Creep Time Step $\Delta\tau$ Calculation	41
CHAPTER 4	VERIFICATION OF ASYMMETRIC CREEP MATERIAL MODEL	43
4.1	Si-SiC C-Rings Compression Creep Test	43
4.2	Asymmetric Creep Laws for Siliconized Silicon Carbide (Si-SiC)	46
4.3	C-Ring Compression Creep Test Simulation by Chuang et al.	48
4.4	C-Ring Compression Creep Test Simulation by Modified Code	50

4.4.1	Model Preparation	50
4.4.2	Simulation Result	53
4.5	Comparison and Discussion	57
CHAPTER 5	FINITE ELEMENT STUDY ON FOUR-POINT BENDING CREEP TEST	60
5.1	Model Preparation	61
5.2	Finite Element Study on Experiment of Jakus and Wiederhorn	64
5.2.1	Observation of Jakus and Wiederhorn	64
5.2.2	Finite Element Modeling	67
5.2.3	Simulation	68
5.2.4	Results and Discussion (Sodalime Silica Glass)	70
5.2.5	Additional Observation for the Total Moment in the Beam Section	73
5.2.6	Results and Discussion (Alumina)	75
5.3	Finite Element Study on Method of Hollenberg et al.	79
5.3.1	Simulation	79
5.3.2	Estimation of Creep Parameters by the Method of Hollenberg et al.	84
5.3.3	Frictional Effect on Estimation of Creep Parameters	86
5.3.4	Discussion	88
5.4	Finite Element Study on Chuang's Method	89
5.4.1	Simulation	89
5.4.2	Evaluation of Chuang's Method	94
5.4.3	Frictional Effect on Chuang's Method	95
5.4.4	Discussion	97
CHAPTER 6	EVALUATION OF BEND TEST SET-UP	101
6.1	Recommended Bend Creep Test Set-up	101

6.2	Simulation of the Recommended Bend Creep Test Set-up	103
6.3	Discussion	107
CHAPTER 7	CONCLUSTIONS AND RECOMMENDATIONS	108
7.1	Conclusions	108
7.2	Recommendations	110
REFERENCES		111

## LIST OF TABLES

2.1	Sample uniaxial creep test data	11
2.2	Sample bend creep test data	19
2.3	Power-law creep parameters (asymmetric creep)	25
2.4	Predicted values of neutral axis location and curvature rate	26
4.1	Specimen dimension and applied load (Chuang et al., 1991)	45
4.2	Total deflections for contact load simulation vs. nodal load simulation	58
5.1	Load point displacement rate data from simulations	81
5.2	Curvature rate data from simulations	82
5.3	Summary of results	86
5.4	Load point displacement rate data from simulations (with friction)	86
5.5	Frictional effect on estimation of creep parameters	87
5.6	Curvature rate data from simulations	92
5.7	Curvature rate data from Chuang's equations	95
5.8	Curvature rates from Chuang's equations vs. simulations	95
5.9	Curvature rates from simulation depending on friction	96
6.1	Curvature rates comparison between normal and recommended test settings	106
6.2	Rolled angles of rollers at time=27 hr ( $\sigma_e = 90$ )	106

## LIST OF FIGURES

1.1	Curvature as a function of distance along the bend bar (Jakus et al, 1988)	4
2.1	Strain vs. time behavior during creep under constant load (Dowling, 1993)	11
2.2	Strain vs. time curves for several stress levels (Dowling, 1993)	12
2.3	Log-log plot of applied stress vs. strain rate	13
2.4	Diagram of four-point bending bar (Keller et al., 1991)	14
2.5	Log-log plot of outer-fiber elastic stress vs. load-point displacement rate	20
2.6	Schematic sketches of four-point bend beam (asymmetric creep)	22
3.1	Geometric model for four-point bending creep test simulation	27
3.2	Dynamic Relaxation Algorithm for Load Increment $i$	31
3.3	Procedure for element internal force calculation (elastic material)	32
3.4	Procedure for Element Internal Force Calculation (Symmetric Creep Material)	35
3.5	Four-point bending creep-80,000 sec creep-dynamic relaxation cycles	37
3.6	Procedure for creep strain increment calculation (asymmetric creep)	39
3.7	Diagram for creep law equations (asymmetric creep) (Chuang 1986)	40
4.1	Schematic diagram of the C-ring compression creep test (Chuang et al., 1991)	44
4.2	Creep curve of a C-ring (Chuang et al., 1992)	45
4.3	Uniaxial tension and compression creep tests at 1300°C (Wiederhorn et al., 1988)	47
4.4	The two-dimensional finite element model of C-ring (Chuang et al., 1992)	48
4.5	Comparison of Chuang's simulation and Experiment (Chuang et al., 1992)	49
4.6	Finite element model of C-ring	52
4.7	Contact surfaces of the model	52
4.8	Von Mises stress at time $t = 0$ (elastic solution)	54
4.9	Von Mises stress at time $t = 100$ hr (creep solution)	54
4.10	Time evolution of the stress $\sigma_{yy}$ at the ring apex	55

4.11a	Total deflection vs. time (modified code)	56
4.11b	Deflection rate vs. time (modified code)	56
4.12a	Total deflection vs. time (comparison)	57
4.12b	Deflection rate vs. time (comparison)	57
4.13	Contact point shift in the C-ring compression test	59
4.14	Total deflection vs. time (comparison)	59
5.1	Geometric model of four-point bending creep test	62
5.2	Finite element model	63
5.3	Contact surfaces definition	63
5.4	Curvature as a function of distance along the flexure bar (Jakus et al., 1988)	66
5.5	Specimen dimension of the experiment of Jakus et al.	67
5.6	The finite element model for the simulation of Jakus's experiments	67
5.7	Beam deflection data from simulation	68
5.8	Von Mises stress distribution after 900 sec creep	70
5.9	Curvature curve from simulation without friction ( $\mu = 0$ )	71
5.10	Curvature curve from simulation with friction ( $\mu = 1$ )	71
5.11	Curvature curve of specimen (C) (Jakus et al., 1988)	72
5.12	Stress distribution at beam cross section ( $n = 1$ )	74
5.13	Stress ( $\sigma_{xx}$ ) distribution after 900 sec creep ( $n = 1$ )	74
5.14	Von Mises stress distribution after 2,7000 sec	75
5.15	Curvature curve from simulation without friction between loading roller and specimen ( $\mu = 0$ )	76
5.16	Curvature curve from simulation with friction between loading roller and specimen ( $\mu = 1$ )	76
5.17	Curvature curve of specimen (A) (Jakus et al., 1988)	77
5.18	Von Mises stress distribution after 22 hr creep (neutral axis is in the beam center due to symmetric creep)	79
5.19	Stress ( $\sigma_{xx}$ ) distribution in the beam section as a function of time (linear elastic stress distribution becomes non-linear because of $n > 1$ )	80

5.20	Stress ( $\sigma_{xx}$ ) distribution after 22hr creep ( $\sigma_e = 90$ MPa)	80
5.21	Mid span displacement $y_R$ (Fett et al., 1991)	81
5.22	Nodal displacement data from simulation ( $\sigma_e = 90$ MPa)	83
5.23	Load-point displacement rate ( $\dot{y}_{node13}$ ) and mid-span displacement rate ( $\dot{y}_R$ ) with $\sigma_e = 90$ MPa	83
5.24	Log-log plot of outer-fiber elastic stress vs. load-point displacement rate	85
5.25	Log-log plot of outer-fiber elastic stress vs. curvature rate	85
5.26	Log-log plot of outer-fiber elastic stress vs. load-point displacement rate	87
5.27	The finite element model for the simulations	89
5.28	Von Mises stress distribution after 27 hr creep with $\sigma_e = 90$ MPa	90
5.29	Stress ( $\sigma_{xx}$ ) distribution in the beam section as a function of time	91
5.30	Stress ( $\sigma_{xx}$ ) distribution after 27 hr creep ( $\sigma_e = 90$ MPa)	91
5.31	Nodal displacement data from simulation ( $\sigma_e = 90$ MPa)	93
5.32	Mid-span displacement rate ( $\dot{y}_R$ ) as a function of time ( $\sigma_e = 90$ MPa)	93
5.33	Curvature rate changes depending on friction between loading roller and specimen	96
5.34	Stress ( $\sigma_{xx}$ ) distribution at time = 0 ( $\sigma_e = 90$ MPa)	98
5.35	Stress ( $\sigma_{xx}$ ) distribution at time = 27 hr ( $\sigma_e = 90$ MPa)	99
5.36	Creep Strain ( $\varepsilon_{xx}$ ) distribution at time = 27 hr ( $\sigma_e = 90$ MPa)	100
6.1	Normal four-point bending creep test set-up	101
6.2	Recommended four-point bending creep test set-up (Krause et al, 1991) (ASTM C 1211)	102
6.3	Finite element model for recommended creep test set-up	103
6.4	Stress ( $\sigma_{xx}$ ) distribution at time = 27 hr ( $\sigma_e = 80$ MPa)	104
6.5	x-translation (exaggerated) visualized at time = 27 hr ( $\sigma_e = 80$ MPa)	105

# CHAPTER 1

## INTRODUCTION

### 1.1 Creep in Engineering Ceramics

Engineering Ceramics have high strength and oxidation and corrosion resistance at elevated temperature. Ceramics are promising material for high temperature load-bearing applications. So, predicting creep behavior of ceramics is vital in design to avoid failure due to creep because the excessive creep deformation can adversely affect the dimensional stability of the part.

Because of the complexity of creep behavior, the analysis of creep problems is often based on equations obtained from the curve-fitting of tensile creep test data. In the equations the creep strain  $\varepsilon_c$  or creep strain rate  $\dot{\varepsilon}_c$  is represented as a functions of stress  $\sigma$ , temperature  $T$ , and time  $t$ . One of the common equations is the Bailey-Norton equation which has the power form (Bailey, 1929) (Norton, 1929)

$$\dot{\varepsilon}_c = At^{k-1}\sigma^n; 0 < k < 1, n > 1 \quad (1-1)$$

which is widely used for creep strain in transient creep range.

For long-term applications in steady state and at isothermal conditions, engineering ceramics usually show power-law creep behavior in a form

$$\dot{\varepsilon}_{cs} = A\sigma^n \quad (1-2)$$

where  $\dot{\varepsilon}_{cs}$  is the steady state creep strain rate,  $A$  is a pre-exponent constant depending

only on the test temperature and the material's properties,  $n$  is a stress exponent which may or may not depend on stress (Chuang, 1986) .

Another important creep behavior of engineering ceramics is asymmetric creep property. Many ceramics shows much higher creep strain rate in tension than in compression (Seltzer, 1977) (Morrell et al., 1973). It can be expressed with the following two equations.

$$\dot{\epsilon}_{sc} = A_c \sigma^{n_c} \quad \sigma \text{ in compression} \quad (1-3a)$$

$$\dot{\epsilon}_{st} = A_t \sigma^{n_t} \quad \sigma \text{ in tension} \quad (1-3b)$$

where  $\dot{\epsilon}_s$  is steady-state creep strain rate;  $A$  and  $n$  are material constants,  $\sigma$  is the normal stress. The subscripts  $c$  and  $t$  refer to the case in compression and in tension respectively (Chuang, 1986).

## 1.2 Four-Point Bending Creep Test vs. Direct Tensile & Compressive Creep Test

The most common method of creep testing is to apply a constant load directly in tension or compression to a specimen. For engineering ceramics, preparing tensile specimen is expensive and the fixturing required to grip the specimen is also expensive. Also, researchers are experiencing premature failure at the neck or head region (Wang et al., 1997) (Krause et al., 2001). For a compressive test, specimen has less expensive geometry and loading is much simpler. But, alignment between the specimen and loading rams is difficult and it can lead to high bending stress.

Researchers and engineers often resort to four-point bending creep tests because specimens are inexpensive rectangular bars, and loading and fixturing are simple and

stable. However, the stress distribution in the bending specimen is nonlinear, so a proper interpretation method is needed to extract the power-law creep parameters from the steady state bend test data. Hollenberg et al. (1971) developed a method to get creep parameters from bend test data with assumption that neutral axis is not moving, creep rates in tension and compression are same. This method is easy to apply because it has a closed-form solution. But, application is restricted to ceramics which have symmetric creep properties ( $A_t = A_c, n_t = n_c$ ). Significant errors can occur if this method is applied to asymmetric creep where the neutral axis can migrate towards compression side of the specimen.

Finnie (1966) and Talty and Dirks (1978) partially generalized this method for asymmetric creep case with some restrictions like  $A_t \neq A_c$ , but  $n_t = n_c = 1$  or  $A_t \neq A_c$ , but  $n_t = n_c = n$ . Chuang (1986) completely generalized the method for the asymmetric creep case where  $A_t \neq A_c$ , and  $n_t \neq n_c$ . In Chuang's method the equations are highly nonlinear, so a numerical iteration and graphic solution scheme is used to solve the equations.

### **1.3 Validity of the Methods to Extract Creep Parameters from Bend Test Data**

Quinn and Morrell (1991) reviewed the problems of using bend test data for design purposes. They doubted bending creep test for quantitative creep analysis on the basis of Jakus and Wiederhorn's observation (1988) on curvatures of crept bend specimens and experimental errors in bending creep test such as load point friction. Jakus and Wiederhorn (1988) measured the surface curvature of a bend specimen after the four-

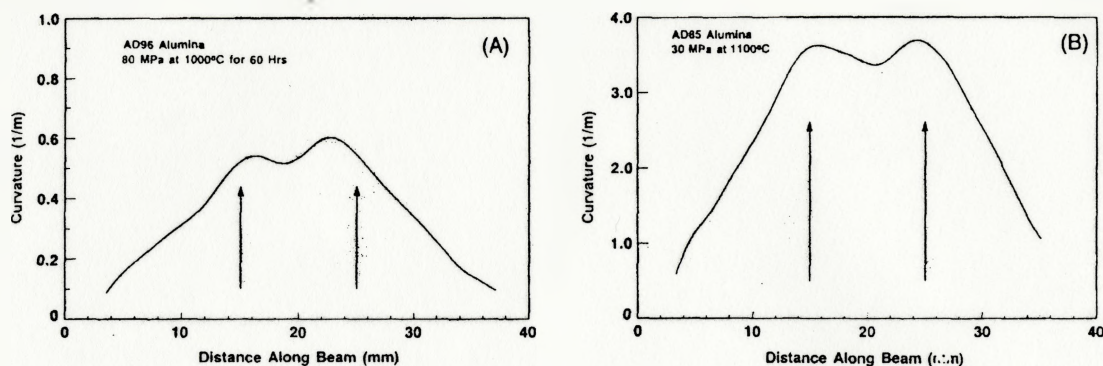


Figure 1.1 Curvature as a function of distance along the bend bar (Jakus et al, 1988)

point bending creep test. In the mid span, one would expect the radius of curvature to be constant because the bending moment is constant. However from the experiment the curvature was greatest under the inner loading points and not constant in the mid span (see Figure 1.1). This result deviates from expectation of simple beam theory which assumes that the moment and therefore the radius of curvature of the beam are constant between the load points.

Both Hollenberg's and Chuang's analyses use the simple beam theory at one point to relate the curvature rate to load-point displacement rate. Curvature rate is the appropriate parameter to measure the creep response of a bend specimen, but curvature rate is difficult to measure. Instead, it is general practice to measure the load-point displacement rate. Hollenberg et. al (1971) and Chuang (1986) begin the analysis with curvature rate and at the final stage they relate curvature rate to load-point displacement

rate by the assumption that bending moment is constant in the mid-span and linearly reduces to zero in the outer span.

So questions arise here if the methods of Hollenberg et al. (1971) and Chuang (1986) are still valid in spite of Jakus and Wiederhorn's observation and how friction affects the estimations of the methods.

#### **1.4 Finite Element Analysis for Verification of Hollenberg's and Chuang's Methods**

The best way to verify the methods of Hollenberg et al. and Chuang, while avoiding limitations of testing and measurement, is to perform tension, compression, and bend creep tests together, and to compare creep parameters measured from tension and compression tests with the parameters extracted from bending creep test data by the methods. At this time there is very little literature which has tension, compression and bend creep test data together. Ferber et al. (1990) performed tension, compression and bend creep tests together, but the estimation by Chuang's method didn't agree well with experimental results because in his bend creep tests the specimens at the two highest applied stresses failed before they reached the steady state. Chen and Chuang (1990) performed compression and bend creep tests together and showed his estimated compression creep strain rate is in fair agreement with compression creep test result.

To fully test the methods of Hollenberg et al. (1971) and Chuang (1986), finite element analysis can be effectively applied. Four-point bending creep test simulations can be performed with tensile and compressive creep parameters ( $A_t, n_t$  and  $A_c, n_c$ ) as inputs. The data collected from simulations such as load-point displacement rates are

used to estimate the tensile and compressive creep parameters by the methods of Hollenberg et al. and Chuang. The estimated parameters can be compared with original input parameters and the validity of the methods be evaluated.

### **1.5 Explicit Finite Element Method for Ceramics Creep Test Simulation**

To make simulations meaningful for comparison, contact and friction between loading rollers and specimen must be considered in the simulation, and material model for asymmetric behavior (different creep rate in tension and compression) of ceramics material be applied in the simulation. To handle material non-linearity (creep) and sliding of material interfaces (contact between loading rollers and specimen), explicit finite element method is the preferred choice because traditional implicit methods can encounter difficulties solving this problem.

The ceramics creep test simulation where both contact conditions between loading rollers and specimen and asymmetric creep properties of ceramics are considered together has not appeared in the literature so far. Chuang et al. (1992) simulated ceramics C-ring compression creep test with asymmetric creep properties but without contact conditions between specimen and loading rod considered. Concentrated nodal loads were applied in their simulations. Wang et al. (1997) performed ceramics tensile creep test simulations with contact between specimen and loading pin considered but assuming symmetric creep properties for the ease of calculation. Lim et al. (1997) performed four-point bending creep test simulations and ceramics C-ring compression creep tests with asymmetric creep properties considered but only point loads were

considered in the simulations.

It seems intractable to perform ceramics creep test simulation by implicit methods with both contact conditions and asymmetric creep properties considered together because in implicit solutions, equilibrium iterations must be performed at each load level and the contact conditions cause abrupt changes in the stiffness of system and asymmetric creep properties make the solution unstable.

Therefore, in this thesis the explicit finite element method was used to simulate ceramics creep tests with both contact conditions and asymmetric creep properties considered together.

## **1.6 Objectives of This Thesis**

The main objectives of this thesis are :

- 1) To develop asymmetric creep material model and to implement into the explicit module of the in-house general purpose finite element code.
- 2) To verify the developed asymmetric creep material model
- 3) To perform four-point bending creep simulations with contact conditions and asymmetric creep properties considered
- 4) To evaluate the methods of Hollenberg et al. and Chuang by comparing with simulation data

Also, in the course of pursuing the above points the various aspects of four-point bending creep tests which are hard to see in the experiments are to be investigated from simulations.

## 1.7 Outline of Methodology

The following points summarize the methodology of this thesis.

- 1) The methods of Hollenberg et al. (1971) and Chuang (1986) to extract creep parameters from bend test data are studied for their use in a later chapter. (chapter 2)
- 2) Modifications are done on material constitutive routine of the in-house general purpose finite element program for simulation of asymmetric creep behavior of ceramics. (chapter 3)
- 3) To verify the modified program, ceramics C-ring compression test is simulated and the result is compared with published experimental data. (chapter 4)
- 4) The bend creep experiment of Jakus and Wiederhorn (1988) is simulated, and the reason for the non-uniform curvature distribution in the mid-span is searched. (section 5.2)
- 5) A set of bend creep simulations are performed with symmetric creep property (  $A_t = A_c = A$  ,  $n_t = n_c = n$  ) at different loads. Load-point displacement rate is collected from simulation at each load. From this data, creep parameters (  $A$  and  $n$  ) are estimated by using the method of Hollenberg et al. (1971). By comparing the estimated creep parameters with simulation input creep parameters, validity of the Hollenberg's method is discussed. The mid-span curvature rates are also collected from simulations and compared with the estimation of the

method. Validity of measuring load-point displacement rate (which is simple and common) instead of curvature rate is discussed. (section 5.3)

- 6) A set of bend creep simulations are performed with asymmetric creep properties ( $A_t \neq A_c, n_t \neq n_c$ ) at different loads. Mid-span curvature rate is collected from simulation at each load. Also, mid-span curvature rate for each load is estimated by Chuang's method. By comparing the curvature rates from simulations with the curvature rates estimated by Chuang's method, validity of Chuang's method is discussed. (section 5.4)
- 7) Simulations in steps 5) & 6) above are repeated with friction between loading rollers and specimen and how friction affects bending creep test and estimation of creep parameters is discussed. (sections 5.3 & 5.4)
- 8) Simulation is performed to establish a better bend creep test set-up to reduce friction. (chapter 6)

## CHAPTER 2

# METHODS TO EXTRACT CREEP PARAMETERS FROM CREEP TEST DATA

This chapter introduces methods to extract creep parameters from creep test data. First how to decide creep parameters from direct tension/compression creep tests is explained as reference. Two methods to extract creep parameters from bend creep test data which will be evaluated in this thesis are explained in detail. For each method an example is given to demonstrate how to use the method to extract creep parameters.

### 2.1 Direct Tension and Compression Creep Tests

Creep is time-dependent inelastic deformation under sustained load and elevated temperature. A typical creep curve (see Figure 2.1) shows four main features; 1) initial elastic, plastic deformation which happens instantaneously with applied load, 2) a period of decreasing deformation rate (transient creep), 3) a period of constant deformation rate (steady-state creep), 4) a period of increasing deformation rate (tertiary creep) (Dowling, 1993).

For long-term applications in steady state, engineering ceramics usually show power-law creep behavior in a form  $\dot{\epsilon}_s = A\sigma^n$ , where  $\dot{\epsilon}_s$  is steady state creep strain rate and  $A$  is a pre-exponent and  $n$  is a stress exponent (Chuang, 1986).

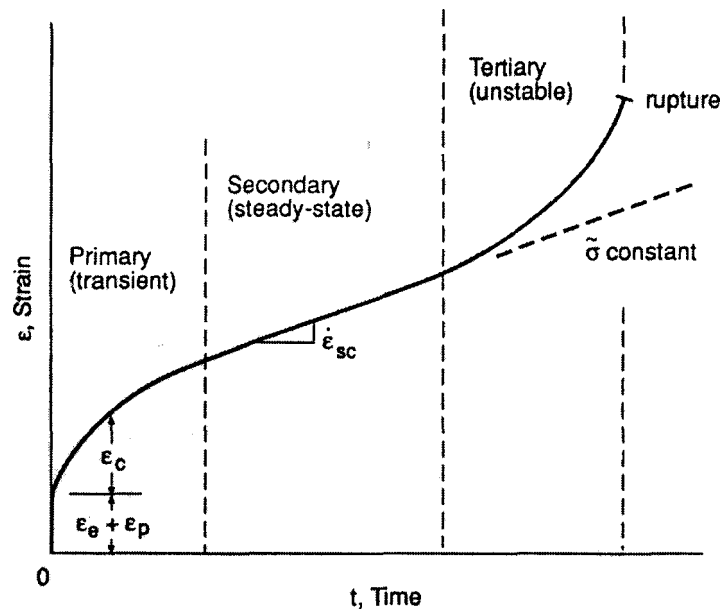


**Fig. 2.1** Strain vs. time behavior during creep under constant load (Dowling, 1993)

In simple tension or compression, tests are performed at different stress levels under constant temperature. Strain is directly measured from axial displacement of specimen, while steady state creep strain rate is collected at each stress level. Table 2.1 and Figure 2.2 are typical examples of such data.

**Table 2.1** Sample uniaxial creep test data

Specimen No.	Stress $\sigma$ (MPa)	Creep rate $\dot{\epsilon}_s$ ( $\text{sec}^{-1}$ )
1	100	$9.261 \times 10^{-10}$
2	150	$15.269 \times 10^{-10}$
3	200	$17.875 \times 10^{-10}$

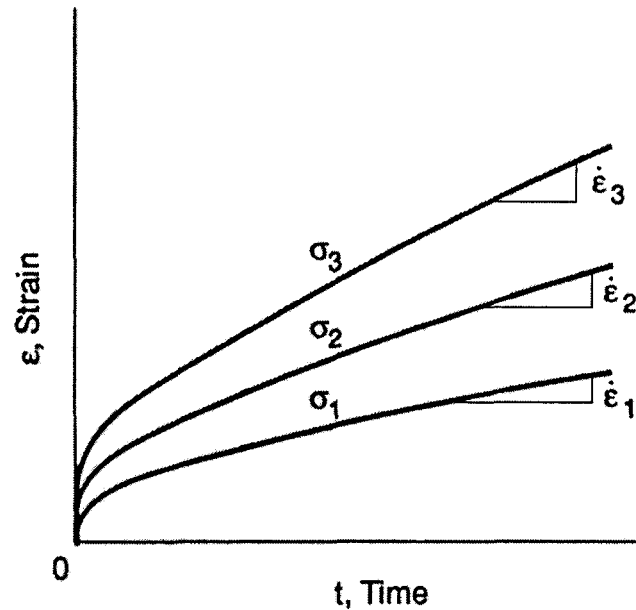


**Figure 2.2** Strain vs. time curves for several stress levels (Dowling, 1993)

Taking the natural log of both sides of creep power law equation gives

$$\log \dot{\epsilon}_s = \log A \sigma^n$$

or

$$\log \dot{\epsilon}_s = n \log \sigma + \log A$$

The creep strain rate ( $\dot{\epsilon}_s$ ) vs. the applied stress ( $\sigma$ ) on a log-log plot is approximated with a line by least squares fit so that the slope becomes stress exponent ( $n$ ) and intercept with y axis becomes log of pre-exponent ( $A$ ).

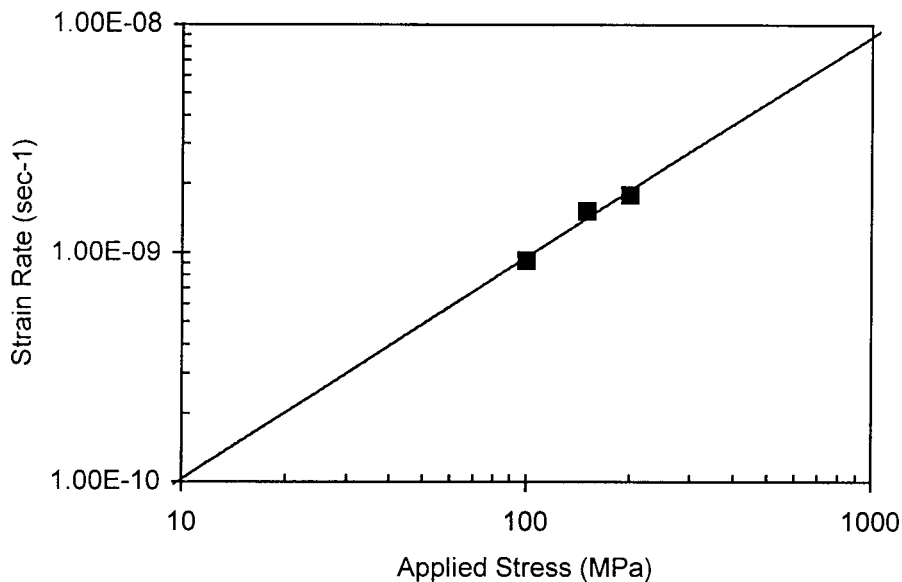


**Figure 2.3** Log-log plot of applied stress vs. strain rate

Linear regression analysis with the above data gives  $n = 0.97$  and  $A = 1.111 \times 10^{-11}$ . So, the steady state creep equation for this material is  $\dot{\epsilon}_s = 1.111 \times 10^{-11} \sigma^{0.97}$ . Therefore, the creep parameters are obtained directly from tensile or compressive creep test data.

## 2.2 Four-Point Bending Creep Test (Hollenberg's Method)

Creep tests on engineering ceramics are often performed in four-point bending to avoid the problems of gripping and alignment associated with direct tensile and compressive tests. However, stress distribution in the bending specimen is nonlinear and a proper interpretation method is needed to get creep parameters from bend test data.

Hollenberg et al. (1971) developed a method with assumptions that the neutral

axis is not moving, creep rates in tension and compression are same (symmetric creep). This method (from now on, the method will be called as Hollenberg's method) can be easily applied to ceramics which has symmetric creep properties because it has a closed-formed solution. The following sub-sections 2.2.1, 2.2.2 and 2.2.3 are the summaries of procedures from Hollenberg's paper (Hollenberg et al., 1971).

### 2.2.1 Stress Equations

At steady-state the stress distribution in a bending specimen is nonlinear and the stress state is not changing with time. And the strain rate ( $\dot{\epsilon}_s$ ) is linearly dependant on  $Y$ , the distance away from the neutral axis where  $\dot{\epsilon}_s = 0$ . In this analysis, the neutral axis is assumed to be at the center of the beam.

$$\epsilon_s = \frac{Y}{\rho} = KY \text{ and } \dot{\epsilon}_s = \dot{K}Y \quad (2-1)$$

where  $\rho$  is radius of curvature and  $\dot{K}$  is curvature rate.

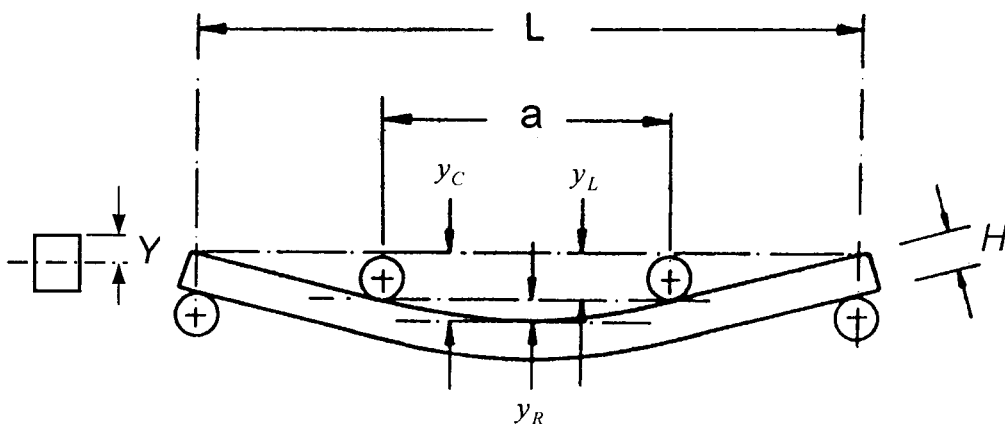


**Figure 2.4** Diagram of four-point bending bar (Keller et al., 1991)

As mentioned previously, the material is assumed to behave in the steady state according to a power law of the form

$$\dot{\epsilon}_s = A\sigma^n \quad (2-2)$$

Combining Equation (2-1) and Equation (2-2), the nonlinear stress distribution over the cross-section of is

$$\sigma(Y) = \left( \frac{Y\dot{K}}{A} \right)^{1/n} \quad (2-3)$$

For a rectangular beam of width B and H, the bending moment about the neutral axis is

$$M = \int_{-H/2}^{H/2} Y\sigma B dY \quad (2-4)$$

Substitution of Equation (2-3) into Equation (2-4) and a subsequent integration give

$$M = \frac{I_n}{(A/\dot{K})^{1/n}} \quad (2-5a)$$

with

$$I_n = \frac{2B \left[ \frac{H}{2} \right]^{\frac{2n+1}{n}}}{(2n+1)n} \quad (2-5b)$$

$I_n$  is defined as the complex moment of inertia. By solving Equation (2-5) in terms of  $\dot{K}$ , substituting into Equation (2-3), and remembering the definition of  $I_n$ , the following expression is obtained for the stress,  $\sigma(Y)$ , at a distance  $Y$  from the neutral axis:

$$\sigma(Y) = \frac{Y^{1/n} \left( \frac{2n+1}{n} \right) M}{2B \left[ \frac{H}{2} \right]^{\frac{2n+1}{n}}} \quad (2-6)$$

The stress in the outer fiber ( $\sigma_{\max}$ ), i.e. at  $Y=H/2$ , is

$$\sigma_{\max} = \frac{3(L-a)P}{BH^2} \frac{(2n+1)}{3n} \quad (2-7)$$

or

$$\sigma_{\max} = \sigma_e \frac{(2n+1)}{3n} \quad (2-8a)$$

where  $\sigma_e$  is the stress in the outer fiber from elastic bending with the same applied load.

$$\sigma_e = \frac{3(L-a)P}{BH^2} \quad (2-8b)$$

### 2.2.2 Strain Equations with Curvature Rate

Although special devices are required, techniques are available to measure curvature rate in laboratory (Fett et al., 1991). The following procedure relates the curvature rate  $\dot{K}$  to outer-fiber elastic stress  $\sigma_e$ .

In Equation (2-1), strain rate was related to curvature rate, which is

$$\dot{\epsilon}_s = \dot{K}Y \quad (2-1)$$

where  $Y$  is the distance from the neutral axis. Therefore the strain rate in the outer fiber ( $\dot{\epsilon}_{s,\max}$ ), i.e. at  $Y=H/2$ , is

$$\dot{\epsilon}_{s,\max} = \dot{K} \frac{H}{2} \quad (2-9)$$

Substituting Equations (2-8) and (2-9) into Equation (2-2) and solving for  $\dot{K}$  gives

$$\dot{K} = \sigma_e^n \frac{2A}{H} \left[ \frac{(2n+1)}{3n} \right]^n \quad (2-10)$$

Taking the natural log to both sides,

$$\log \dot{K} = n \log \sigma_e + C_1 \quad (2-11)$$

The constant  $C_1 = \log \frac{2A}{H} \left[ \frac{(2n+1)}{3n} \right]^n$ . Thus the creep exponent ( $n$ ) can be evaluated in steady-state creep test by plotting the curvature rate ( $\dot{K}$ ) vs. the applied elastic stress ( $\sigma^e$ ) on a log-log plot. The slope of the line is  $n$  and the intercept is  $C_1$ , which will lead to the estimation of creep pre-exponent ( $A$ ).

### 2.2.3 Strain Equations with Load-Point Displacement Rate

As shown in the preceding section, curvature rate ( $\dot{K}$ ) is the proper parameter to measure the creep behavior of bend bar. But, measuring load-point displacement rate is easier than measuring curvature rate of a beam. Quite often load-point displacement rate is measured instead of curvature rate and applied to estimate creep parameters.

To determine the relationship between the load-point displacement rate and the outer fiber strain rate, the curvature rate must be determined in terms of the beam deflection. For small deflection, the common assumption is that

$$K = \frac{d^2 y}{dx^2} \quad \text{and} \quad \dot{K} = \frac{d^2 \dot{y}}{dx^2} \quad (2-12)$$

where  $\dot{y}$  is the displacement rate at a position  $x$  along the beam. The load-point

displacement rate ( $\dot{y}_L$ ) can be solved by integration of  $\dot{K}$  along the beam length  $x$ , with linear moment distribution in the outer span and a constant maximum moment in the inner span. Setting the origin of the coordinate system at the mid-span of the deformed beam, the boundary conditions are  $y(0)=0$  and  $\dot{y}(0)=0$  due to symmetry. After the deformed shapes  $y = \dot{y}(x)$  are solved, the load-point displacement rate is given by  $\dot{y}_L = \dot{y}(L/2) - \dot{y}(a/2)$  where  $L$  and  $a$  are the lengths of major and minor spans respectively. The solution of Equation (2-12) is

$$\dot{K} = \frac{4(n+2)}{(L-a)[L+a(n+1)]} \dot{y}_L \quad (2-13)$$

Substitution of Equation (2-13) into Equation (2-9) gives

$$\dot{\epsilon}_{s,\max} = \frac{2H(n+2)}{(L-a)[L+a(n+1)]} \dot{y}_L \quad (2-14)$$

Substituting Equations (2-8) and (2-14) into Equation (2-2) and solving for  $\dot{y}_L$  gives

$$\dot{y}_L = \sigma_e^n \frac{A(L-a)[L+a(n+1)]}{2H(n+2)} \left[ \frac{(2n+1)}{3n} \right]^n \quad (2-15)$$

Finally, taking the natural log of both sides,

$$\log \dot{y}_L = n \log \sigma_e + C_2 \quad (2-16a)$$

where

$$C_2 = \log \frac{A(L-a)[L+a(n+1)]}{2H(n+2)} \left[ \frac{(2n+1)}{3n} \right]^n \quad (2-16b)$$

The creep exponent ( $n$ ) can be evaluated by plotting the load-point displacement rate ( $\dot{y}_L$ ) vs. the applied elastic stress ( $\sigma^e$ ) on a log-log plot. The slope of the line is  $n$  and the

intercept is  $C_2$ , which will lead to the estimation of creep pre-exponent ( $A$ ).

#### 2.2.4 Example (Hollenberg's Method)

Table 2.2 is the example bending creep test data, which shows applied outer-fiber elastic stresses and load-point displacements. Geometric data are given as: Beam height  $H=2.770$  mm, Outer-span  $L=40$  mm, mid-span  $a=10$  mm.

If we plot the load-point displacement rate ( $\dot{y}_L$ ) vs. the applied outer-fiber elastic stress ( $\sigma_e$ ) on a log-log plot and draw a line with least squares fit, the slope becomes stress exponent ( $n$ ) and intercept with y axis becomes  $C_2$  of Equation (2-16) (see Figure 2.5).

From the plot  $n=1.185$ ,  $C_2 = -25.04$ , and from  $C_2$  we get  $A = 1.35 \times 10^{-10}$ . So, the steady state creep equation for this material is  $\dot{\epsilon}_s = 1.35 \times 10^{-10} \sigma^{1.185}$ .

**Table 2.2** Sample bend creep test data (load-point displacement)

Specimen No.	Outer-Fiber Elastic Stresses $\sigma$ (MPa)	Load-Point Displacement Rates $\dot{y}_L$ (m sec <sup>-1</sup> )
1	20	$5.185 \times 10^{-10}$
2	20	$4.719 \times 10^{-10}$
3	30	$6.311 \times 10^{-10}$
4	30	$6.656 \times 10^{-10}$
5	40	$11.50 \times 10^{-10}$
6	40	$11.57 \times 10^{-10}$

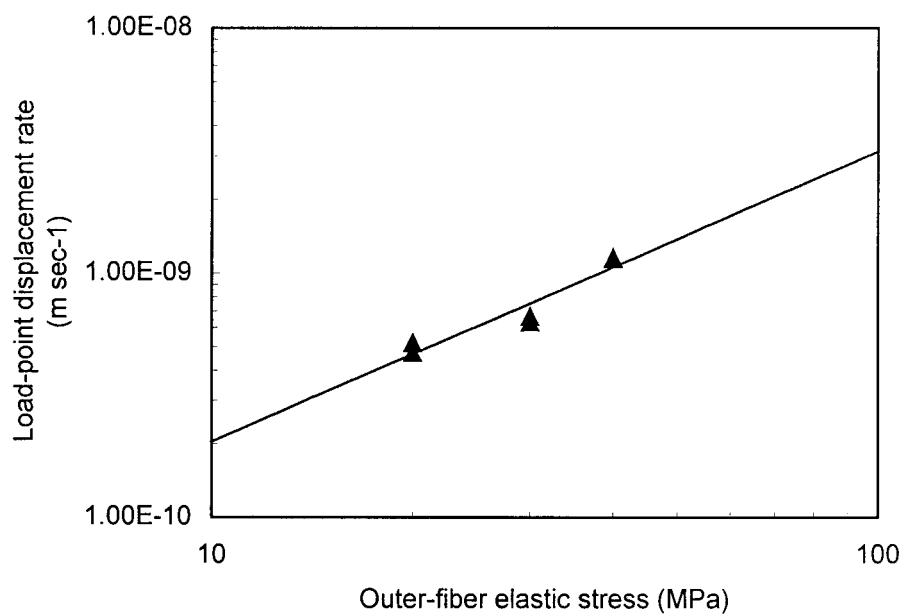


**Figure 2.5** Log-log plot of outer-fiber elastic stress vs. load-point displacement rate

### 2.3 Four-Point Bending Creep Test (Chuang's Method)

Many engineering ceramics show higher creep rate in tension than in compression. As we saw in the previous section, method of Hollenberg et al. (1971) assumed that the neutral axis is invariant, while creep rates in tension and compression are the same (symmetric creep). Significant errors can occur if this method is applied to asymmetric creep case where neutral axis migrate towards compression side of the specimen.

A more generalized method for asymmetric creep which was developed by Chuang (1986) is introduced, and the following sub-sections 2.3.1, 2.3.2 and 2.3.3 are the summaries of the procedures.

#### 2.3.1 Analysis

For ceramics which show asymmetric creep properties, the steady-state strain rate and the applied stress can be related by the following two power-law creep equations.

$$\dot{\epsilon}_{sc} = A_c \sigma^{n_c} \quad \sigma \text{ in compression} \quad (2-17a)$$

$$\dot{\epsilon}_{st} = A_t \sigma^{n_t} \quad \sigma \text{ in tension} \quad (2-17b)$$

where  $A$  and  $n$  are creep constants and the subscripts  $c$  and  $t$  refer to the case in compression and in tension respectively. Assuming that planar sections remain planar during bending, the strain ( $\epsilon$ ) is linearly dependent on the distance  $Y$  from the neutral axis;  $\epsilon = KY$  where  $K$  is curvature.

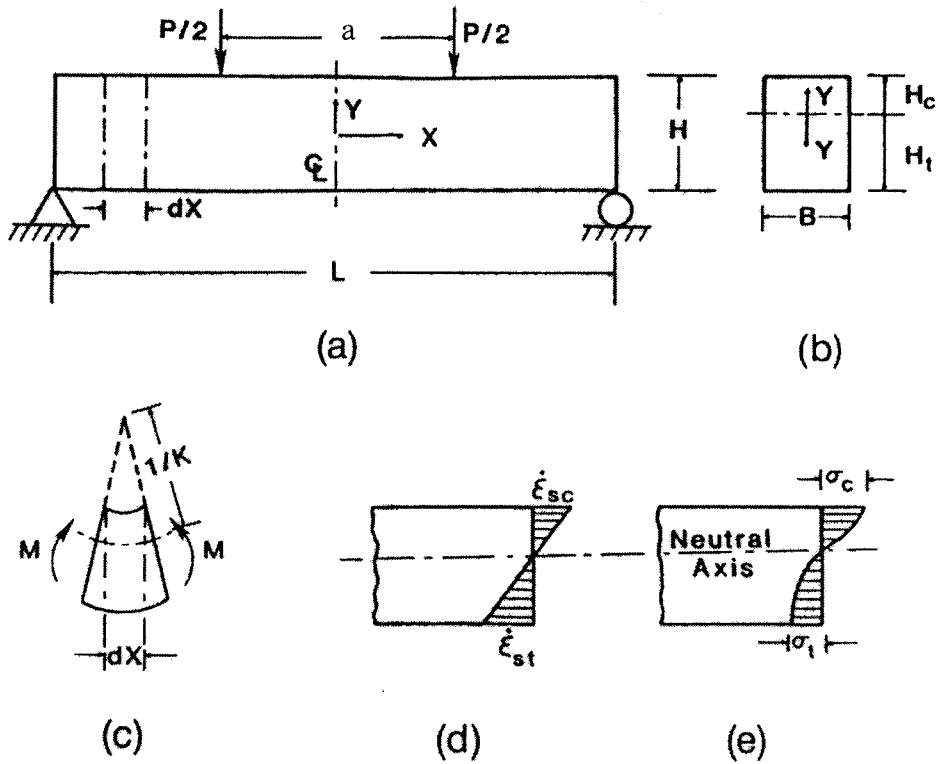


**Figure 2.6** Schematic sketches of four-point bend beam (asymmetric creep)

And the strain rate is deduced to  $\dot{\epsilon} = \dot{K}Y + K\dot{Y}$ . The second term is generally negligible because during steady-state, the neutral axis migration rate is very small.

$$\dot{\epsilon} = \dot{K}Y \quad (2-18)$$

Thus, Equations (2-17a) and (2-17b) become

$$\sigma(Y) = \left( \frac{Y\dot{K}}{A} \right)^{1/n} \quad (2-19)$$

regardless of the sign of the stress. From the equilibrium requirement, the total force acting

on the compression side of the cross-section must be balanced by the total force on the tensile side. This means  $F_c = F_t$  or  $B \int_0^{H_c} \sigma dY = B \int_0^{H_t} \sigma dY$  where  $B$  is the beam width and  $H(= H_c + H_t)$  is the beam height. By integrating  $\sigma$  using Equations (2-19) and (2-17), and after some mathematical manipulations, this force balance equation finally reduces to

$$R_1 \left[ \dot{K}H / A_c \right]^{C_1} (H_c / H)^{C_2} + (H_c / H) = 1 \quad (2-20a)$$

where

$$R_1 = (A_t / A_c)^{[1/(1+nt)]} [(n_c + n_c n_t) / (n_t + n_c n_t)]^{[nt/(1+nt)]} \quad (2-20b)$$

$$C_1 = [(n_t - n_c) / (n_c + n_c n_t)] \quad (2-20c)$$

$$C_2 = [(n_t + n_c n_t) / (n_c + n_c n_t)] \quad (2-20d)$$

Equation (2-20a) is a nonlinear algebraic equation which can be used to predict the location of the neutral axis.

In addition, the requirement that the total summation of moments produced by local tractions be equal to the external moment ( $M$ ) forms the second governing equations,

$$M = \int_0^{H_c} \sigma Y B dY + \int_0^{H_t} \sigma Y B dY$$

Substitution of Equation (2-19) and recognition of  $H_t + H_c = H$  result in the equation

$$M / (BH^2) = \left[ \dot{K}H / A_c \right]^{C_3} \left\{ \left[ \dot{K}H / A_c \right]^{C_4} (R_3 / C_5) (1 - H_c / H)^{C_5} + (1 / C_6) (H_c / H)^{C_6} \right\} \quad (2-21a)$$

where

$$R_3 = 1 / (A_t / A_c)^{(1/nt)} \quad (2-21b)$$

$$C_3 = 1/n_c \quad (2-21c)$$

$$C_4 = (1/n_t - 1/n_c) \quad (2-21d)$$

$$C_5 = (2n_t + 1)/n_t \quad (2-21e)$$

$$C_6 = (2n_c + 1)/n_c \quad (2-21f)$$

Equations (2-20a) and (2-21a) constitute a system of algebraic equations for the two unknowns  $H_c$  and  $\dot{K}$ , while the remaining parameters such as the applied moment  $M$  and the values of the materials parameters  $A$  and  $n$  are being treated as given. These two coupled non-linear algebraic equations can be solved numerically. A computer program is used which contains the following tasks: first to solve  $H_c$  from Equation (2-20a) by a Newton-Raphson iteration scheme. Inputs to this subroutine are  $A_t/A_c$ ,  $n_t$ ,  $n_c$  and  $\dot{K}$ . Once  $H_c$  is successfully solved, it can then be used as input, together with the  $\dot{K}$ , to Equation (2-21a) for the computation of  $M$ . At the end, a total of three one-dimensional arrays are generated for  $M$ ,  $\dot{K}$ ,  $H_c$ . The solutions are then displayed in graphical form for  $\dot{K}$  against  $M$  and  $H_c$  against  $M$  with any given values of  $A$  and  $n$ .

More details and examples are on Chuang's paper (Chuang, 1986) (Ferber et al., 1990).

### 2.3.2 Example (Chuang's Method)

To demonstrate how to use Chuang's method, a computer program to do numerical iterations and graphic solutions is needed. In this thesis, instead of following whole iteration steps of Chuang's method, Equations (2-20) and (2-21) were used to

calculate curvature rates from given creep constants ( $A_t, A_c, n_t, n_c$ ) and applied moments ( $M$ ), and finite element simulations were performed with the same given creep constants ( $A_t, A_c, n_t, n_c$ ) and applied moments ( $M$ ) as input. The curvature rates from Equations (2-20a) and (2-21a) and the curvature rates from finite element simulations were compared, and the validity of Chuang's method was evaluated.

Following is an example to demonstrate how to calculate curvature rates from given creep constants and applied moments by using Chuang's equations (Feber et al, 1990). Specimen size is 3 mm Height  $\times$  4 mm Width  $\times$  50 mm Long. Inner loading span ( $l$ ) is 20 mm and outer span ( $L$ ) is 40 mm. Creep constants are shown below.

**Table 2.3** Power-law creep parameters (asymmetric creep)

	$n$	$A$ ( $\epsilon/\text{sec}$ )
Tension	5.6	$2.972 \times 10^{-17}$
Compression	1.7	$5.555 \times 10^{-13}$

By using Equations (2-20a) and (2-21a) it is possible to predict neutral axis location and curvature rate at steady state. First  $H_c/H$  is chosen, which is in the range of ( $0 < H_c/H < 1$ ), and  $\dot{K}$  is calculated from Equation (2-20a) and then with  $H_c/H$  and  $\dot{K}$  as input the moment  $M$  is calculated from Equation (2-21a). The  $H_c/H$  is then varied until the calculated moment is equal to the applied moment. For example, given moment of 510 N-mm, a value of 0.3 for  $H_c/H$  was chosen and substituted into Equation (2-20a). This yields a value of  $1.065 \times 10^{-9}$  for  $\dot{K}$ , and then these two values were substituted into

Equation (2-21a) to find a moment of 306.8, which differs from the applied moment 510 N-mm. More iterations were repeated with different  $H_c/H$  values and finally we get  $H_c/H=0.197$  and  $\dot{K}=8.00\times 10^{-9}$  for  $M=510$ . Table 2.4 shows the calculated results for 5 different applied moments and these results will be used later in comparison with finite element simulation results.

**Table 2.4** Predicted values of neutral axis location and curvature rate

Specimen No.	Applied Moment $M$ (N mm)	Neutral Axis Location $H_c/H$	Curvature Rate $\dot{K}$
1	510	0.197	8.00E-9
2	453	0.220	4.88E-9
3	340	0.278	1.57E-9
4	282	0.319	7.82E-10
5	220	0.374	3.28E-10

## 2.4 Summary

In this chapter, the methods of Hollenberg et al. (1971) and Chuang (1986) to extract creep parameters from bend test data were studied in detail. Both of these methods provide a practical means to determine creep properties from bend test data. The methods will be used later to estimate creep parameters from creep test simulation data and their validity will be discussed by comparing the estimated creep parameters with the input creep parameters in simulations.

## CHAPTER 3

### A FINITE ELEMENT MODELING OF ASYMMETRIC CREEP

#### BEHAVIOR OF CERAMICS

In order to simulate four point bending creep tests of ceramics, the following should be considered in the finite element modeling.

- 1) The asymmetric creep behavior of ceramics should be included in the creep material model.
- 2) Instead of using simplified concentrated load, loading rollers with specimen should be modeled like in Figure 3.1 so that friction between loading rollers and specimen, and contact point shift during creep bending can be considered in the simulation.

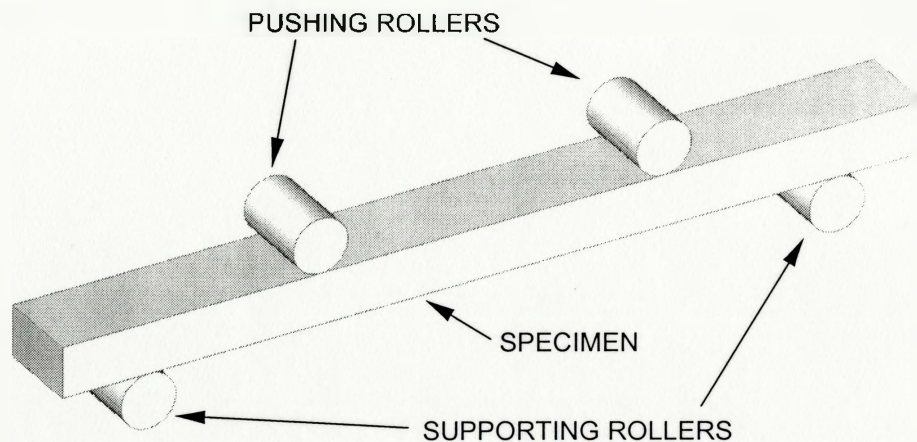


**Figure 3.1** Geometric model for four-point bending creep test simulation

Although creep analysis is routinely done with so called implicit finite element method, the explicit finite element method is the best choice to handle the material non-linearity (creep) and sliding of material interfaces (contact between loading rollers and specimen) with friction. This is because traditional implicit methods can encounter difficulties solving problems where contact conditions cause abrupt change in the stiffness of the system.

In this chapter explicit finite element method is introduced first and formulation of the material model for asymmetric creep is explained in detail.

### **3.1 Explicit Finite Element Method**

The finite element method is a numerical method for formulating a system of equations which models physical problems mathematically. Nonlinear problems which include material non-linearity like creep and plasticity or geometric non-linearity like large deformation and contact can be solved effectively by explicit finite element methods. Typically, explicit methods concern only transient dynamic problems. However, an explicit finite element method applies to non-linear static problems viewed as steady state condition of critically damped dynamic problem. This approach is often called Dynamic Relaxation, and the procedures of its use are described by (Underwood, 1983) (Sauve and Metzger, 1995).

#### **3.1.1 Dynamic Relaxation Algorithm**

The following explanation of the dynamic relaxation algorithm, which is extracted from a paper of Sauve and Metzger (1995), is consistent with its general implementation.

The equations of dynamic motion are given as

$$M\ddot{u} + C\dot{u} + F_{\text{int}}(u) = F_{\text{ext}} \quad (3-1)$$

At steady state, the terms  $M\ddot{u}$  and  $C\dot{u}$  damp away and static solution is obtained.

$$F_{\text{int}}(u) = F_{\text{ext}} \quad (3-2)$$

Therefore, for non-linear static problem  $M$  and  $C$  are chosen artificially so that the static solution can be reached as fast as possible.

In explicit method central difference operator is used to approximate velocity and acceleration.

$$\dot{u}^{k+1} = \frac{u^{k+1} - u^k}{\Delta t}, \quad \ddot{u}^k = \frac{\dot{u}^{k+1/2} - \dot{u}^{k-1/2}}{\Delta t} \quad (3-3)$$

where  $\Delta t$  is a constant time increment and  $k$  is time step. The average value of velocity is taken as

$$\dot{u}^k = (\dot{u}^{k+1/2} + \dot{u}^{k-1/2})/2 \quad (3-4)$$

Substituting Eqs. (3-3) and (3-4) into Eq. (3-1) yields

$$\frac{M}{\Delta t}(\dot{u}^{k+1/2} - \dot{u}^{k-1/2}) + C(\dot{u}^{k+1/2} + \dot{u}^{k-1/2})/2 + F_{\text{int}}^k = F_{\text{ext}}^k \quad (3-5)$$

or

$$\dot{u}^{k+1/2} = \left(\frac{M}{\Delta t} + \frac{C}{2}\right)^{-1} \times \left[ (F_{\text{ext}}^k - F_{\text{int}}^k) + \left(\frac{M}{\Delta t} - \frac{C}{2}\right) \dot{u}^{k-1/2} \right] \quad (3-6)$$

To make the mode associated with the applied loading distribution critically damped, a critical damping matrix  $C$  is used which is

$$C = 2\omega M \quad (3-7)$$

where  $\omega$  is undamped natural frequency corresponding to the participating mode of

loading and  $M$  is the diagonal lumped mass matrix.

The equation (3-6) can be simplified to

$$\dot{u}^{k+1/2} = \frac{1}{1 + \omega\Delta t} \left[ \Delta t M^{-1} (F_{ext}^k - F_{int}^k) + (1 - \omega\Delta t) \dot{u}^{k-1/2} \right] \quad (3-8)$$

The current displacements are obtained as

$$u^{k+1} = u^k + \Delta t \dot{u}^{k+1/2} \quad (3-9)$$

In dynamic relaxation algorithm the  $\omega$ ,  $\Delta t$  and  $M$  are chosen judiciously so that the transient response disappears fast, resulting in static solution to

$$F_{int} = F_{ext} \quad (3-10)$$

The following flow chart shows the dynamic relaxation algorithm and the algorithm is the main structure of in-house non-linear finite element code H3DMAP (Sauve, 1999) which will be used for four-point bending creep simulation. **Step 7** is highlighted because in this step the material model is included and modification is to be done for asymmetric creep model. The H3DMAP code has modular structure and the dynamic relaxation algorithm is included in the module named CEXPRES which is dynamic relaxation solution module for creep analysis.

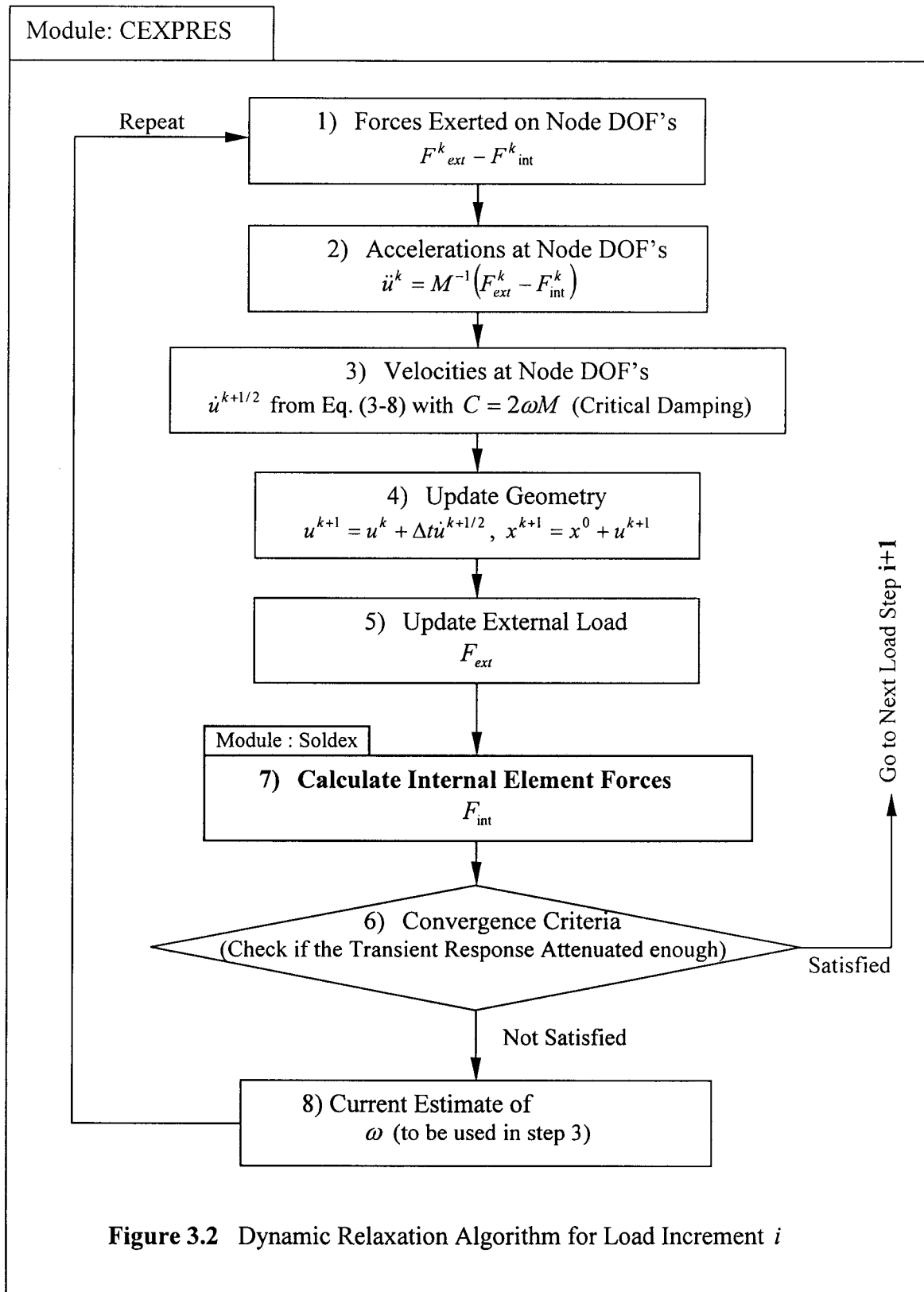


**Figure 3.2** Dynamic Relaxation Algorithm for Load Increment  $i$

The step 7) of the dynamic relaxation algorithm (Figure 3.2) is one module named SOLDEX and it is shown in detail below. The step b) and c) of Figure 3.3 comprise a material constitutive module which is a sub-module of SOLDEX and in Figure 3.3 elastic material model is shown as example.

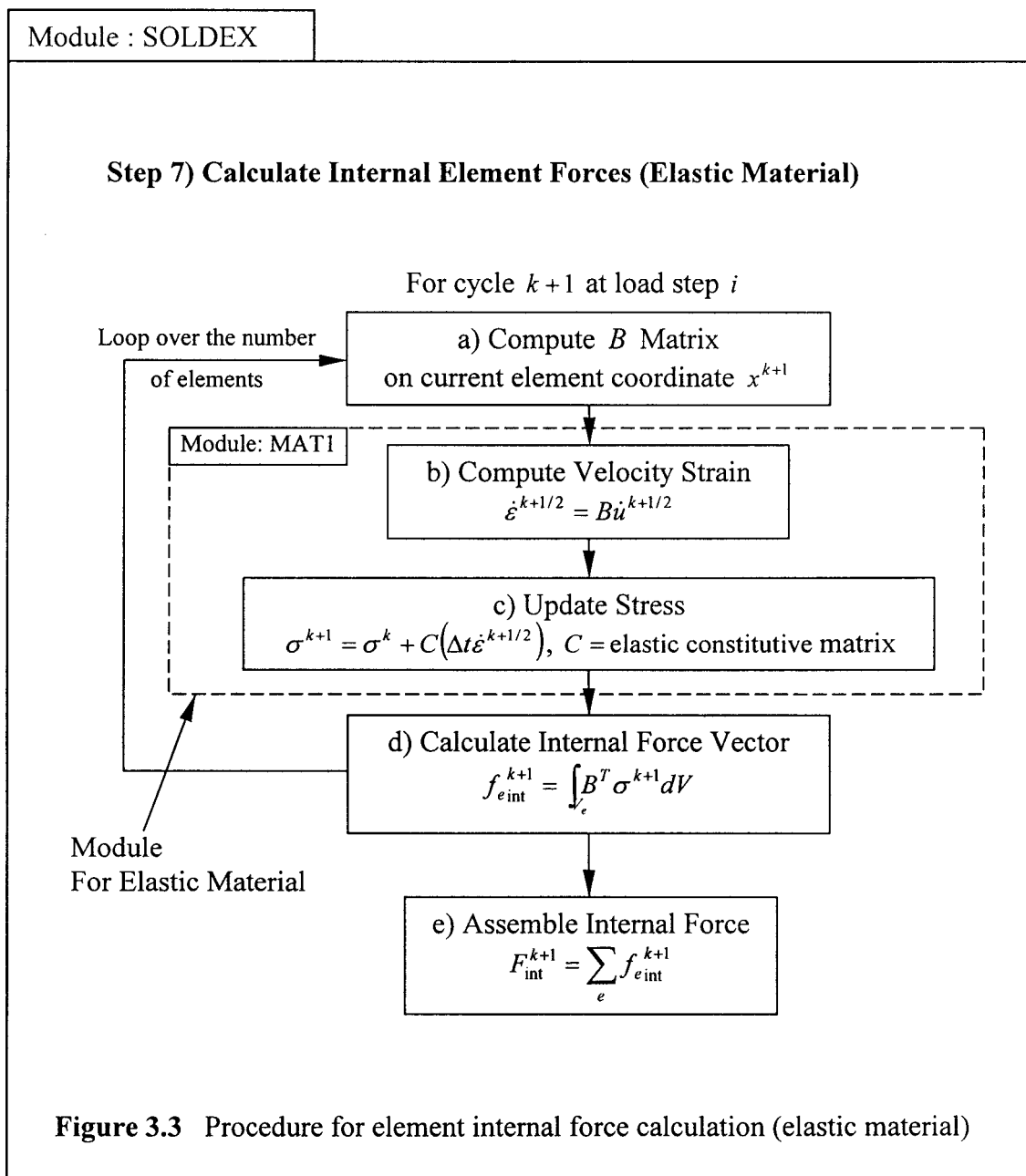


**Figure 3.3** Procedure for element internal force calculation (elastic material)

### 3.1.2 Stability of Dynamic Relaxation Algorithm

Explicit method is easy to apply in finite element code but this method is conditionally stable. If the time step exceeds the critical value  $\Delta t_{cr}$ , converged solution is not obtained. It has been mathematically shown that the time step must be less than or equal to two divided by the highest natural frequency (Bathe, 1982) that is  $\Delta t \leq 2 / \omega_{max}$ . The highest natural frequency and therefore the critical time step  $\Delta t_{cr}$  depend on element size and material properties. In the dynamic relaxation algorithm the mass is chosen so that  $\omega_{max} = 2$ ,  $\Delta t = 1$  (Sauve and Metzger, 1995), the details of which are not shown in the above flow chart of Figure 3.2.

## 3.2 Finite Element Modeling for Asymmetric Creep Behavior of Ceramics

In order to implement an asymmetric creep model, a material model for symmetric creep and the algorithm for creep calculation, which already exist in a material constitutive module named MAT14 of in-house code H3DMAP, is considered first. Then, modification to the existing material model for asymmetric creep is addressed.

### 3.2.1 Material Model for Symmetric Creep

In the analysis of creep, the response of the system is dependent both on external loading and the strain time history. In general, the creep is governed by a creep law which relates effective creep strain rate  $\dot{\epsilon}_c$  in terms of stress  $\sigma$ , time  $\tau$ , temperature  $T$ , etc., temperature  $T$ , etc. (Sauve et al, 1992) which is

$$\frac{d\varepsilon_c}{d\tau} = \dot{\varepsilon}_c = f(\sigma, \tau, T, \text{etc.}) \quad (3-11)$$

In this research, power law equations ( $\dot{\varepsilon}_c = A\sigma^n$ ) were assumed for ceramics creep behavior, and time  $\tau$  and temperature  $T$  terms were not included in the creep equations because only the steady state creep is studied here and the simulation is conducted with constant temperature. Therefore at the current cycle the creep strain rate is given by

$$\dot{\varepsilon}_c^k = f(\sigma) = A(\sigma^k)^n \quad (3-12)$$

The creep strain increment is obtained using a creep time increment  $\Delta\tau$  as

$$\Delta\varepsilon_c^{k+1} = \Delta\tau\dot{\varepsilon}_c^k \quad (3-13)$$

The element stress  $\sigma^{k+1}$  is obtained as

$$\sigma^{k+1} = \sigma^k + C(\Delta t\dot{\varepsilon}^{k+1/2} - \Delta\varepsilon_c^{k+1} + \Delta\varepsilon_c^k) \quad (3-14)$$

Thus, at dynamic relaxation cycles within one creep time increment, the revised creep strain increment  $\Delta\varepsilon_c$  is continually updated and the solution proceeds to equilibrate the unbalanced stress due to creep.

The above creep model is included in material constitutive module named MAT14 which is called by internal force calculation module named SOLDEX of dynamic relaxation algorithm (see Figure 3.2). The internal force calculation module SOLDEX with creep material module MAT14 is shown on the following flow chart (compare with Figure 3.3). The highlighted **step c**) is a sub-module which is called by MAT14 and this module is modified to model the asymmetric creep behavior of ceramics for this research.

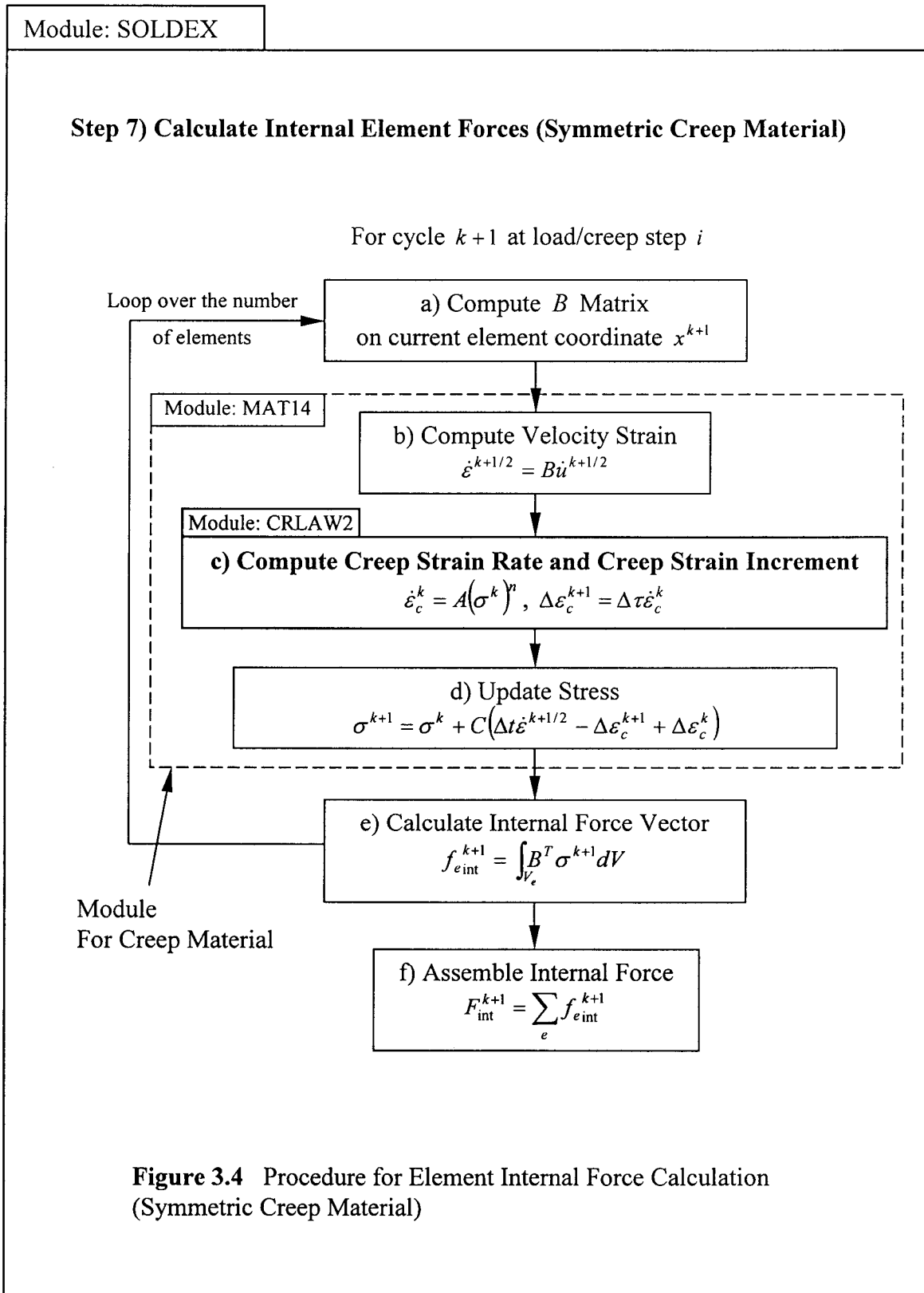


**Figure 3.4** Procedure for Element Internal Force Calculation (Symmetric Creep Material)

### 3.2.2 Stability of Dynamic Relaxation for Creep Calculation

As can be seen from the flow chart of Figure 3.4, in the creep calculation algorithm there are two kinds of time steps  $\Delta t$  and  $\Delta \tau$ . The time step  $\Delta t$  is for dynamic relaxation cycles (iterations in solving a set of non-linear algebraic equations) and  $\Delta \tau$  is a real time interval for creep deformation. As explained in section 3.1.2,  $\Delta t$  is artificially set to unity (like iteration counter) by the code via automatically adjusting the mass to keep the stability of solution, but  $\Delta \tau$  is given manually as load steps. Within one load/creep step, iterations goes on while  $\Delta \varepsilon_c$  is continually updated and the converged state is the solution of the given load/creep time step. In the Figure 3.5, dynamic relaxation cycle vs. displacement of four-point bending creep test simulation is shown. During iterations within each load/creep step, the displacement continually changed and reached converged solution and based on the converged condition, iteration goes on with next load/creep step.

As cycle time step  $\Delta t$  does, creep time step  $\Delta \tau$  affects the solution stability. If  $\Delta \tau$  is greater than critical value  $\Delta \tau_{cr}$ , the solution diverges. A rule of thumb for stable creep time step calculation is that the creep strain increment should not exceed one half of the total elastic strain (Zienkiewicz, 1991). For simulations in this thesis, the critical creep time step was calculated from the following formula which is from (Corneau, 1975) (Sauve et al, 1989)

$$\Delta \tau_{cr} \leq \frac{2\bar{\sigma}}{EAn\bar{\sigma}^n} \quad (3-15)$$

where  $\Delta \tau_{cr}$  is critical creep time step,  $E$  is modulus of elasticity,  $\bar{\sigma}$  is effective stress, and

$A$  and  $n$  are creep constants from steady state power law equation  $\dot{\epsilon}_c = A\sigma^n$ . Thus, stability conditions with respect to the dynamics relaxation transient and creep response can be obtained.

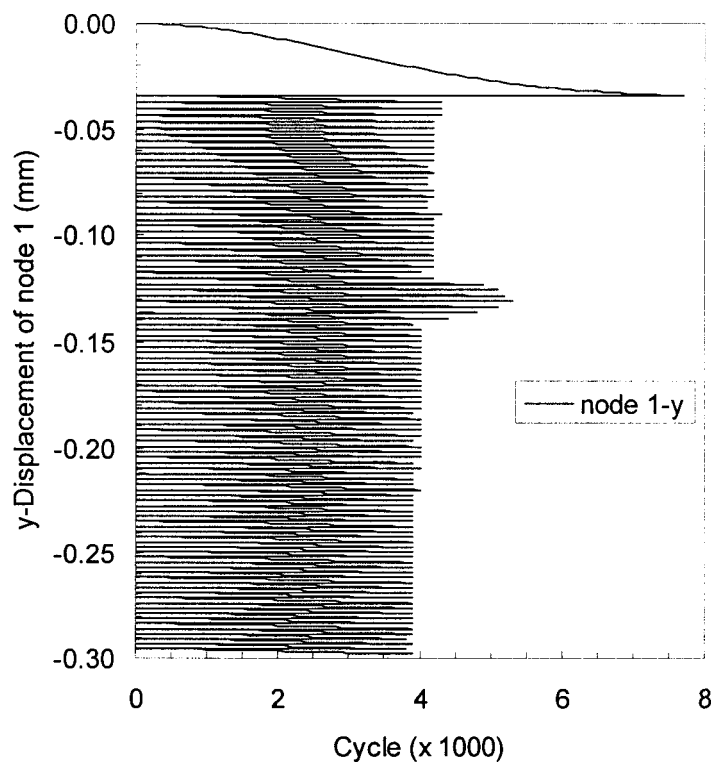


**Figure 3.5** Four-point bending creep-80,000 sec creep-dynamic relaxation cycles

### 3.2.3 Material Model for Asymmetric Creep

The modifications to the creep material model used to perform bending creep test simulations in this thesis need to be addressed.

For ceramics which show asymmetric creep behavior, with respect to different creep rates in tension and in compression, the creep is governed by the following two equations.

$$\dot{\epsilon}_{sc} = A_c \sigma^{n_c} \quad \sigma \text{ in compression} \quad (3-16a)$$

$$\dot{\epsilon}_{st} = A_t \sigma^{n_t} \quad \sigma \text{ in tension} \quad (3-16b)$$

$A$  and  $n$  are creep constants and the subscripts  $c$  and  $t$  refers to the case in compression and in tension respectively

In the existing code the **step c) Compute Creep Strain Rate and Creep Strain Increment** is a module named CRLAW2 which is called by creep material constitutive module MAT14 and this module calculates and returns creep strain increment based on current stresses using a given power law creep equation  $\dot{\epsilon} = A\sigma^n$ . To model the asymmetric creep behavior, a simple modification was performed in this subroutine. Instead of using the single creep equation, the two equations of (3-16a) and (3-16b) were used selectively to calculate creep strain. The hydrostatic stress was initially used to decide compression/tension condition of the element. The modified module CRLAW2 for asymmetric creep is shown in Figure 3.6.

Module: CRLAW2 (MODIFIED)

**c) Compute Creep Strain Rate and Creep Strain Increment  
(Asymmetric Creep Material)**

For cycle  $k + 1$  at load/creep increment  $i$

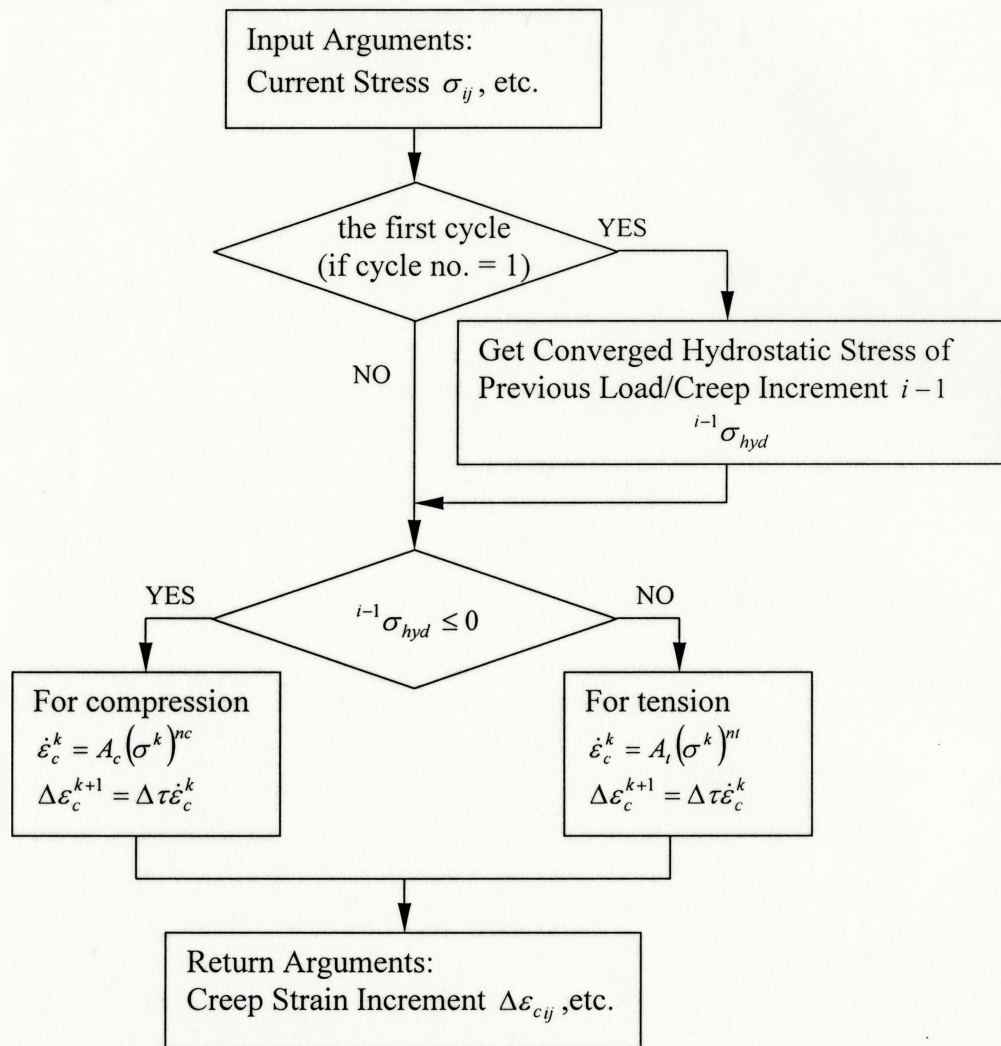


**Figure 3.6** Procedure for creep strain increment calculation (asymmetric creep)

### 3.2.4 Stability of Dynamic Relaxation for Asymmetric Creep Calculation

Instability problems were encountered in the asymmetric modification when current hydrostatic stress was used to decide compression/tension condition of elements. In bending creep simulation, at elements near neutral axis the hydrostatic stresses fluctuate between tension and compression during dynamic relaxation iterations. Different creep law equations are used for tension and compression and the creep rate abruptly changes when the hydrostatic stress changes from tension to compression or from compression to tension during iterations.

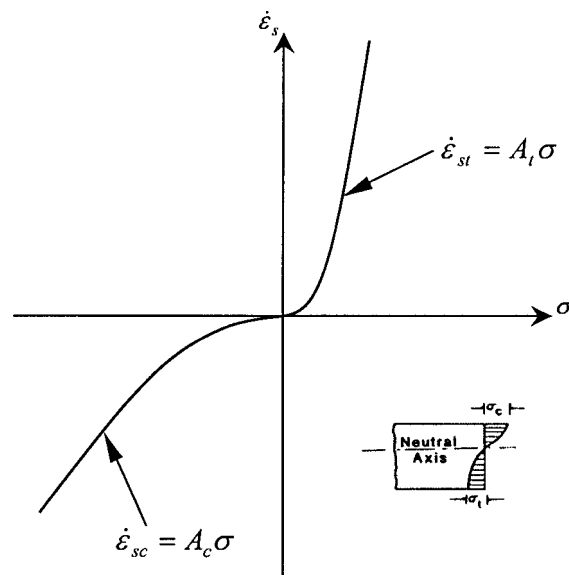


**Figure 3.7** Diagram for creep law equations (asymmetric creep) showing distinct behaviors between tension and compression (Chuang 1986)

This problem was solved when the converged hydrostatic stress of last load/creep time step was used to decide compression/tension condition of the element. That means during iterations within one load/creep time step, a single creep law is applied ( $\dot{\epsilon}_{sc} = A_c \sigma^{nc}$  or  $\dot{\epsilon}_{st} = A_t \sigma^{nt}$  depending on stress condition of previous load/creep time step) for creep strain increment.

### 3.2.5 Stable Creep Time Step $\Delta\tau$ Calculation

As explained in section 3.3.2,  $\Delta\tau$  should be selected and given manually in the simulations as load steps and theoretical formula for critical creep time step is given as

$$\Delta\tau_{cr} \leq \frac{2\bar{\sigma}}{EAn\bar{\sigma}^n} \quad (3-17)$$

But in actual applications one-tenth of the calculated value by the formula was stable for creep simulation. In some simulation cases, the creep exponent was big and the stable time step was too small. For example, in one case the parameters were

$$E = 300 \text{ GPa}, n = 5.6, A = 2.972 \times 10^{-17} \text{ (1/sec)}, \bar{\sigma} = 90 \text{ MPa}$$

and the calculated stable creep time step is

$$\Delta\tau_{cr} = \frac{2(90)}{(300E3)(2.972E-17)(5.6)(90)^{5.6}} \times 0.1 = 4 \text{ sec}$$

which is too small to practically simulate the duration of a useful creep test. Therefore the implicit creep time stepping scheme option was used for creep strain increment calculation. In the in-house code, creep strain increment  $\Delta\epsilon_c$  in creep time interval  $\Delta\tau$  is calculated using time stepping scheme such as

$$\Delta\epsilon_c = \left[ (1-\gamma)\dot{\epsilon}_c^\tau + \gamma\dot{\epsilon}_c^{\tau+\Delta\tau} \right] \Delta\tau \quad (3-18)$$

If  $\gamma = 0$  option is used, it is the explicit creep time stepping scheme because the creep strain increment is determined from conditions at step  $\tau$ . If  $\gamma = 1$  option is used, it becomes implicit creep time stepping scheme because the creep strain increment is determined using the creep strain rate corresponding to the end of the time interval. With  $\gamma = 1$  option, the scheme is unconditionally stable theoretically. The detailed procedures to use these time stepping schemes were not shown in the algorithms of Figure 3.4 but have been previously established in the finite element code (Sauve et al., 1992).

To use longer creep time step,  $\gamma = 1$  option was used for the simulations in this thesis. But not to lose accuracy by using too longer creep time step, the calculated value from the formula (3-13) was used as creep time step. By doing this, 10 times longer creep time step could be applied in simulations than by using explicit creep time stepping scheme.

## **CHAPTER 4**

### **VERIFICATION OF ASYMMETRIC CREEP MATERIAL MODEL**

The asymmetric creep material model which is implemented in the finite element method must be tested and verified before it is used in the bending creep test simulations of this research. For this purpose C-ring compression creep test simulation is performed with modified code and the result is compared with published experimental data and simulation.

#### **4.1 Si-SiC C-Rings Compression Creep Test**

The mechanics of C-ring tests have been of interest to researchers because the C-ring specimen geometrically bridges the gap between simple one-dimensional lab test specimens and the three-dimensional structural components. C-ring specimens are cost effective because specimens can be cut directly from a tube, and experimental design is simple because a simple push rod can be used to apply the load directly to the specimen (Chuang et al., 1992).

Chuang et al. (1991) performed compression creep tests with siliconized silicon carbide (Si-SiC) C-rings and the load-point displacements were continually monitored as a function of time.

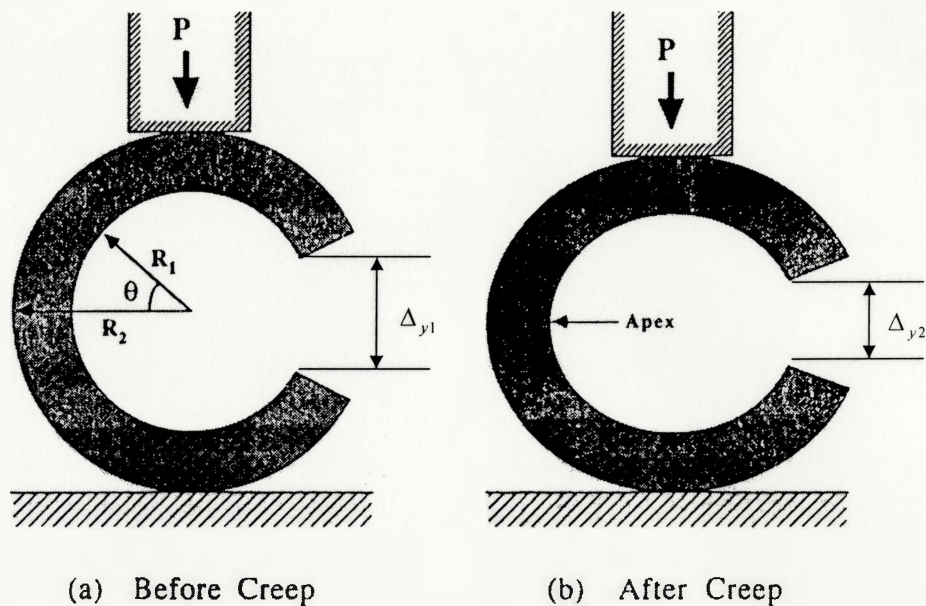


**Figure 4.1** Schematic diagram of the C-ring compression creep test (Chuang et al., 1991)

Si-SiC is two-phase ceramic composite containing metallic silicon matrix with SiC grains. It is promising material for load-bearing applications such as turbine engines and heat generation systems. The main feature of the creep response for this two-phase composite is its asymmetric property in tension and compression (Chuang, 1992). In their tests, a number of Si-SiC C-ring specimens were cut from tubular components. The C-ring was placed between two SiC push rods inside a furnace, a constant compression load was applied at 1300 °C in air, and the long-term creep behavior of specimen was investigated. The separation distance of C-ring opening slit was measured ( $\Delta y = \Delta y_1 - \Delta y_2$ ) as a function of time, using a traveling optical microscope (Chuang et al., 1991).

The table 4.1 shows the dimensions and applied load for one C-ring specimen which will be the object of comparison for the verification.  $B$  is the specimen width and  $\sigma_e$  is the theoretically predicted elastic stress developed at the out edge of the ring apex.

**Table 4.1** Specimen dimensions and applied load (Chuang et al., 1991)

Specimen	$B$ (mm)	$R_1$ (mm)	$R_2$ (mm)	$P$ (N)	$\sigma_e$ (MPa)
KX01-C4	6.38	15.950	19.050	117.89	200

The Figure 4.2 is the measured deflection of the C-ring vs. time where the stages of transient, steady state, and tertiary creep are shown. But, for engineering ceramics at mild service load, the transient and tertiary stages are short, and thus not important. The steady state stage (steady state creep rate) is the main concern of researchers and designers. The measured creep deflection rate for this specimen is  $11.55 \mu\text{m/h}$  at steady state.

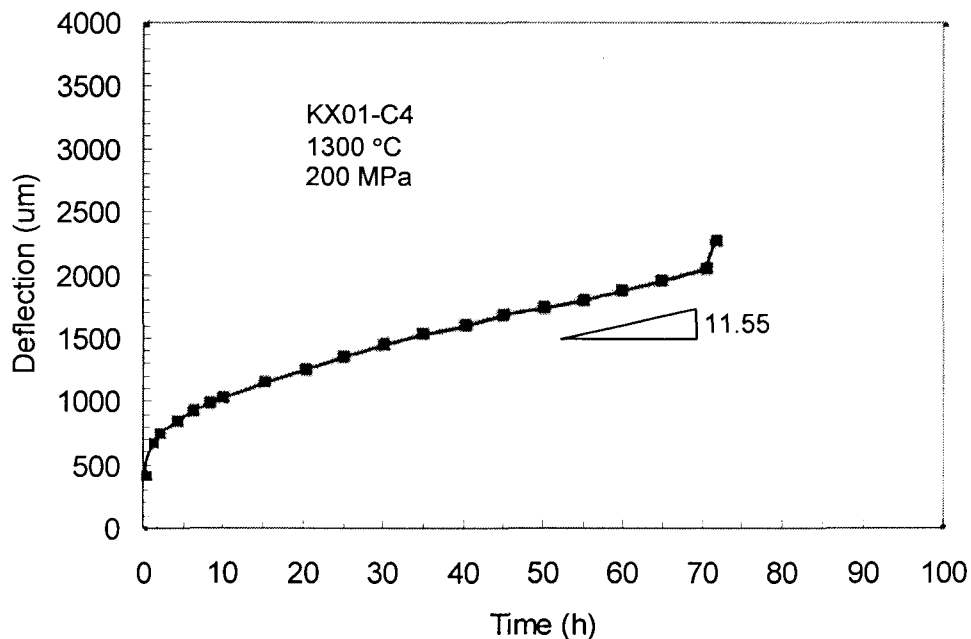


**Figure 4.2** Creep curve of a C-ring (Chuang et al., 1992)

## 4.2 Asymmetric Creep Laws for Siliconized Silicon Carbide (Si-SiC)

Uniaxial tension and compression creep test had been performed for Si-SiC and the corresponding creep laws were established previously (Wiederhorn et al., 1988). This material showed asymmetric creep response in tension and compression, which means creep rates in tension and in compression are different. Also, bi-linear behavior for both tension and compression were investigated. The creep law is given as follows.

$$\dot{\varepsilon}_s = A_t \left( \frac{\sigma}{\sigma_0} \right)^n \quad \text{for } \sigma \leq \sigma_0 \quad (4-1a)$$

$$= A_t \left( \frac{\sigma}{\sigma_0} \right)^N \quad \text{for } \sigma > \sigma_0 \quad \text{in tensile creep} \quad (4-1b)$$

$$\dot{\varepsilon}_s = \lambda A_t \left( \frac{\sigma}{\sigma_0} \right)^n \quad \text{for } \sigma \leq \beta \sigma_0 \quad (4-1c)$$

$$= \lambda A_t \left( \frac{\sigma}{\sigma_0} \right)^N \quad \text{for } \sigma > \beta \sigma_0 \quad \text{in compressive creep} \quad (4-1d)$$

where  $\dot{\varepsilon}_s$  is effective creep strain rate at steady state,  $\sigma$  is effective stress and  $\sigma_0$  is threshold stress. At 1300°C creep parameters have the following values.

$A_t = 5 \times 10^{-9} \text{ s}^{-1}$ ,  $\sigma_0 = 100 \text{ MPa}$ ,  $N = 10$ ,  $n = 4$ ,  $\beta = 2$  and  $\lambda = 0.1$  (Wiederhorn et al., 1988)

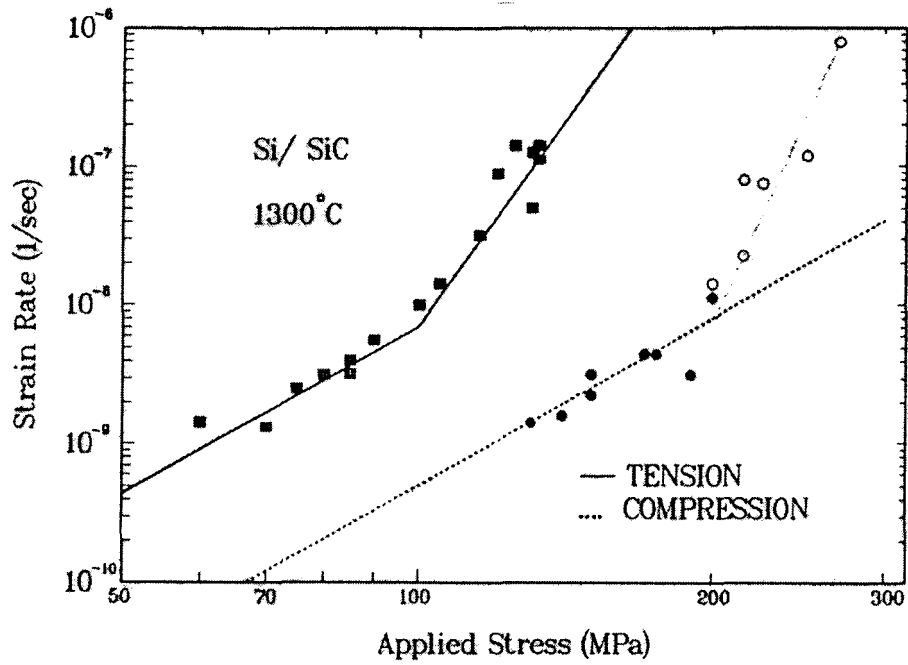


**Figure 4.3** Uniaxial tension and compression creep tests at 1300°C (Wiederhorn et al., 1988)

### 4.3 C-Ring Compression Creep Test Simulation by Chuang et al.

With the creep laws and specimen dimensions given in the previous sections, Chuang et al. (1992) performed a finite element simulation of C-Ring Compression Creep Test. They used a two-dimensional finite element model with plane strain conditions as shown in Figure 4.4. 240 8-node quadratic elements were used to model the C-ring and concentrated load was applied to one node on top.

From the finite element solution, the load-point displacement,  $\Delta_p$  vs. time  $t$ , and displacement rate,  $\dot{\Delta}_p$  vs. time  $t$ , were plotted together with experimental data which were introduced in section 3.2 as in Figure 4.5.

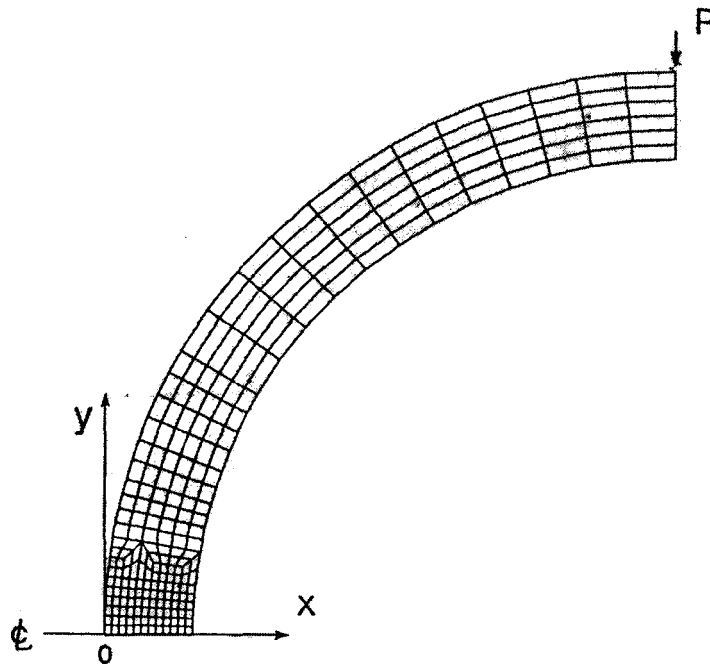


**Figure 4.4** The two-dimensional finite element model of C-ring (Chuang et al., 1992)

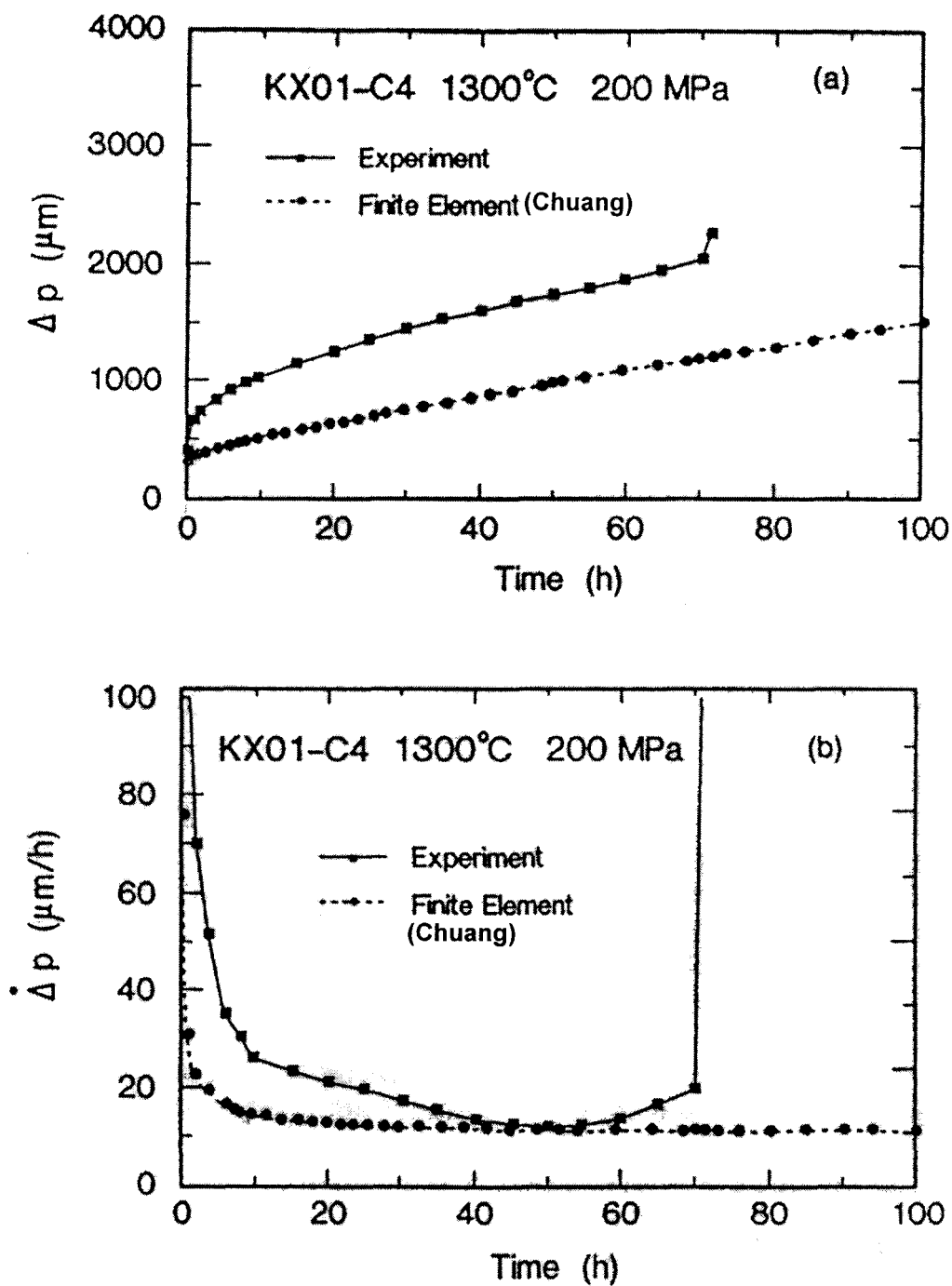


**Figure 4.5** Comparison of Chuang's simulation and Experiment (Chuang et al., 1992)

From the displacement curve it can be seen that total deflections of simulation and experiment differ considerably. This is because the input creep law equations were for steady state creep, so the transient term was not included in creep law. As explained already steady state creep rate is the main concern of researchers. If one considers the creep rate as a function of time, the effect of primary creep becomes insignificant (Chuang et al., 1992) (Zhu and Weng, 1989). The displacement rate from the simulation was  $11.00 \mu\text{m}/\text{h}$  at  $t = 100 \text{ h}$  which is in good agreement with the experimental data of  $\dot{\Delta}_p = 11.55 \mu\text{m}/\text{h}$  although some discrepancies are apparent (Chuang et al., 1992).

#### 4.4 C-Ring Compression Creep Test Simulation by Modified Code

To verify the asymmetric creep material model which is implemented in explicit finite element code, the C-ring compression creep test simulation was performed with the same creep constants, specimen dimensions and load.

##### 4.4.1 Model Preparation

Because of symmetry of geometry and load with respect to the apex of the ring, upper half of the ring was modeled. The quarter ring on the right side of the load was included in the model because in the experiment which is introduced in section 3.2, “The load-point displacements were monitored as a function of time by measuring the separation distance of the opening slit, using a traveling optical microscope.” (Wiederhorn et al., 1991). Therefore, the change of separation distance is twice the  $\Delta_d$  of Figure 4.6 and  $\Delta_y = \Delta_{y1} - \Delta_{y2}$  of Figure 4.1. Due to symmetry in thickness, one half of

the thickness was considered and a half of the load was applied on the model.

Nodes on the  $y=0$  surface were fixed in  $y$  displacements but free in  $x$  and  $z$  displacements. And all nodes on the front surface of the ring were fixed in  $z$  displacements but nodes on the back surface of the ring were free to move so that thickness could change as the ring bent.

Instead of concentrated nodal loads, a pushing rod was modeled with rigid surface and contact elements were modeled both on the rigid surface and on top surface of the ring, which is shown on the following Figure 4.7.

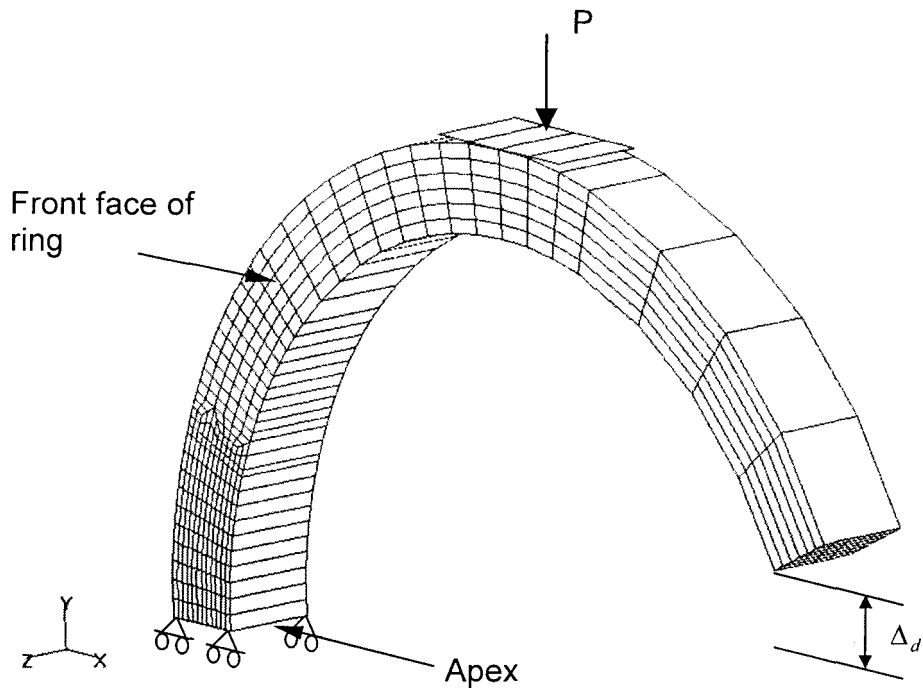


**Figure 4.6** Finite element model of C-ring

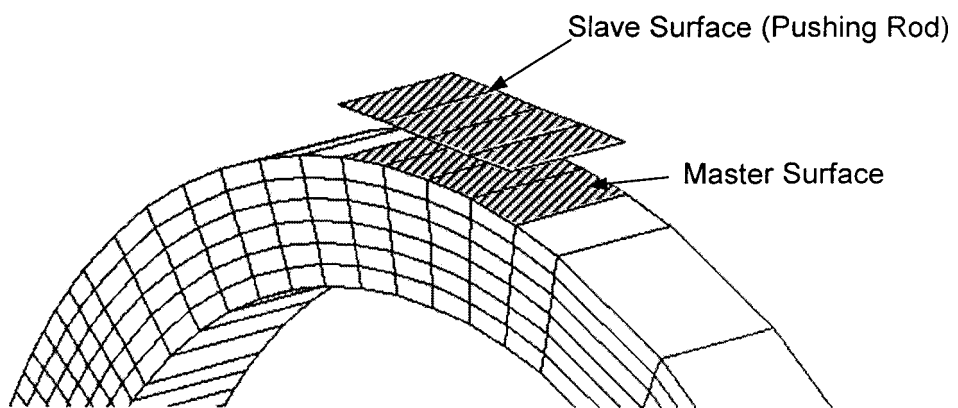


**Figure 4.7** Contact surfaces of the model

#### 4.4.2 Simulation Result

The explicit code with the asymmetric creep model was run to simulate the C-ring compression creep test. The same creep laws which was given in section 4.3 was used. The creep time step (50 sec) was calculated from the formula (3-13) and 360,000 sec (100 hr) creep was simulated. The friction coefficient between the pushing rod and C-ring was assumed as  $\mu = 1$ , which is reasonable because at creep test the pushing rod and specimen are almost stuck together due to high temperature.

Figure 4.8 and Figure 4.9 are the von Mises stress distributions at time  $t = 0$  and  $t = 100$  hr. At around the apex, the neutral axis ( $\sigma = 0$ ) shift toward compression side is observed because of higher creep rate in tension. Figure 4.10 shows the stress redistribution across the thickness at apex as time. The stresses were collected from the elements at the first row near apex.

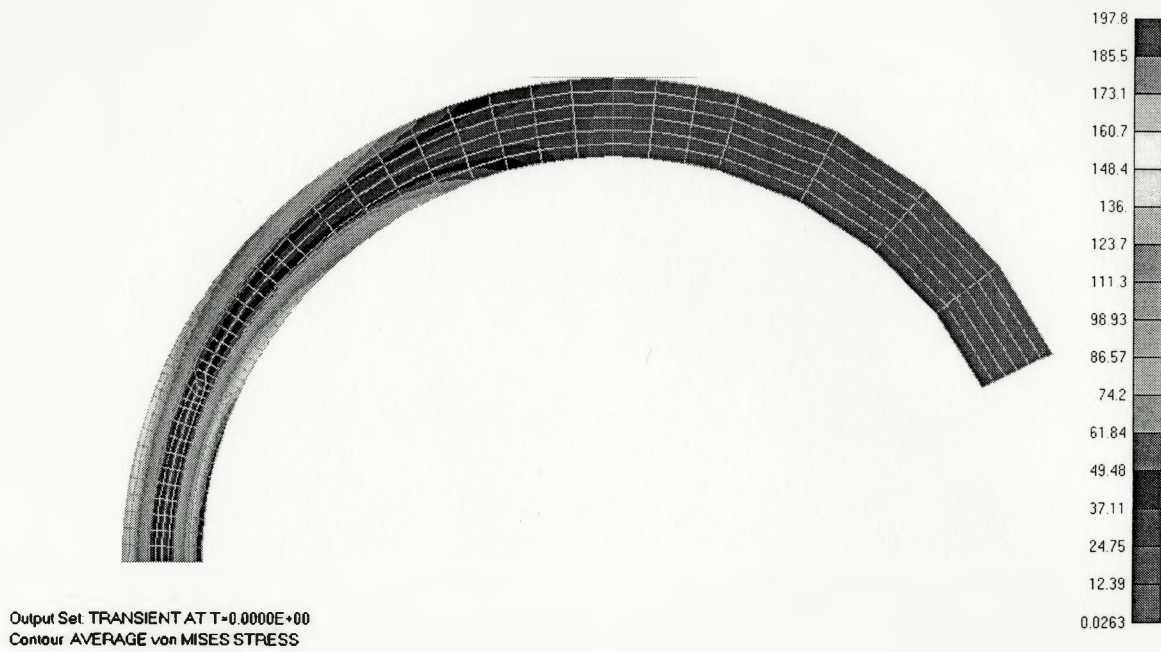


Figure 4.8 Von Mises stress at time  $t = 0$  (elastic solution)

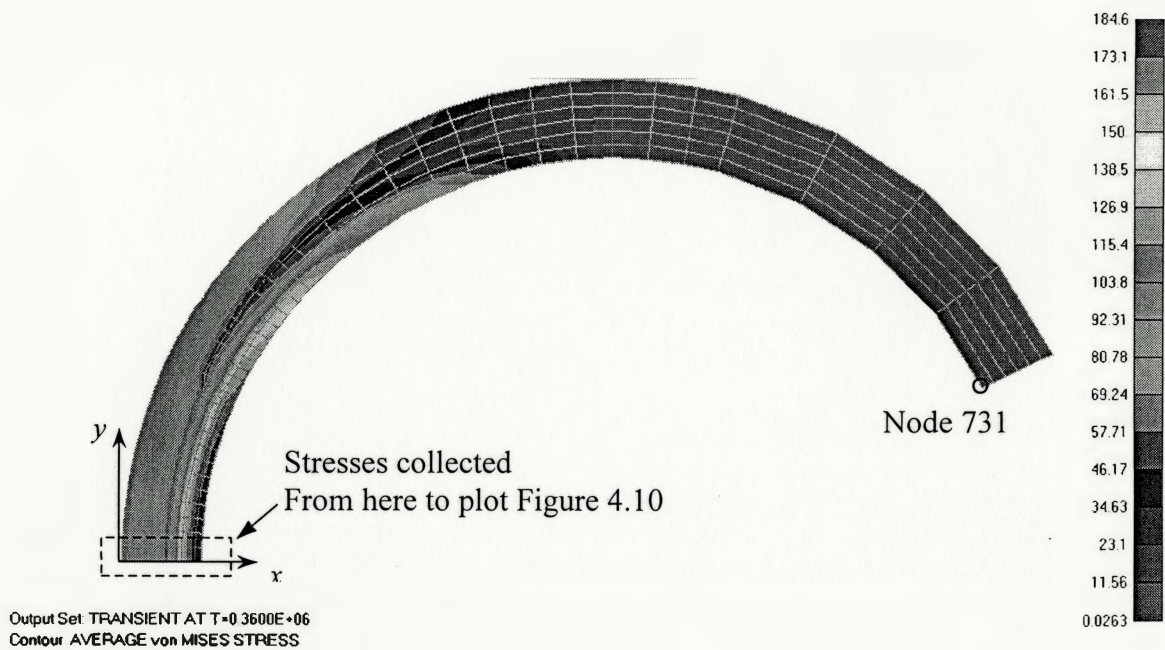
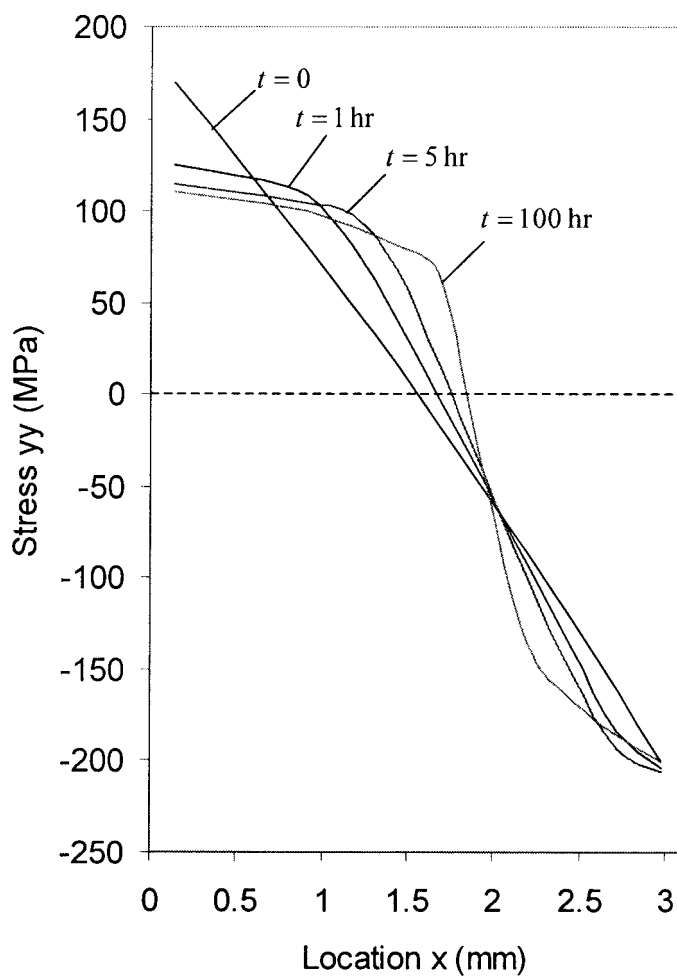
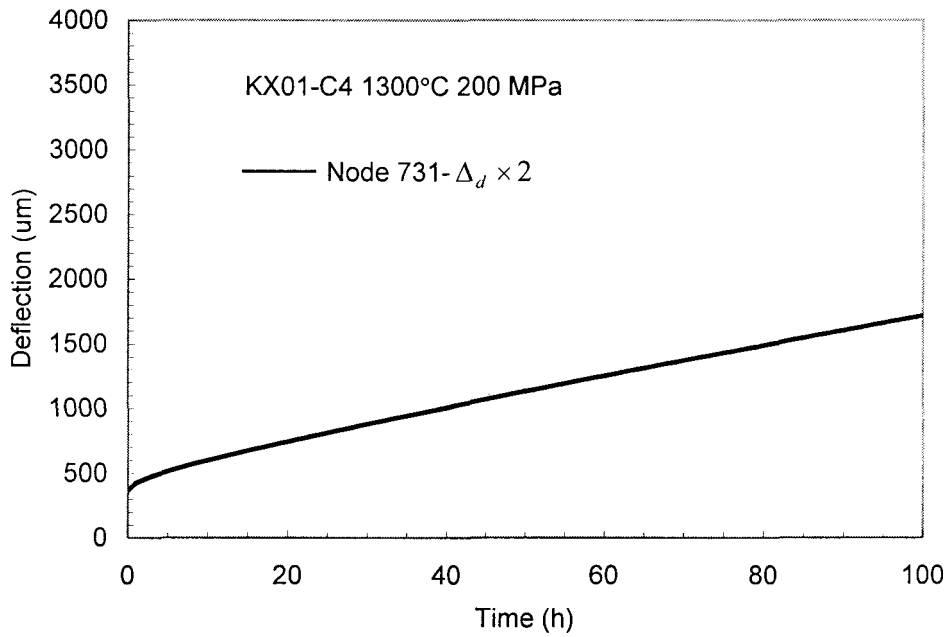


Figure 4.9 Von Mises stress at time  $t = 100$  hr (creep solution)



**Figure 4.10** Time evolution of the stress  $\sigma_{yy}$  at the ring apex



**Figure 4.11a** Total deflection vs. time (modified code)

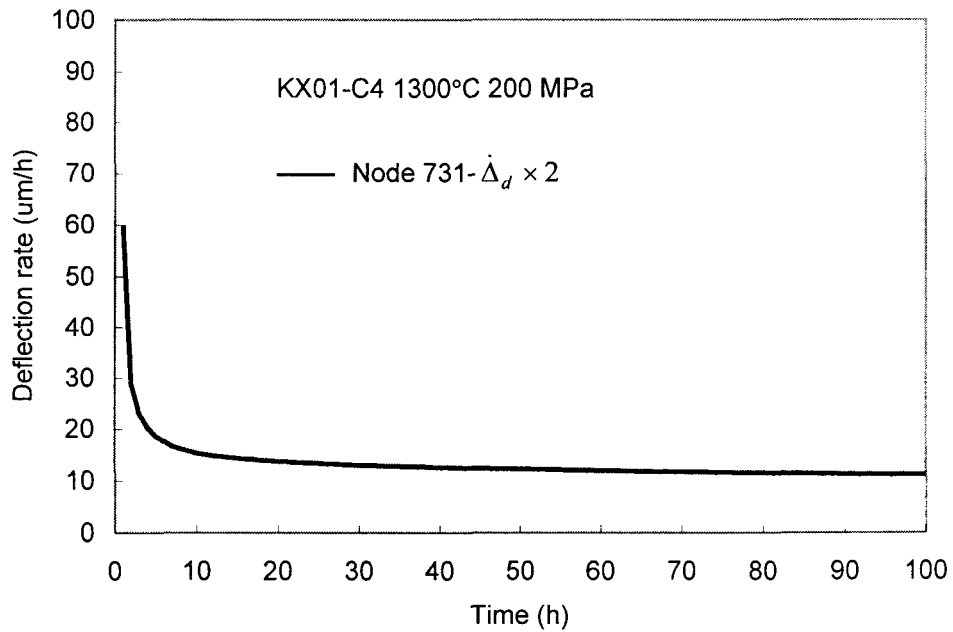


**Figure 4.11b** Deflection rate vs. time (modified code)

#### 4.5 Comparison and Discussion

For comparison, curves on Figure 4.5 and Figure 4.11 are plotted together for deflection vs. time and deflection rate vs. time as follows.

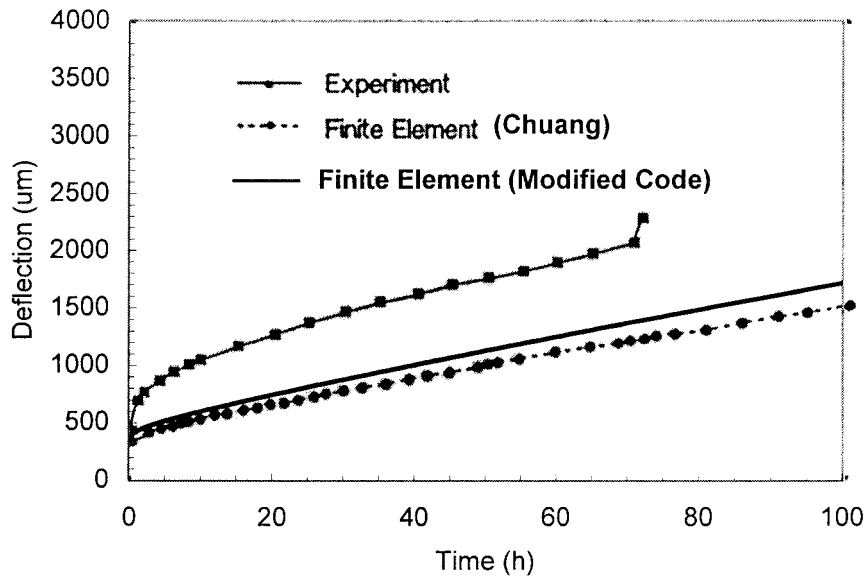


Figure 4.12a Total deflection vs. time (comparison)

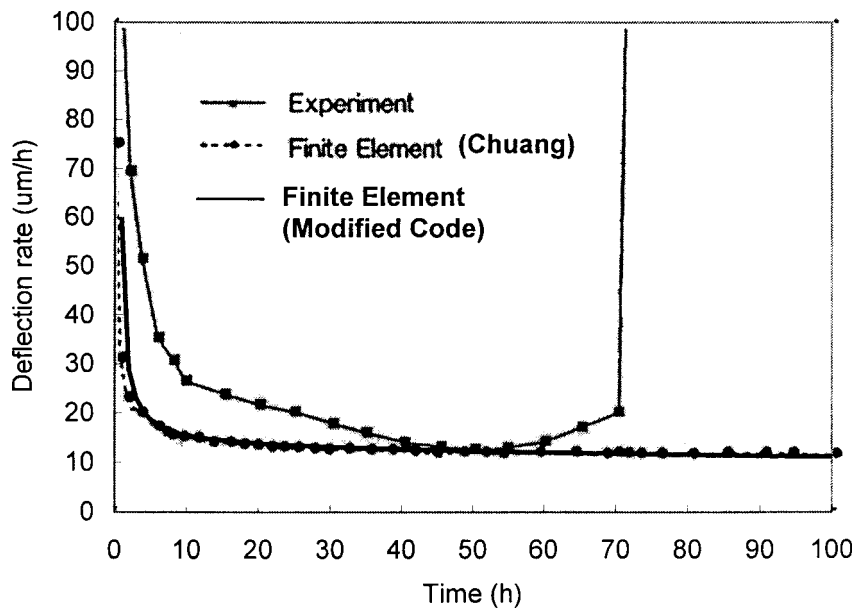


Figure 4.12b Deflection rate vs. time (comparison)

As can be seen from Figure 4.12a and Figure 4.12b, the data from current simulation are in very good agreement with both experimental data and data from Chuang's simulation. The deflection rate from current simulation is  $11.23 \mu\text{m}/\text{h}$  at 100 hr, which is compared with  $11.55 \mu\text{m}/\text{h}$  from experiment and  $11.00 \mu\text{m}/\text{h}$  from Chuang's simulation. The total deflections of current simulation differ from experiment considerably because the transient creep is considered in the simulation. But the steady-state creep rate is the main concern of this research. Therefore the accuracy of asymmetric creep model implemented in the in-house code is convincing from the comparison.

To see the error of using nodal loads instead of including contact conditions between the pushing rod and C-ring, another simulation was performed with simplified nodal loads. In the C-ring compression test, the contact point migrates toward the inside of C-ring as can be seen from Figure 4.13. With nodal load, this contact point shift is not considered in the simulation and the applied moment gets bigger than the actual applied moment as deformation goes. In the current simulations, the effect of contact shift was minor as can be seen from the table 4.2 and Figure 4.13., but the difference increases as deformation goes. Thus caution is required to use simplified nodal load in the simulations with large deformation.

**Table 4.2** Total deflections for contact load simulation vs. nodal load simulation

	Total deflection ( $\mu\text{m}$ ) at $t = 0$	Total deflection ( $\mu\text{m}$ ) at $t = 100$ hr
Simulation with contact load	367	1715
Simulation with nodal load	371	1763

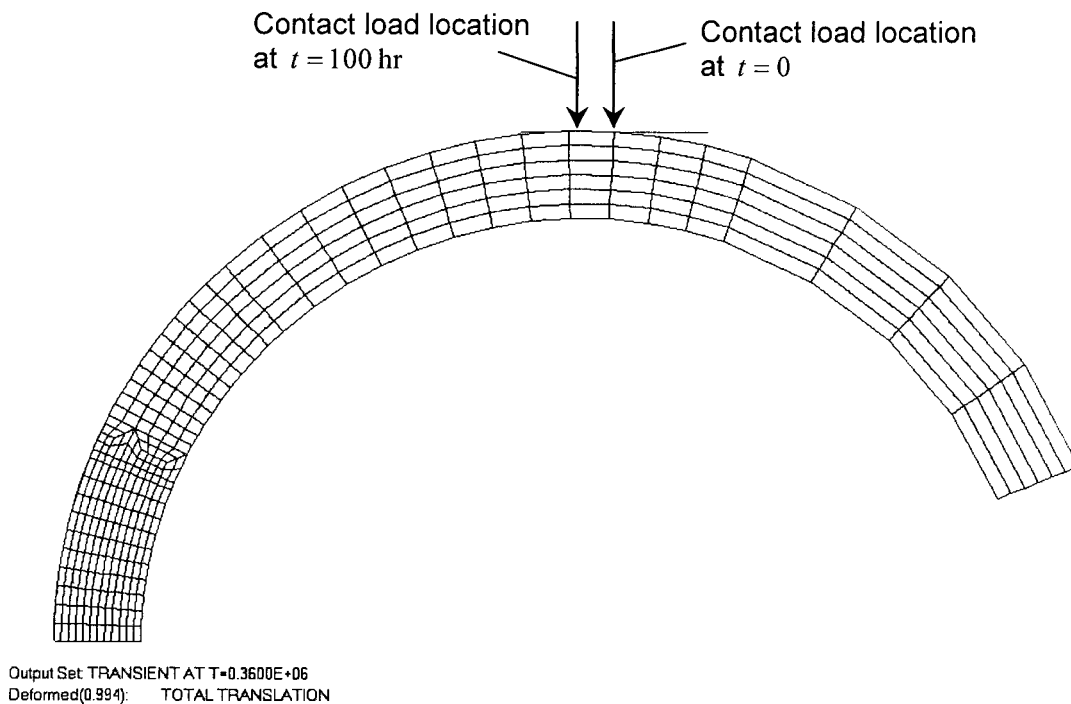


**Figure 4.13** Contact point shift in the C-ring compression test (deformed shape 2% exaggerated)

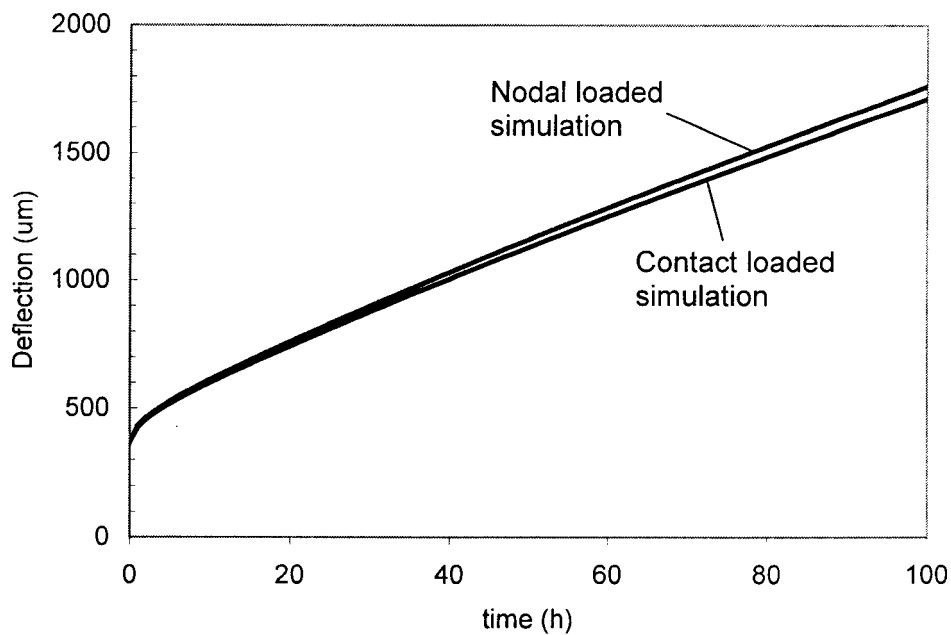


**Figure 4.14** Total deflection vs. time (comparison)

## CHAPTER 5

### FINITE ELEMENT STUDY ON FOUR-POINT BENDING CREEP TEST

In this chapter, the methods of Hollenberg et al. (1971) and Chuang (1986) to extract creep parameters from bend test data are evaluated by comparing with various simulations. The asymmetric creep material model which was developed in chapter 3 and verified in chapter 4 is used for the simulations of ceramics which have asymmetric creep property.

First, the observation of Jakus and Wiederhorn (1988) is studied with finite element analysis. Their experiments are simulated with various creep parameters and the reason for the non-linear curvature distribution in the mid-span of four-point bending creep test specimen is searched.

And then, the methods of Hollenberg et al. (1971) and Chuang (1986) to extract power-law creep parameters from bend creep test data which was introduced in chapter 2 are evaluated by comparing with simulation results. Both methods assumes constant moment and therefore constant curvature in the mid-span to relate the curvature rate to load-point displacement rate which is more easily measurable than curvature rate. Therefore it will be tested if the methods are still valid in spite of the Jakus and Wiederhorn's observation (non-linear curvature distribution in the mid span).

Then, frictional effect on the estimation of creep parameters by the methods will be studied. Also, various aspects of bend creep test which are hard to see in real experiments are examined through simulations.

### **5.1 Model Preparation**

It is quite common to simplify the finite element model using concentrated nodal load and skipping detailed geometries in finite element analyses. But in the current research, more realistic simulations were designed by including loading rollers in the finite element modeling which interact with a bending specimen through contact surfaces. By doing this the frictional effects on bend creep test were studied. To take advantage of symmetry the right half of a specimen and half thickness of it were modeled, and a half of loading roller in proximity to the specimen and half thickness of it were modeled. Linear quadrilateral solid elements were used to model the bending specimen and shell elements were used to model the loading rollers. The mesh was refined in the region of contacts of the specimen and the rollers, and all nodes on supporting roller were fixed. The nodes on pushing roller were tied to each other so that they work as rigid surface, and the total force ( $P$ ) was applied on one node in the pushing roller (see Figure 5.3). All nodes on left edge surface were fixed in x-translation and nodes on front surface were fixed in z-translation. Contact surfaces were set on four elements in the specimen and in the roller. It was enough because the contact point shift was small, and it saved calculation time by reducing the targets of contact searching algorithm.

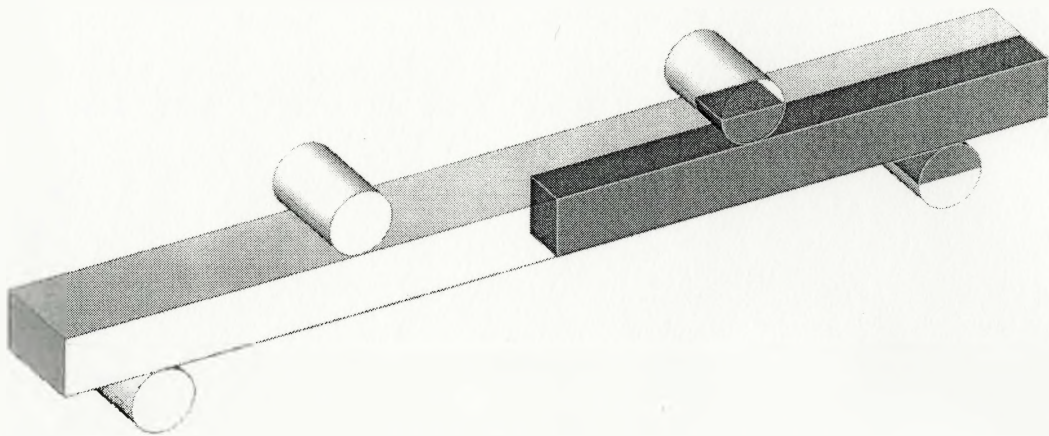
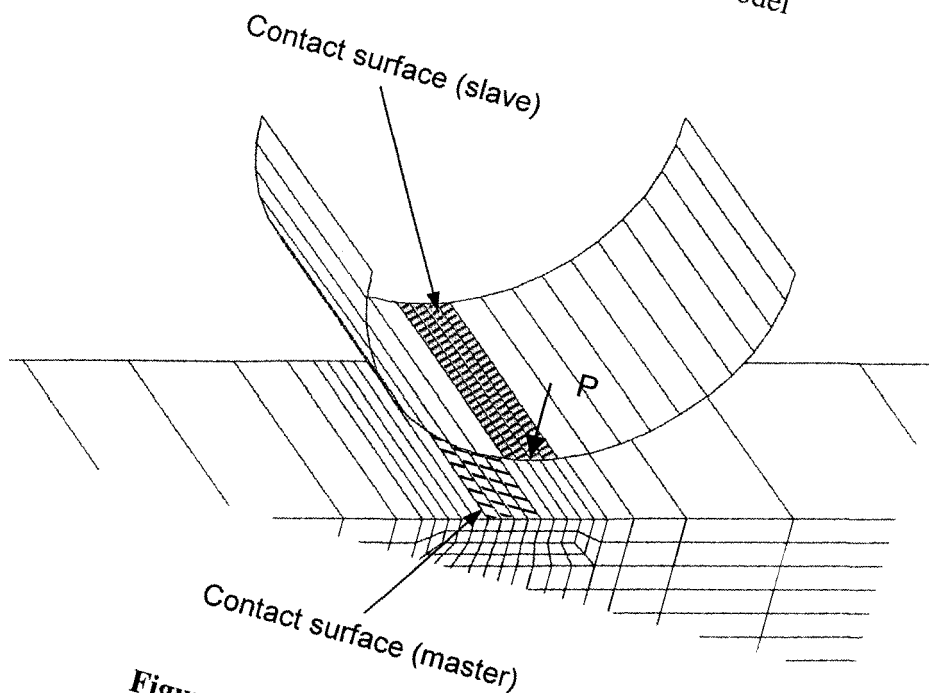
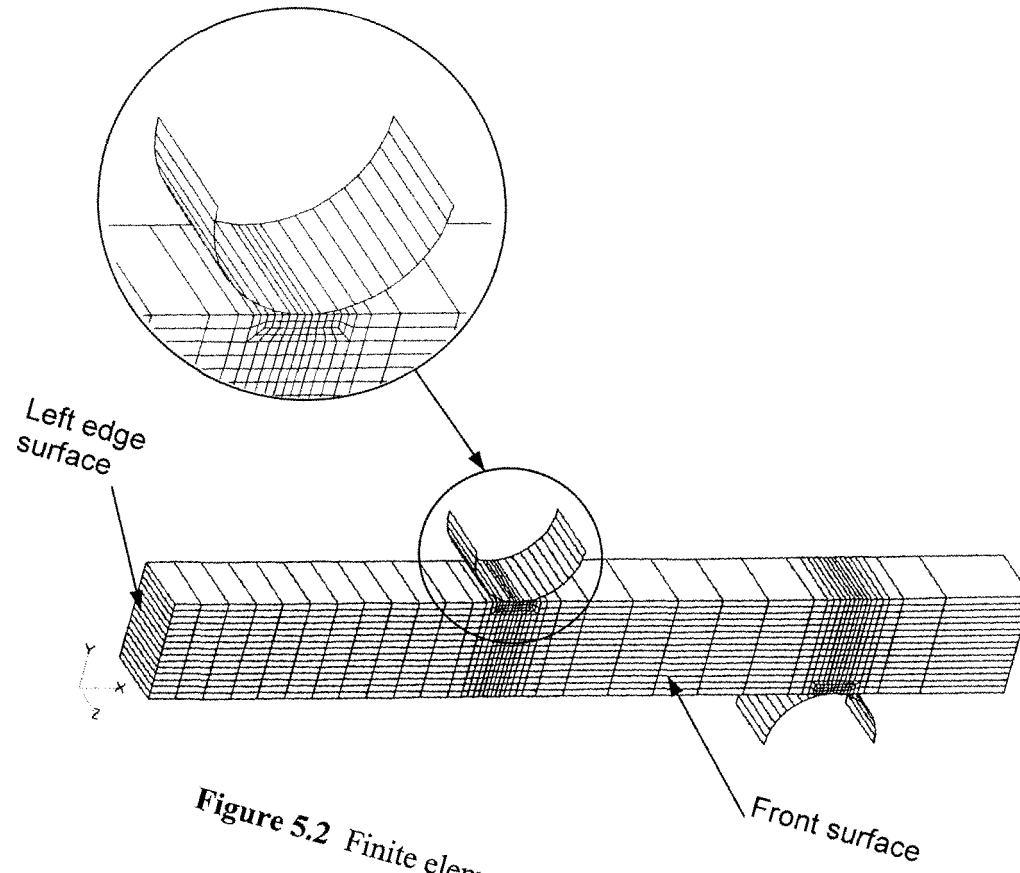


**Figure 5.1** Geometric model of four point bending creep test  
(a quarter of the model was used for finite element modeling)



## 5.2 Finite Element Study on Experiment of Jakus and Wiederhorn

The experiment of Jakus et al. (1988) exhibits non-constant curvature in the mid-span. From Figure 5.4, one can also notice that specimen (A) and (B) don't show constant curvature in the mid-span, but specimen (C) shows the constant curvature region inside the mid span which is tilted possibly because of the friction difference between left and right loading points. The reasons for this are sought through detailed finite element simulations.

### 5.2.1 Observation of Jakus and Wiederhorn

Jakus and Wiederhorn (1988) investigated four-point bending test as a method of studying the creep of ceramics at elevated temperature. In their tests, ceramic specimens were dead-weight loaded in four-point bending at elevated temperatures. The creep process was periodically interrupted by cooling the specimen to room temperature under load, after which the curvature was determined as a function of position along the tensile surface from the measurement of the deformation of the specimen (Jakus et al., 1988).

Figure 5.4 shows the curvature of three crept specimens. The nominal size of the specimen was 3 by 5 by 50 mm and the inner loading span was 10 mm and the outer span was 40 mm. The curves generally follow the simple beam theory, but in the mid span it deviates from the theory. From simple beam theory the constant moment and therefore radius of curvature expected in the mid span but from the experiment the curvature was greatest under the inner loading points and not constant in the mid span ( Jakus et al. 1988).

The methods of Hollenberg et al. (1971) and Chuang (1986) to extract creep parameters from bend creep tests, which were explained in chapter 2, assumed constant moment in the inner span to relate the curvature rate to load-point displacement rate. With the above observation as one of the reasons, Jakus and Wiederhorn (1988) concluded that “the necessity of performing creep tests in uniaxial tension and compression is apparent.”

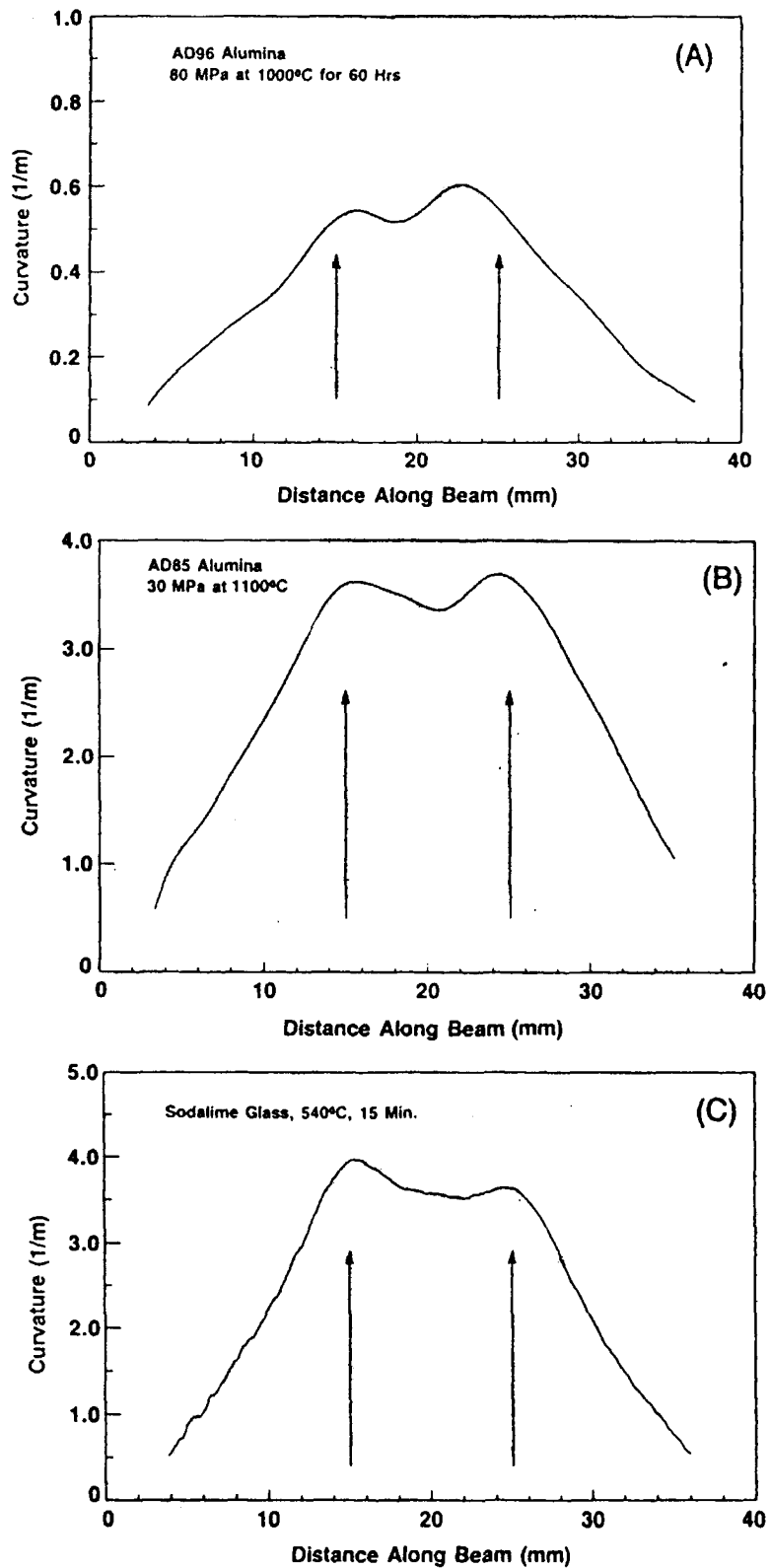


**Figure 5.4** Curvature as a function of distance along the flexure bar (Jakus et al., 1988)

### 5.2.2 Finite Element Modeling

The Finite element model was prepared with the way which had been explained in section 5.2. A total of 772 elements and 1,660 nodes were used. 15 elements were used in the height of specimen to depict the stress distribution in height direction of the specimen.

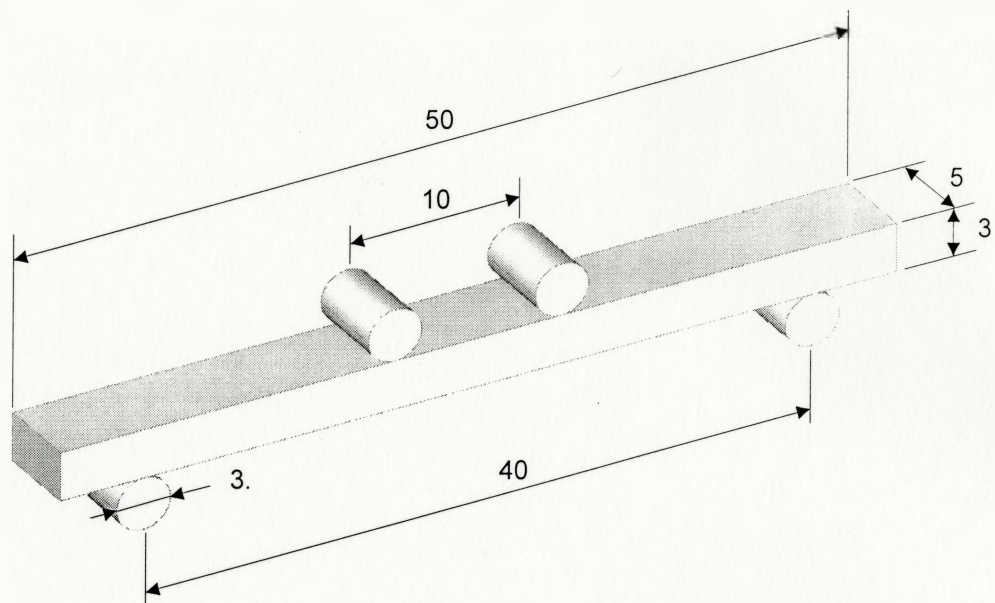


Figure 5.5 Specimen dimension of the experiment of Jakus et al.

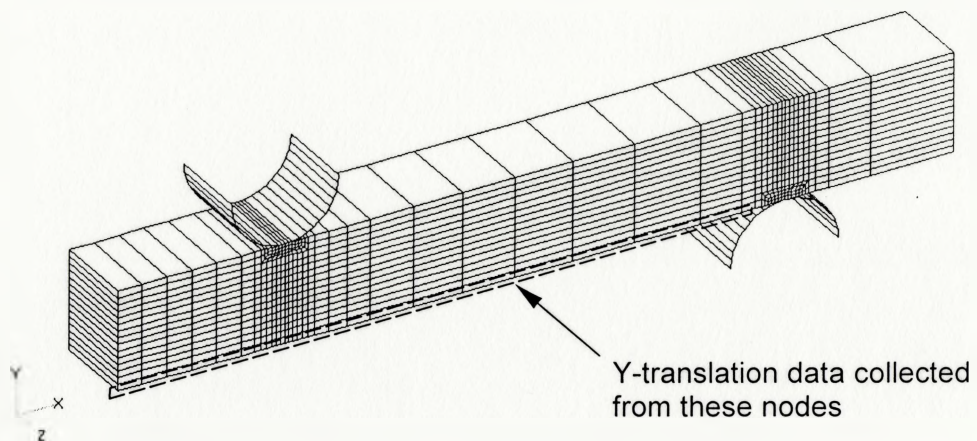
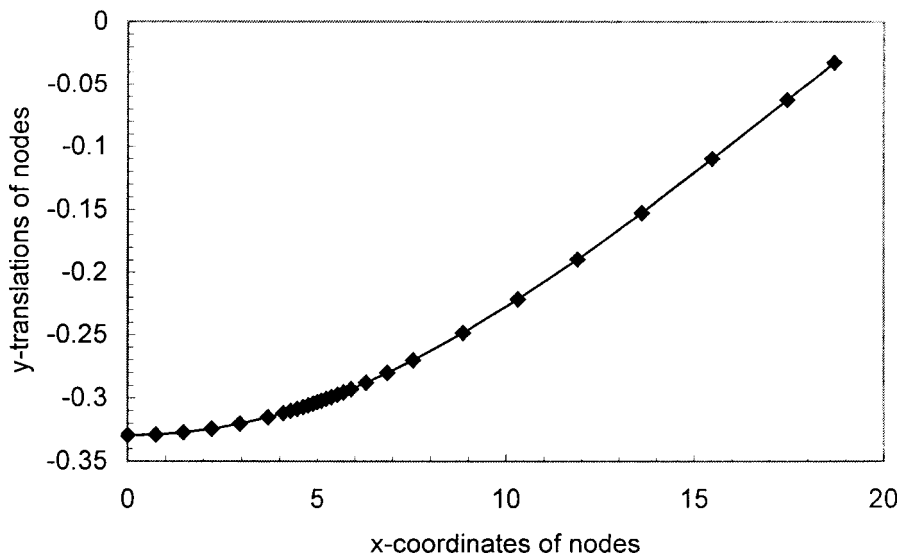


Figure 5.6 The finite element model for the simulation of Jakus's experiments

### 5.2.3 Simulation

Because the creep properties were not given in the paper of Jakus et al. and the purpose of simulations in this section is not a quantitative study of their experiment, various creep properties were assumed based on the limited data in the paper and curvatures of the specimens from the simulations were compared with the curvature curves (Figure 5.4) from the experiments of Jakus et al..

The curvature curve of the crept model of simulation was calculated by the similar way that Jakus et al. used to determine curvature from the measurement of the deformation of the specimen (Jakus et al., 1988). Y-translations of the nodes (Figure 5.6) in tensile surface of the model were collected from the simulation, which are shown in the following Figure 5.7 as graphical form.



**Figure 5.7** Beam deflection data from simulation

The curvature can be determined from beam deflection data by numerically calculating the second derivative of the beam deflection with the following equation assuming small deflection.

$$1/\rho = (d^2 y / dx^2) \quad (5-1)$$

where  $1/\rho$  is the curvature,  $y$  is the beam deflection, and  $x$  is the distance along the beam. When the nodal data were used to calculate curvature, the noise was quite high as Jakus et al. experienced with experimental data because differentiation accentuates scatter in data. To use the localized curve-fitting scheme which was used by Jakus et al., nodal displacement data were connected with smooth line by cubic spline interpolation. By doing this the beam deflection data were collected at every 0.1 mm in x-coordinates along the beam. Twenty to forty adjacent points in the deflection data, corresponding 2 to 4 mm along the beam, were fitted with the following polynomial.

$$y = a_2 x^2 + a_1 x + a_0 \quad (5-2)$$

The second derivative of this equation is  $2a_2$  and this is the curvature of the data segment. This value was considered as the curvature at the center of the segment. The curvature at the next location was calculated by shifting the segment by one data point and the curvature of the center of that segment was calculated. This process was repeated at every location along the beam.

### 5.2.4 Results and Discussion (Sodalime Silica Glass)

First, creep test of specimen (C) of Figure 5.4, sodalime silica glass, was simulated with the following creep parameters which were assumed based on the data given in the paper.

$$A_t = A_c = 1.35 \times 10^{-7} \text{ s}^{-1}, n_t = n_c = 1 ; \text{symmetric creep}$$

where  $n_t = n_c = 1$  was given in the paper mentioning linear viscous creep behavior of sodalime silica glass. The load 7.5 N was applied so that the outer fiber elastic stress of the specimen may become 30 MPa. The creep time step of 30 sec, was used to simulate 900 sec (15 min.) of creep.

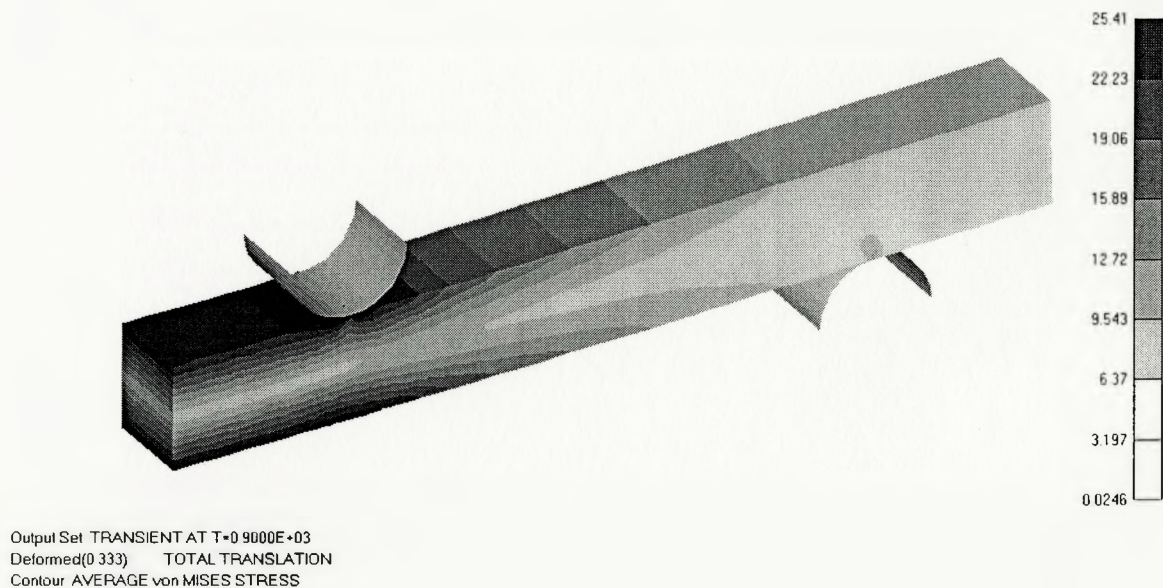


**Figure 5.8** Von Mises stress distribution after 900 sec creep

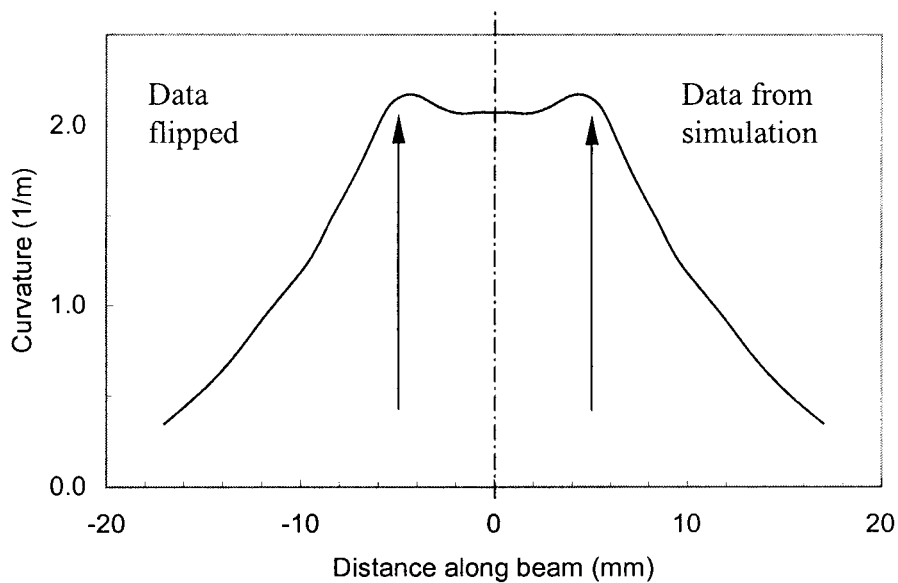


**Figure 5.9** Curvature curve from simulation without friction between loading roller and specimen ( $\mu = 0$ )

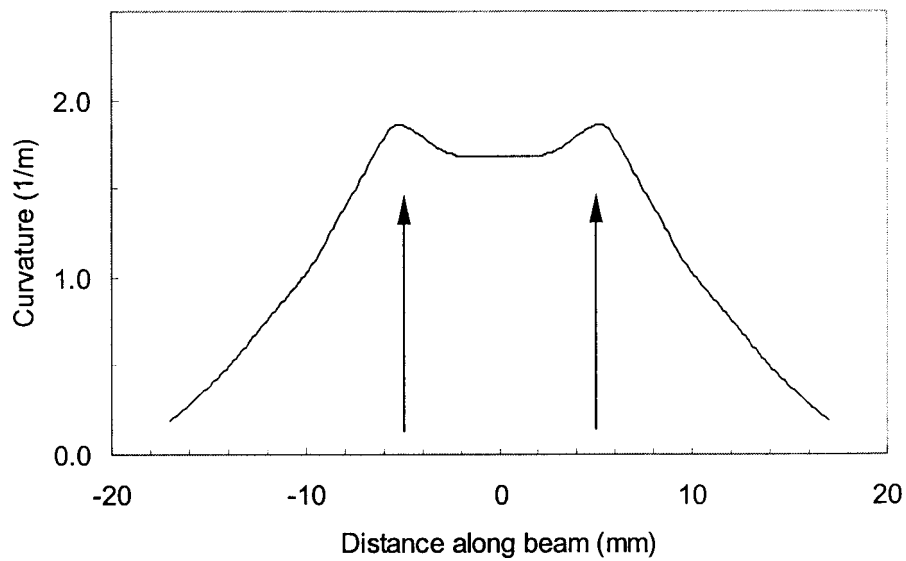


**Figure 5.10** Curvature curve from simulation with friction between loading roller and specimen ( $\mu = 1$ )

Two simulations were performed with different friction coefficients ( $\mu=0$  and  $\mu=1$ ) between pushing rollers and specimen. Figure 5.9 and Figure 5.10 shows the curvature curves from the simulations. To get the curvature curves from the beam deflection data, the method explained in section 5.4.2 were used. The beam deflection data from the simulation were flipped for the opposite half so that the curvature curves for the whole specimen length could be viewed.

The curvature curves from simulations didn't exactly match quantitatively with the curve from the experiment of Jakus et al. because the exact creep parameters were not used in the simulations. However, the general trend is similar to each other. Flat curvature regions were shown for both experiment and simulation. By comparing Figure 5.9 and Figure 5.10, one can notice that friction lowers the curvature at the loading point. Based on this observation, one can see from the curvature curve of specimen (C) of Figure 5.11 that the friction was higher at the right loading point.

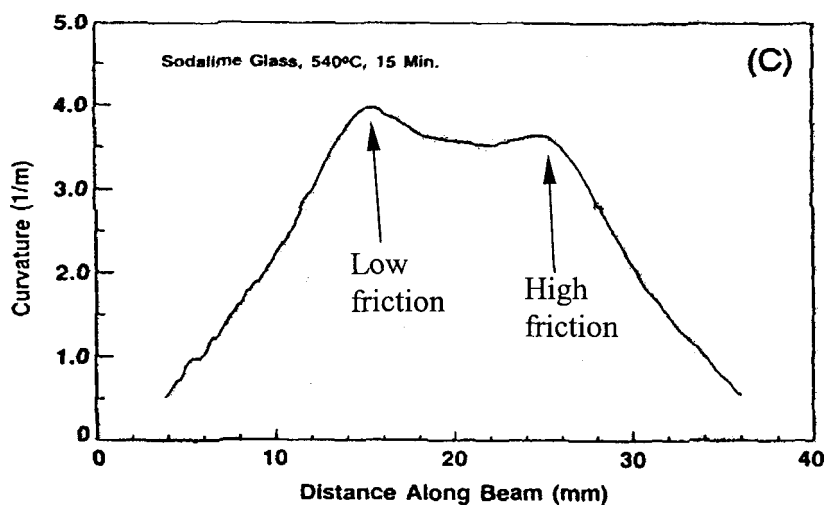


**Figure 5.11** Curvature curve of specimen (C) (Jakus et al., 1988)

### 5.2.5 Additional Observation for the Total Moment in the Beam Section

The stress ( $\sigma_{xx}$ ) distribution at the beam cross section in the mid span was plotted as a function of time (Figure 5.12). It showed the linear stress distribution as expected from creep exponent  $n = 1$ . The total bending moment in the section can be calculated as the summation of moments produced by stresses of elements in the cross section.

From simple beam theory, the bending moment applied to the beam cross section in the mid span must be constant as a function of time in the four-point bending creep test. However, one can notice from the plot that the total bending moment keeps decreasing as time goes. This is why the bending creep tests show that the displacement rate decreases with increase in test time even in the steady-state stage of creep. This is a very important observation of four-point bending creep test. It means that in a four-point bending creep test, steady-state condition will never be clearly discerned and a wise decision of researchers for quasi steady-state data is required.

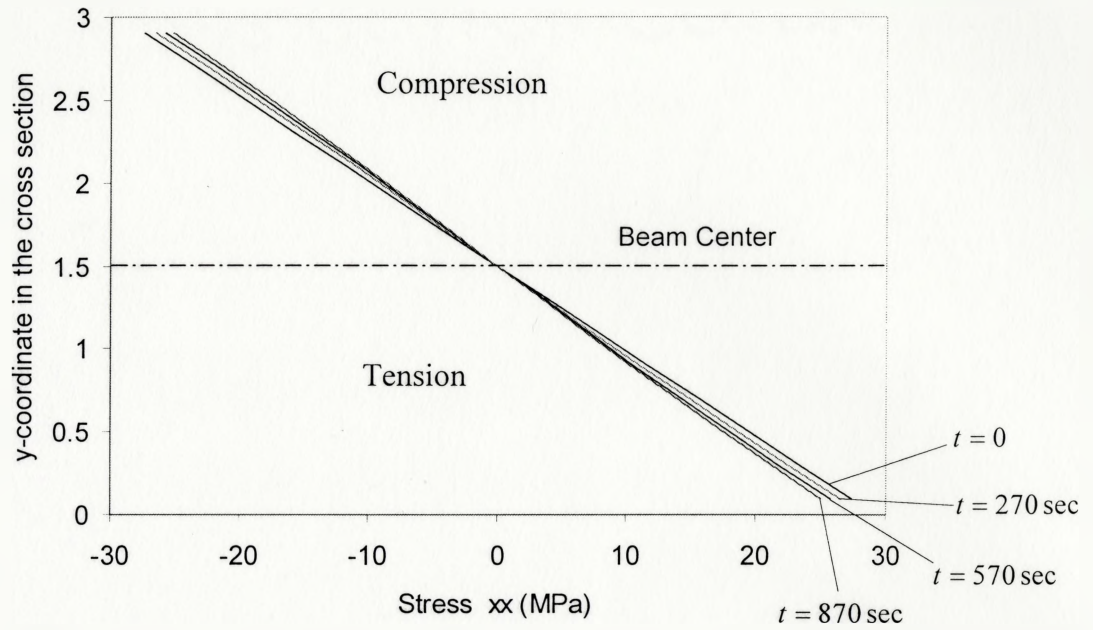
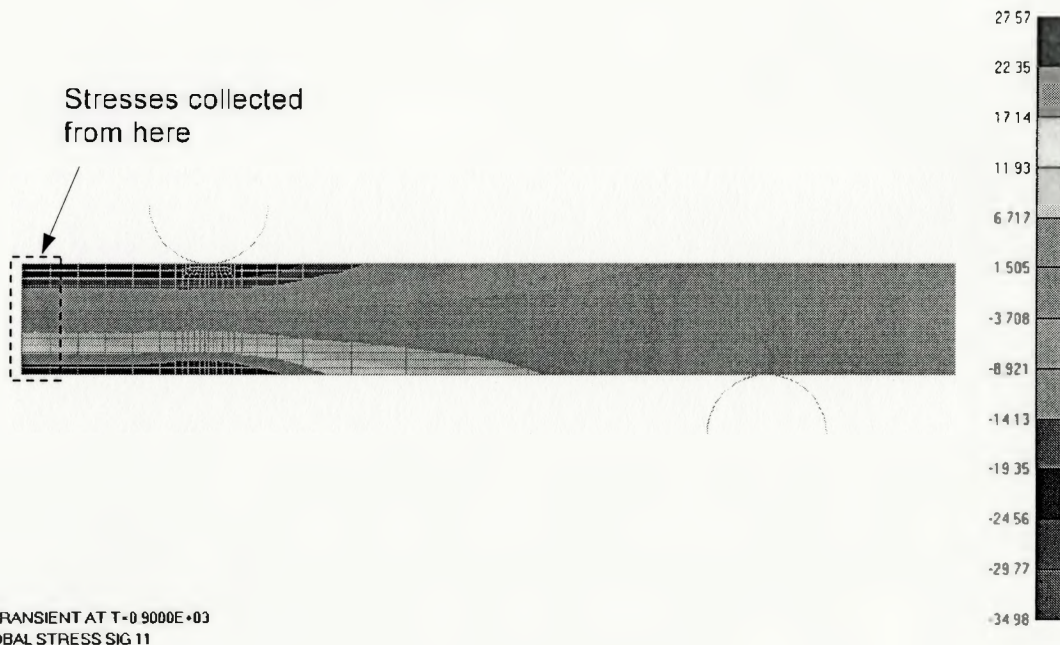


Figure 5.12 Stress distribution at beam cross section ( $n = 1$ )



Output Set: TRANSIENT AT T=0.9000E+03  
 Contour: GLOBAL STRESS SIG11

Figure 5.13 Stress ( $\sigma_{xx}$ ) distribution after 900 sec creep ( $n = 1$ )

### 5.2.6 Results and Discussion (Alumina)

A creep test of specimen (A) and (B), alumina, of Figure 5.4 was simulated with the following creep parameters which were assumed based on the creep parameters estimated for AD86 alumina in Chuang's paper (Chuang, 1986).

$$A_t = 0.885 \times 10^{-13} \text{ s}^{-1}, A_c = 4.25 \times 10^{-9} \text{ s}^{-1}, n_t = 4, n_c = 0.5; \text{ asymmetric creep}$$

The load 7.5 N was applied so that the outer fiber elastic stress of the specimen may become 30 MPa. The creep time step was 100 sec and 2,7000 sec (7.5 hr) creep was simulated. The curvature curve was obtained from the deflection data by the way explained previously. A number of simulations were repeated with different creep parameters to get the curvature curve which is similar to the curves given in Figure 5.4. The creep parameters which are given above were the most successful in matching the non-uniform curvature of crept specimen.

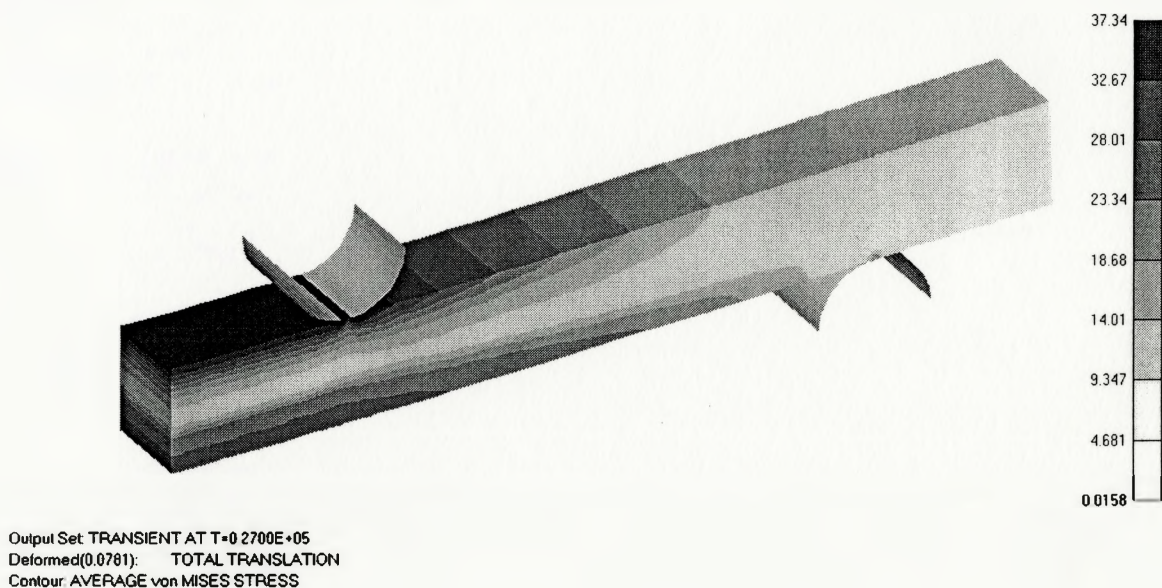
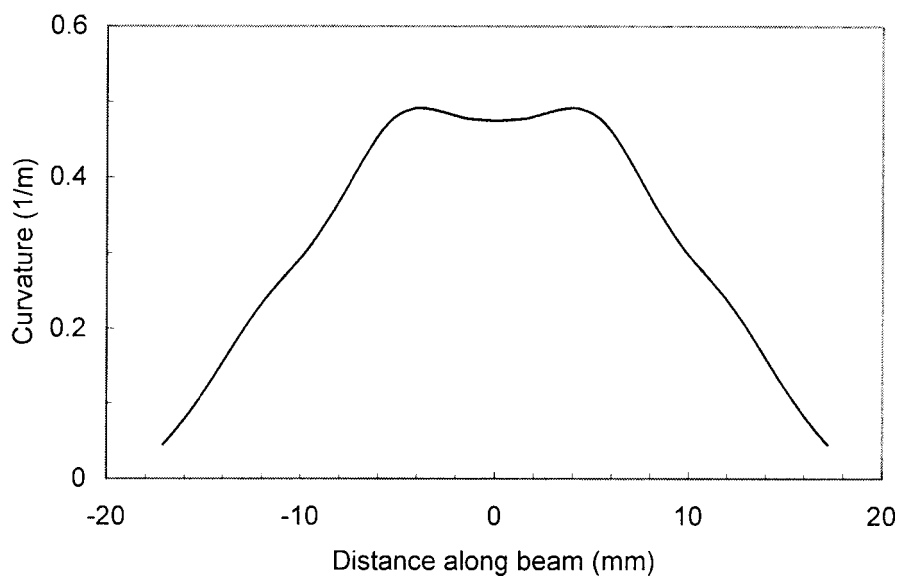
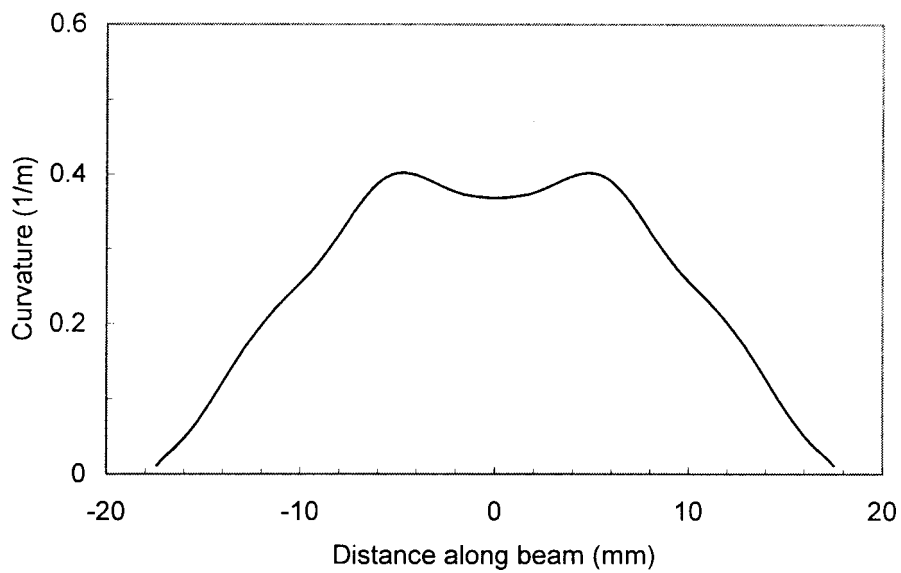


Figure 5.14 Von Mises stress distribution after 2,7000 sec



**Figure 5.15** Curvature curve from simulation without friction between loading roller and specimen ( $\mu = 0$ )



**Figure 5.16** Curvature curve from simulation with friction between loading roller and specimen ( $\mu = 1$ )

Figure 5.15 shows the curvature curve from the simulation where friction was not applied ( $\mu=0$ ) and Figure 5.16 shows the curvature curve from the simulation where friction was applied for loading rollers and specimen contact. The curvature curve from the simulation is only for a right half of the beam and for the better comparison the data flipped for the opposite half so that the whole curvature curve may be obtained.

Like curvature curves from the sodalime silica glass simulations, the curves from simulations didn't match quantitatively with the curves from the experiment because the input creep parameters were assumed. However, the general trend agreed well with the experimental curves. By comparing Figure 5.15 and Figure 5.16, one can notice that friction lowers the curvature at the loading point. Based on this observation, one can see from the curvature curve of specimen (A) of Figure 5.11 that the friction was higher at the left loading point.

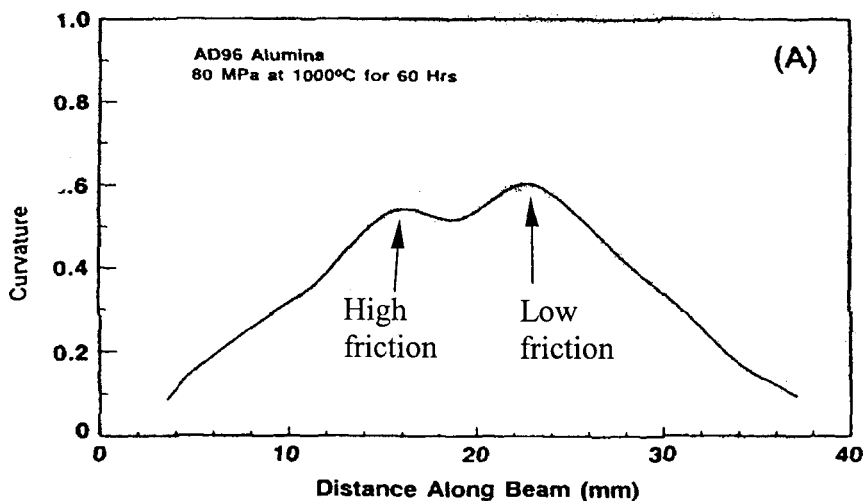


**Figure 5.17** Curvature curve of specimen (A) (Jakus et al., 1988)

From both simulations and the experiments of Jakus et al., the curvature enhancement in the vicinity of the loading points was observed. With symmetric creep parameters ( $n_t = n_c = 1, A_t = A_c$ ), the theoretical constant moment region and therefore constant curvature region in the mid-span were detected. However, with asymmetric creep parameters ( $n_t \neq n_c, A_t \neq A_c$ ) the curvature in the mid-span was non-linear, and a constant region was not evident in both experiments and simulations.

In view of the detailed simulations, the ability to extract creep parameters from bend tests needs further consideration. In particular, the methods to extract creep parameters from bend test data which are based on simple beam theory (constant moment in the mid-span and linearly diminishing moment at the outer-span) and the validity of these methods can be checked with finite element simulations.

### 5.3 Finite Element Study on Method of Hollenberg et al.

Hollenberg's method (Hollenberg et al., 1971) to extract creep parameters from four-point bending creep tests is based on simple beam theory. Here it is evaluated using finite element simulations of four-point bending creep test with given creep parameters ( $A, n$ ) at four different load levels. Symmetric creep parameters ( $A_t = A_c, n_t = n_c$ ) were used because the method of Hollenberg's et al. is only for symmetric creep cases.

#### 5.3.1 Simulation

The specimen size considered was 3 by 5 by 50 mm, the inner loading span was 10 mm, and the outer span was 40 mm. A total of 772 elements and 1,660 nodes were used with creep parameters  $A_t = A_c = 3.273 \times 10^{-12} \text{ s}^{-1}$ ,  $n_t = n_c = 2.2$ .

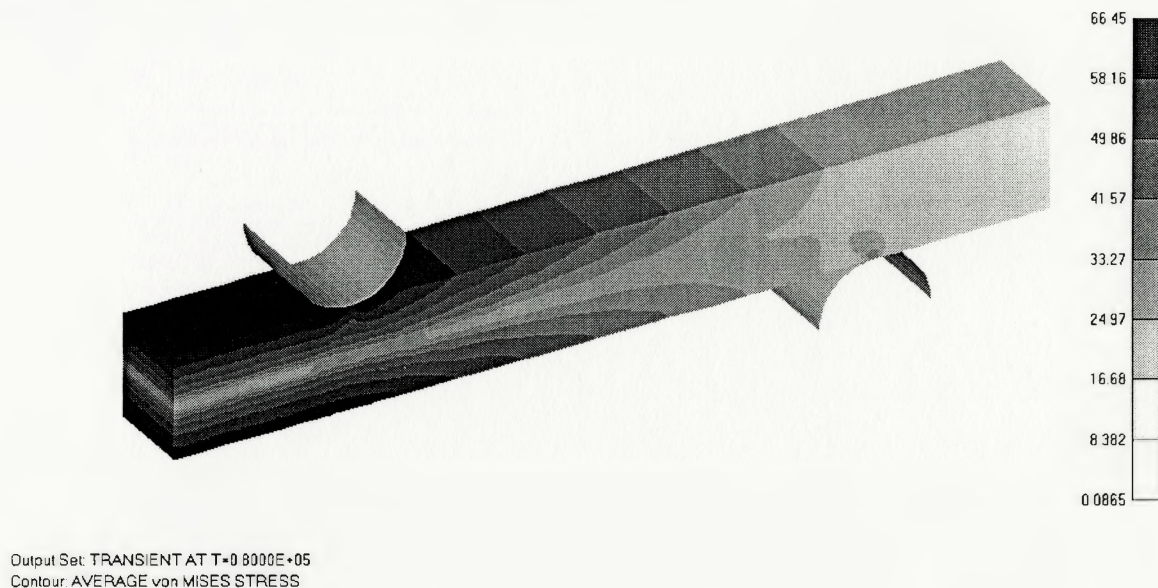


**Figure 5.18** Von Mises stress distribution after 22 hr creep (neutral axis is in the beam center due to symmetric creep)

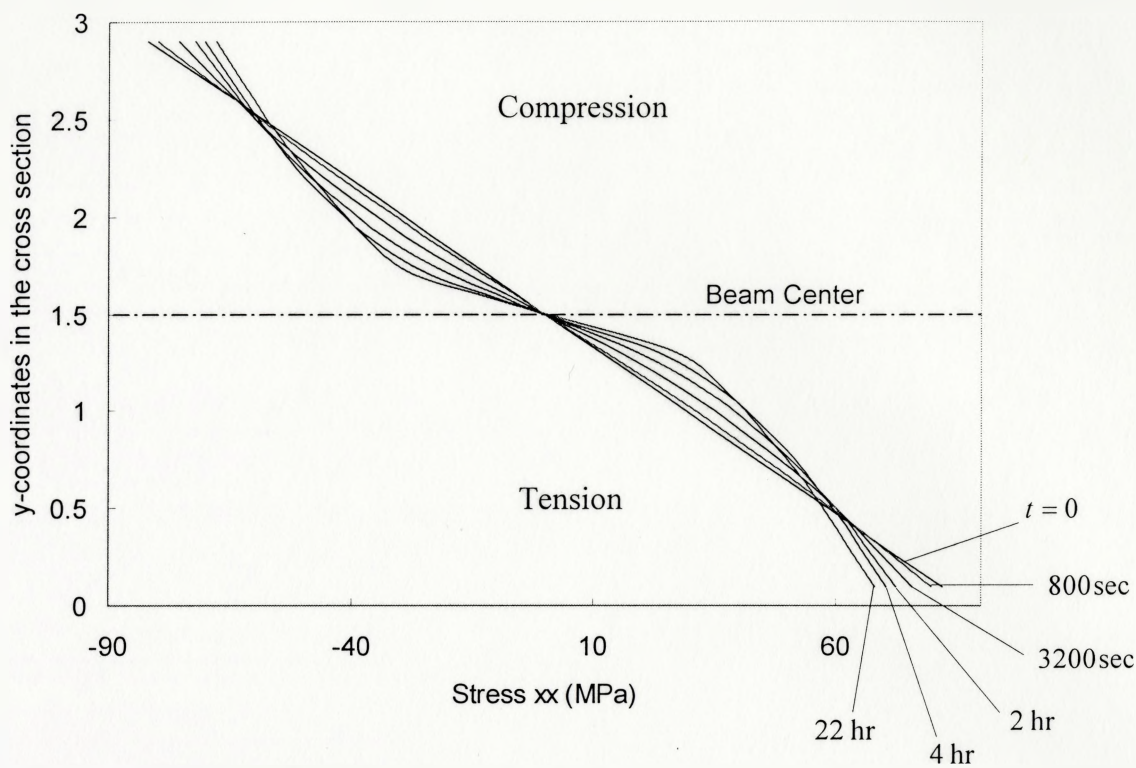
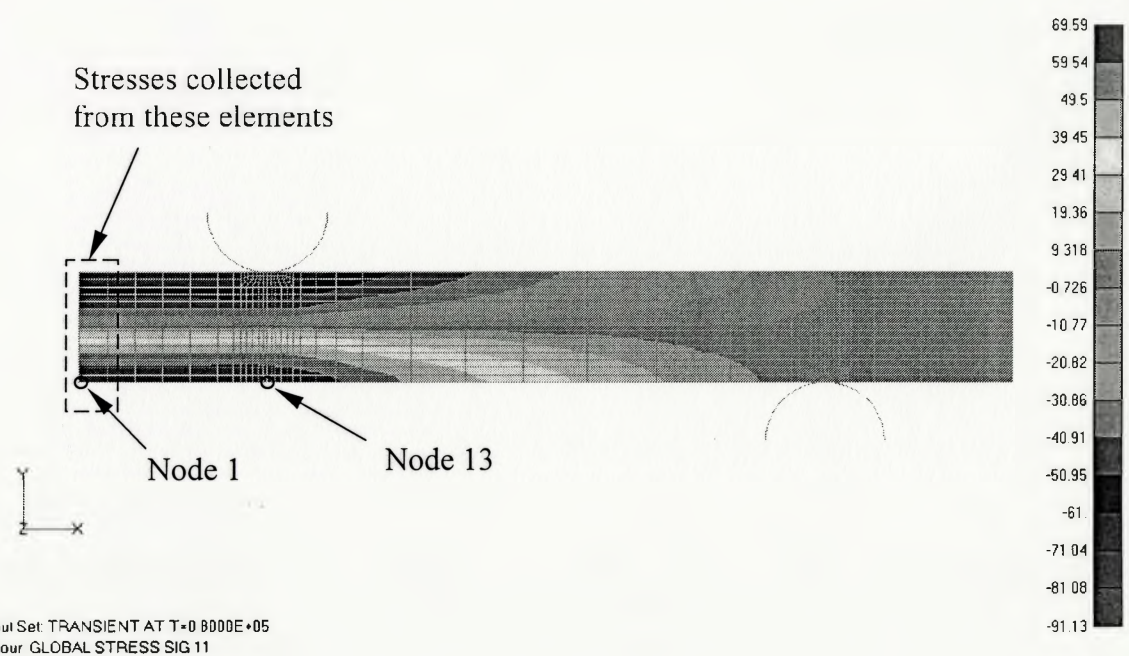


Figure 5.19 Stress ( $\sigma_{xx}$ ) distribution in the beam section as a function of time (linear elastic stress distribution becomes non-linear because of  $n > 1$ )



Output Set: TRANSIENT AT T=0.0000E+05  
 Contour: GLOBAL STRESS SIG 11

Figure 5.20 Stress ( $\sigma_{xx}$ ) distribution after 22hr creep ( $\sigma_c = 90$  MPa)

The load point displacement data were collected as a function of time from node 13 (Figure 5.20 and Figure 5.21) and load point displacement rates were calculated from the displacement data. (Figure 5.22) This process was repeated for simulations with four different load levels. The following table summarizes the results.

**Table 5.1** Load point displacement rate data from simulations

Applied Load P (N)	Outer-Fiber Elastic Stress $\sigma_e$ (MPa)	Steady-State Load Point Displacement Rate $\dot{y}_{node13}$ (mm/sec)
22.5	90	$2.71 \times 10^{-6}$
20.0	80	$2.08 \times 10^{-6}$
15.0	60	$1.03 \times 10^{-6}$
12.0	50	$6.57 \times 10^{-7}$

Displacement data were collected also from node 1 and specimen mid span displacements ( $y_R$ ) were calculated by  $y_R = y_{node1} - y_{node13}$ . (Figure 5.21)

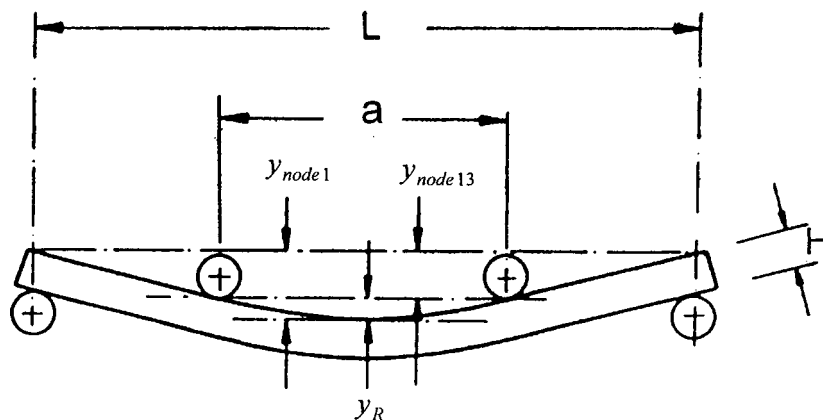


**Figure 5.21** Mid span displacement  $y_R$  (Fett et al., 1991)

Then curvature rates were calculated from the mid-span displacement rates by the following formula.

$$\dot{K} = \frac{8}{a^2} \dot{y}_R \quad (5-3)$$

where  $a$  is inner loading span (10 mm) and  $\dot{K}$  is curvature rate of the inner loading span. This process also was repeated for simulations with four different load levels. The following table summarizes the results.

**Table 5.2** Curvature rate data from simulations

Outer-Fiber Elastic Stress $\sigma_e$ (MPa)	Steady-State Mid Span Displacement Rate $\dot{y}_R$ (mm/sec)	Curvature Rate $\dot{K}$ ( $\text{mm}^{-1}\text{sec}^{-1}$ )
90	$2.75 \times 10^{-7}$	$2.20 \times 10^{-8}$
80	$2.10 \times 10^{-7}$	$1.68 \times 10^{-8}$
60	$1.05 \times 10^{-7}$	$8.40 \times 10^{-9}$
50	$6.67 \times 10^{-8}$	$5.34 \times 10^{-9}$

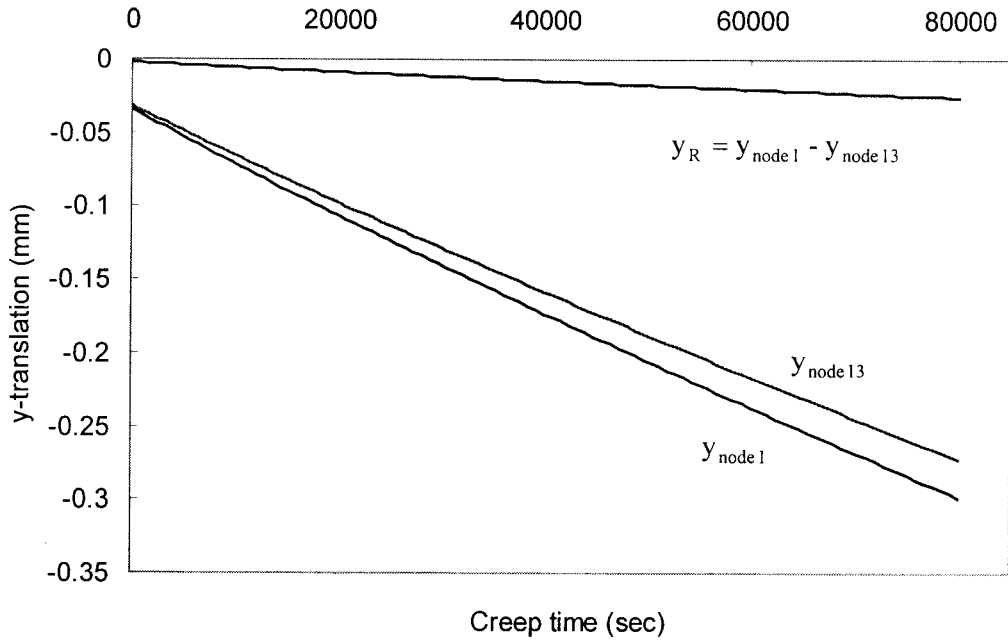


**Figure 5.22** Nodal displacement data from simulation ( $\sigma_e = 90$  MPa)

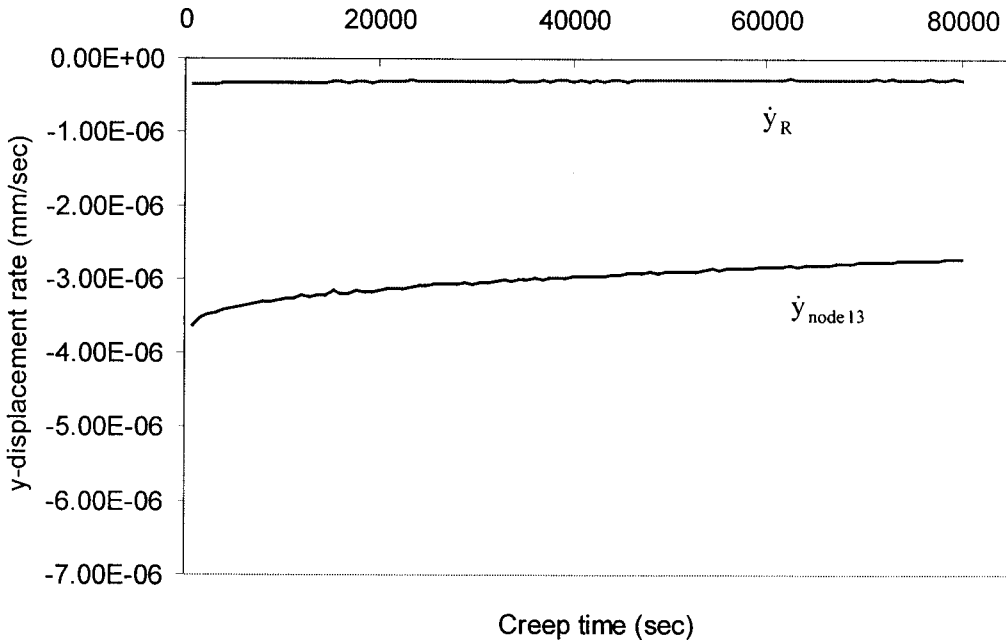


**Figure 5.23** Load-point displacement rate ( $\dot{y}_{\text{node 13}}$ ) and mid-span displacement rate ( $\dot{y}_R$ ) with  $\sigma_e = 90$  MPa

### 5.3.2 Estimation of Creep Parameters by the Method of Hollenberg et al.

As explained above in section 2.2, creep parameters can be estimated from bend creep test data by the method of Hollenberg et al. (Hollenberg et al., 1971) for the symmetric creep. In section 2.2, equations were derived for the curvature rate ( $\dot{K}$ ) and for the load-point displacement rate ( $\dot{y}_{node13}$ ). Therefore, creep parameters can be estimated from the curvature rate data and from the load-point displacement rate data. In practice researchers have preferred to measure the load-point displacement rate because it is much easier to measure than curvature rate. Fett et al. (1991) introduced the method to measure the curvature from bend specimen.

Previously, both the load-point displacement rate data (Table 5.1) and the curvature rate data (Table 5.2) were obtained from bending creep simulations. Using Equation (2-16), the creep parameters can be obtained by plotting the load-point displacement rate vs. applied elastic stress. From the plot in Figure 5.24, the creep exponent  $n = 2.42$  and the intercept  $C_2 = -23.7$  were obtained, and from  $C_2$  and Equation (2-16a) the pre-exponent  $A = 1.028 \times 10^{-12}$  was calculated. Using Equation (2-11), the creep parameters can be obtained also by plotting the curvature rate vs. applied elastic stress. The plot is shown in the below where  $n = 2.41$  and  $C_1 = -28.5$  and from  $C_1$  and Equation (2-11a) the pre-exponent  $A = 1.061 \times 10^{-12}$  was calculated.

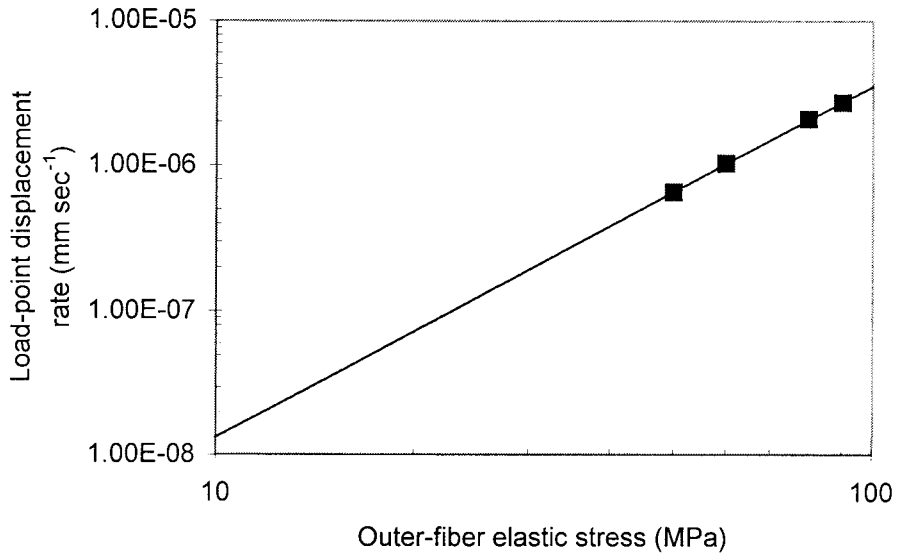


**Figure 5.24** Log-log plot of outer-fiber elastic stress vs. load-point displacement rate

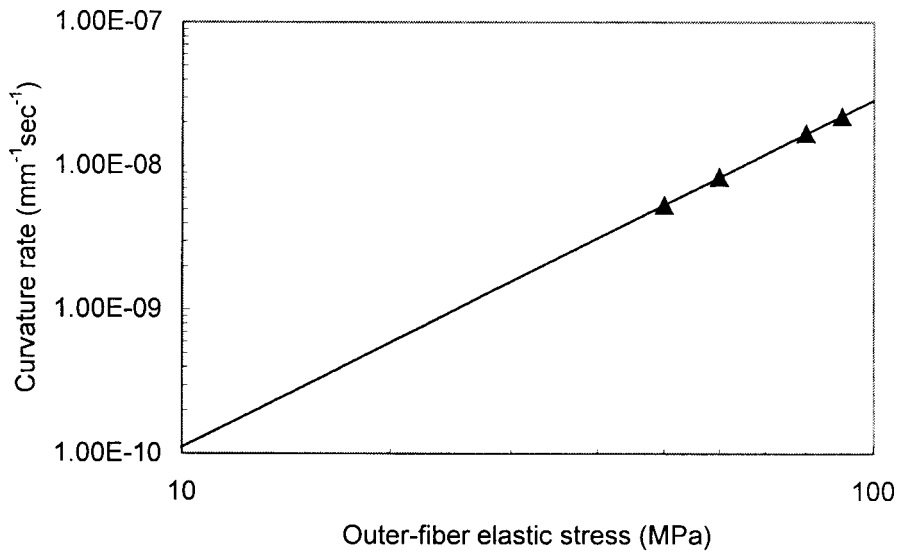


**Figure 5.25** Log-log plot of outer-fiber elastic stress vs. curvature rate

The simulation input creep parameters and the estimated creep parameters are summarized as follows.

**Table 5.3** Summary of results

Creep Parameters	Original Input	By Load-Point Displacement Rate	By Curvature Rate
$n$	2.2	2.42	2.41
$A$	$3.273 \times 10^{-12}$	$1.028 \times 10^{-12}$	$1.061 \times 10^{-12}$

### 5.3.3 Frictional Effect on Estimation of Creep Parameters

The above simulations were performed without friction between loading roller and specimen. To study the frictional effect on bending creep test, another set of simulations were performed with friction ( $\mu = 1$ ). The load point displacement rates were collected from simulations following the same procedures previously explained.

**Table 5.4** Load point displacement rate data from simulations (with friction)

Applied Load P (N)	Outer-Fiber Elastic Stress $\sigma_e$ (MPa)	Steady-State Load Point Displacement Rate $\dot{y}_{node13}$ (mm/sec)
22.5	90	$1.9 \times 10^{-7}$
20.0	80	$1.4 \times 10^{-7}$
15.0	60	$7.0 \times 10^{-8}$
12.0	50	$4.4 \times 10^{-8}$

The above data were plotted in log-log scale and the creep exponent  $n = 2.47$  and the intercept  $C_2 = -26.6$  were obtained. From  $C_2$  the pre-exponent  $A = 5.79 \times 10^{-14}$  was

calculated. The following table compares the creep parameters from simulations with and without frictions.

**Table 5.5** Frictional effect on estimation of creep parameters

Creep Parameters	Original Input	Simulation without Friction ( $\mu = 0$ )	Simulation with Friction ( $\mu = 1$ )
$n$	2.2	2.42	2.47
$A$	$3.273 \times 10^{-12}$	$1.028 \times 10^{-12}$	$5.79 \times 10^{-14}$

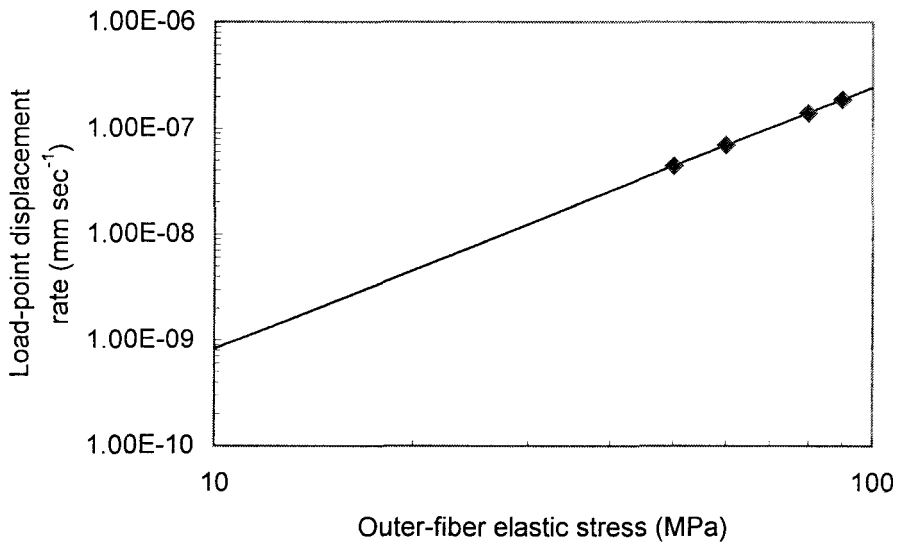


**Figure 5.26** Log-log plot of outer-fiber elastic stress vs. load-point displacement rate

#### 5.3.4 Discussion

By the method of Hollenberg et al., creep parameters were estimated from bend creep test simulation data. There were two ways to estimate creep parameters, one by measuring load-point displacement rate and the other by measuring curvature rate. The estimated creep parameters from displacement rates and from curvature rates didn't show much difference. The estimated creep exponent  $n$  was quite similar to original input  $n$  and the estimated pre-exponent  $A$  was about one third of original input  $A$  which is within allowable error range in ceramics creep tests. Therefore the common practice of measuring load-point displacement rate instead of curvature rate which is possible (Fett et al.) but difficult to measure is reasonable.

The frictions between loading rollers and specimen didn't affect the creep exponent  $n$  estimation much, but the pre-exponent  $A$  was seriously underestimated when friction applied in simulations (Table 5.5).

## 5.4 Finite Element Study on Chuang's Method

In section 5.3 above the method of Hollenberg et al. (1971) was tested using finite element simulations and the validity of this method was discussed. Only symmetric creep parameters were applied to the simulations in section 5.3 because the method of Hollenberg is valid for symmetric creep cases. In this section the generalized method (Chuang's method) to extract creep parameters from bend test data for asymmetric creep is evaluated using finite element simulations.

### 5.4.1 Simulation

The used specimen size was 3 by 4 by 50 mm and the inner loading span was 20 mm and the outer span was 40 mm. A quarter of the geometry was modeled for simulation (see section 5.1). A total of 809 elements and 1,756 nodes were used for finite element model.

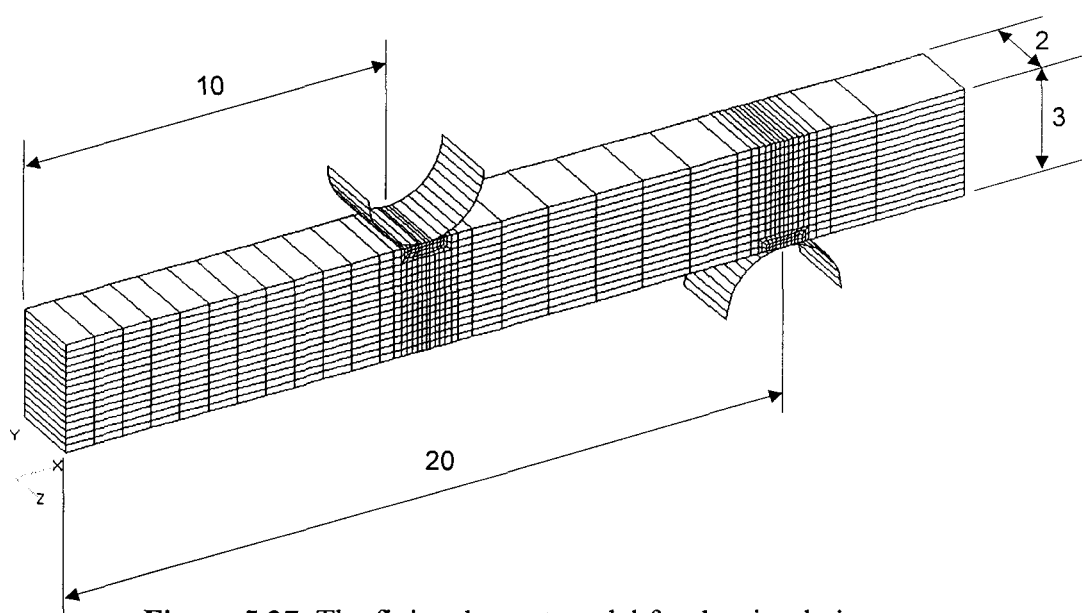


**Figure 5.27** The finite element model for the simulations

## 5.4 Finite Element Study on Chuang's Method

In section 5.3 above the method of Hollenberg et al. (1971) was tested using finite element simulations and the validity of this method was discussed. Only symmetric creep parameters were applied to the simulations in section 5.3 because the method of Hollenberg is valid for symmetric creep cases. In this section the generalized method (Chuang's method) to extract creep parameters from bend test data for asymmetric creep is evaluated using finite element simulations.

### 5.4.1 Simulation

The used specimen size was 3 by 4 by 50 mm and the inner loading span was 20 mm and the outer span was 40 mm. A quarter of the geometry was modeled for simulation (see section 5.1). A total of 809 elements and 1,756 nodes were used for finite element model.

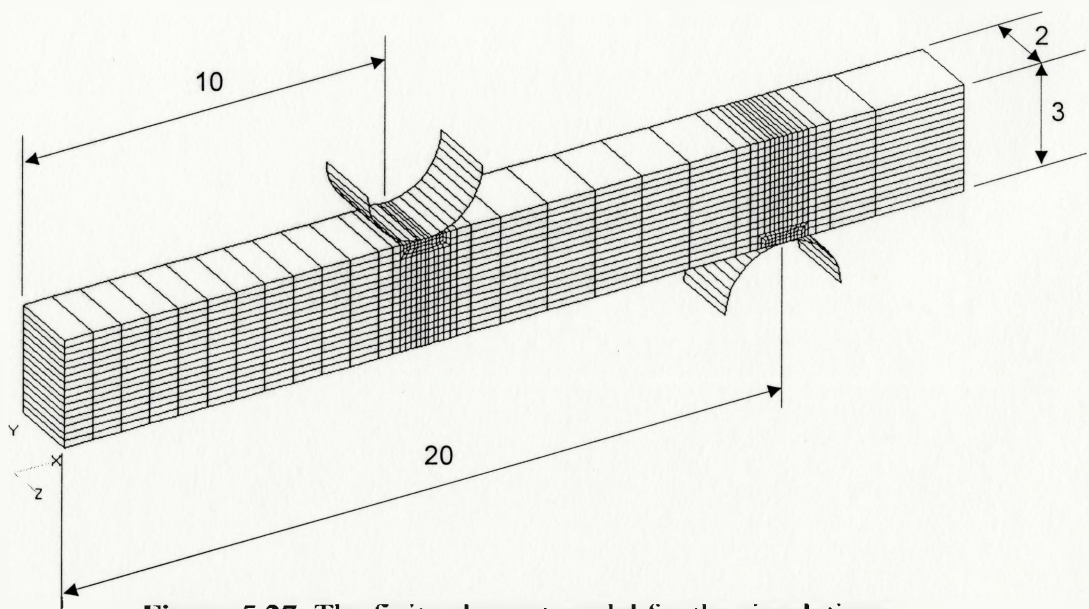


**Figure 5.27** The finite element model for the simulations

The asymmetric creep parameters used are summarized as follows.

$$A_t = 2.972 \times 10^{-17} \text{ s}^{-1}, \quad A_c = 5.555 \times 10^{-13} \text{ s}^{-1}, \quad n_t = 5.6, \quad n_c = 1.7$$

The parameters came from a paper of Ferber et al. (Ferber et al., 1990) They measured the above creep parameters from tensile and compressive tests of AD94 alumina. The modulus of elasticity,  $E = 300 \text{ GPa}$ , and Poisson's ratio,  $\nu = 0.25$ , which are typical for engineering ceramic materials were applied. The simulations were performed at five different load levels. ( $\sigma_x = 90, 80, 60, 50, 39 \text{ MPa}$ )

With the material model for asymmetric creep which was developed in section 3, four-point bending simulations of ceramics which have asymmetric creep properties were performed.

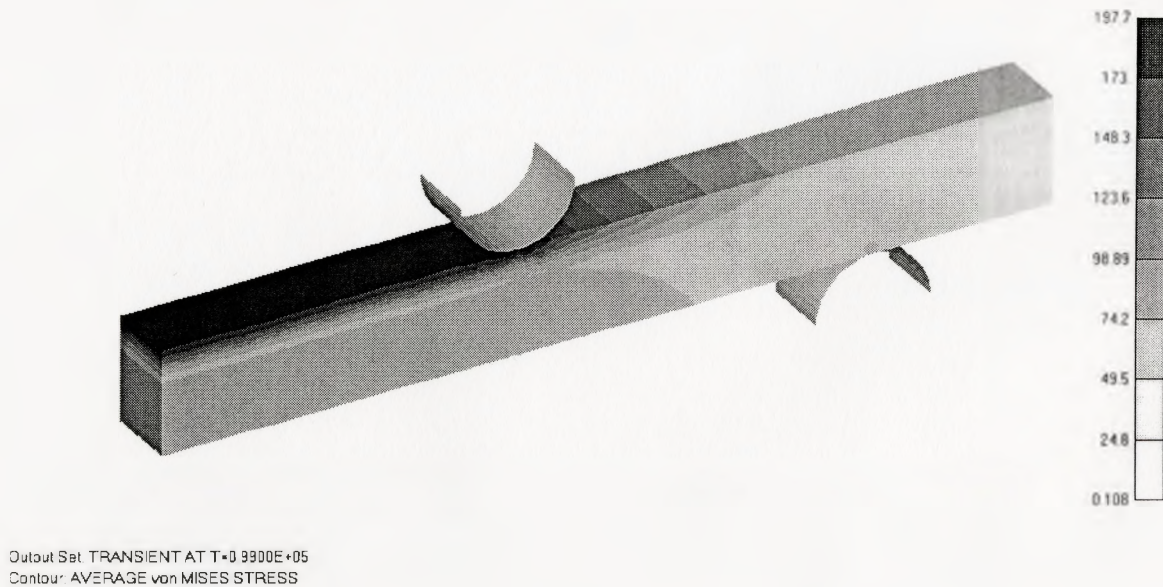


**Figure 5.28** Von Mises stress distribution after 27 hr creep with  $\sigma_x = 90 \text{ MPa}$  (neutral axis migrated toward compression surface)

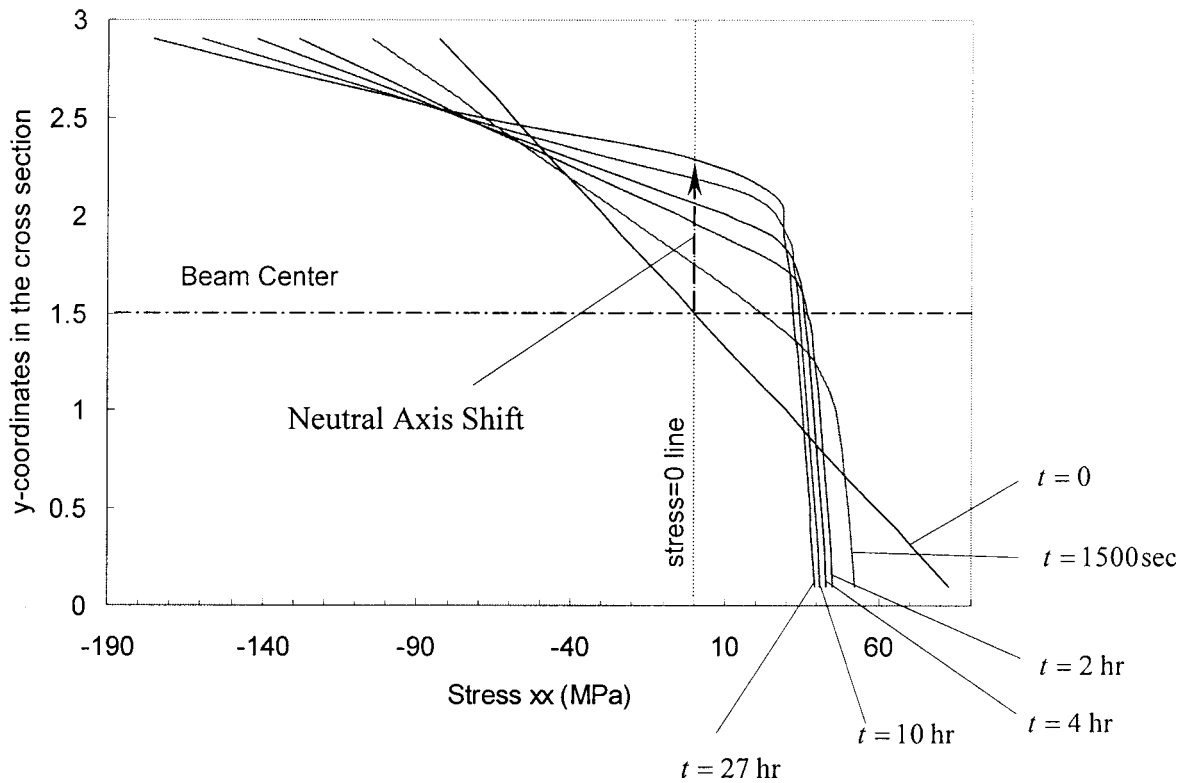


**Figure 5.29** Stress ( $\sigma_{xx}$ ) distribution in the beam section as a function of time (neutral axis migrates toward compression surface)

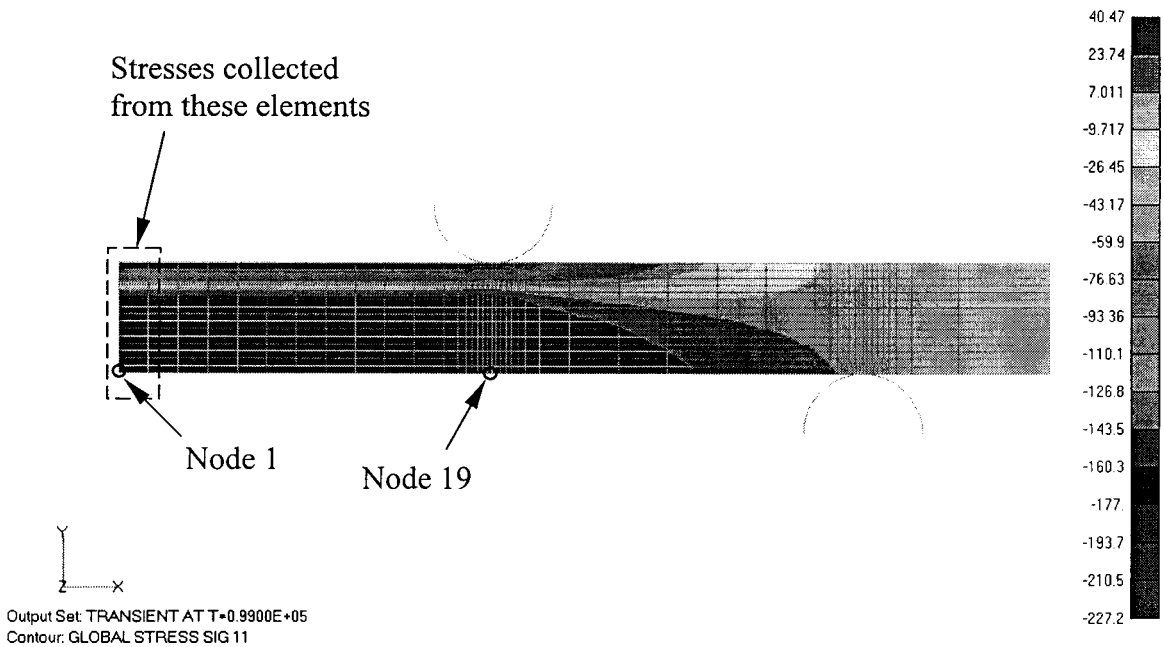


**Figure 5.30** Stress ( $\sigma_{xx}$ ) distribution after 27 hr creep ( $\sigma_e = 90$  MPa)

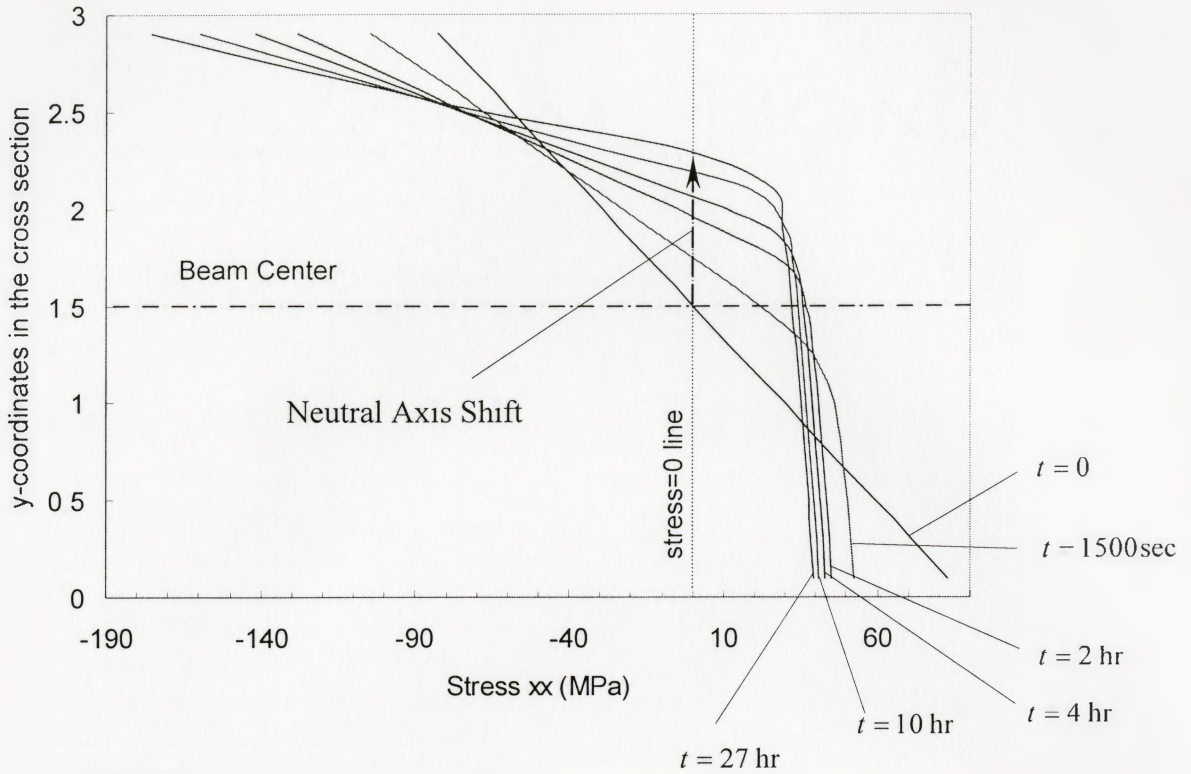


**Figure 5.29** Stress ( $\sigma_{xx}$ ) distribution in the beam section as a function of time (neutral axis migrates toward compression surface)

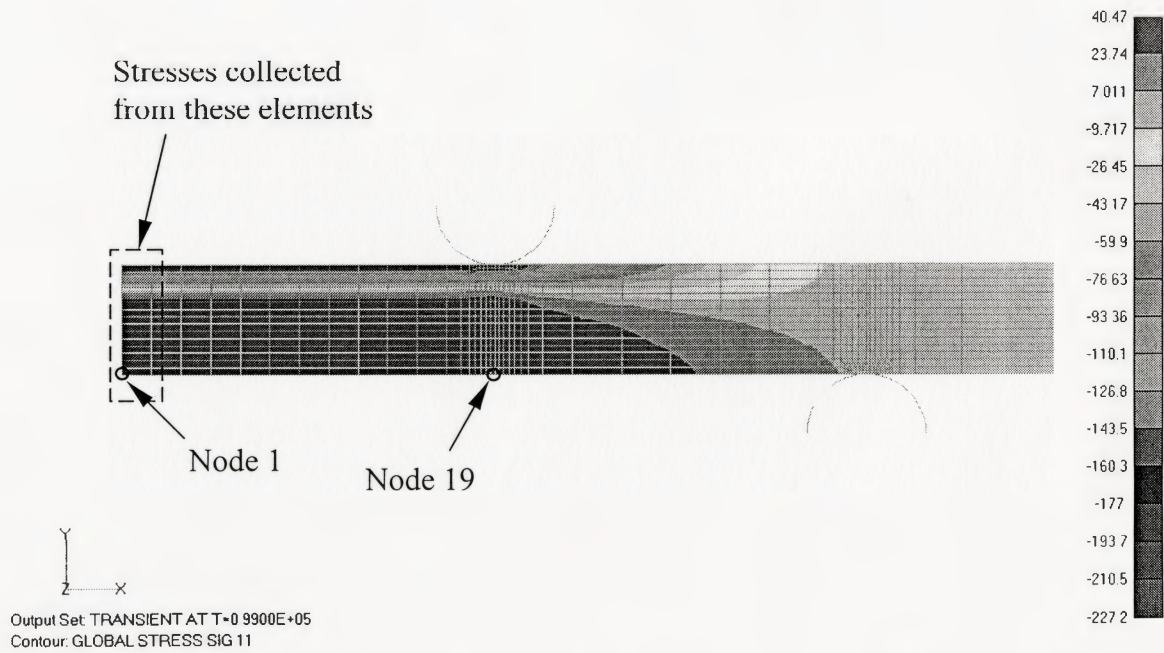


**Figure 5.30** Stress ( $\sigma_{xx}$ ) distribution after 27 hr creep ( $\sigma_r = 90$  MPa)

From each simulation, the nodal displacement data ( $y_{\text{node1}}$  and  $y_{\text{node19}}$ ) were collected for node 1 and node 19 and the mid-span displacement data ( $y_R = y_{\text{node1}} - y_{\text{node19}}$ ) were calculated as in Figure 5.31. Then, mid-span displacement rate ( $\dot{y}_R$ ) was calculated from the mid-span displacement data. A curve fitting scheme similar to the one in section 5.4.2 was used to remove the numerical noise from the displacement rate curve. The steady-state mid-span displacement rate obtained from the curve and then steady-state curvature rate was calculated from the Equation (5-3).

$$\dot{K} = \frac{8}{a^2} \dot{y}_R \quad (5-3)$$

where inner loading span  $a = 20$  mm and  $\dot{K}$  is the curvature rate of the mid-span. The following table shows the obtained steady-state curvature rate from the simulations at different load levels.

**Table 5.6** Curvature rate data from simulations

Outer-Fiber Elastic Stress $\sigma_e$ (MPa)	Steady-State Mid Span Displacement Rate $\dot{y}_R$ (mm/sec)	Curvature Rate $\dot{K}$ ( $\text{mm}^{-1}\text{sec}^{-1}$ )
90	$4.20 \times 10^{-7}$	$8.40 \times 10^{-9}$
80	$2.75 \times 10^{-7}$	$5.50 \times 10^{-9}$
60	$7.80 \times 10^{-8}$	$1.56 \times 10^{-9}$
50	$4.22 \times 10^{-8}$	$8.44 \times 10^{-10}$
39	$1.89 \times 10^{-8}$	$3.78 \times 10^{-10}$

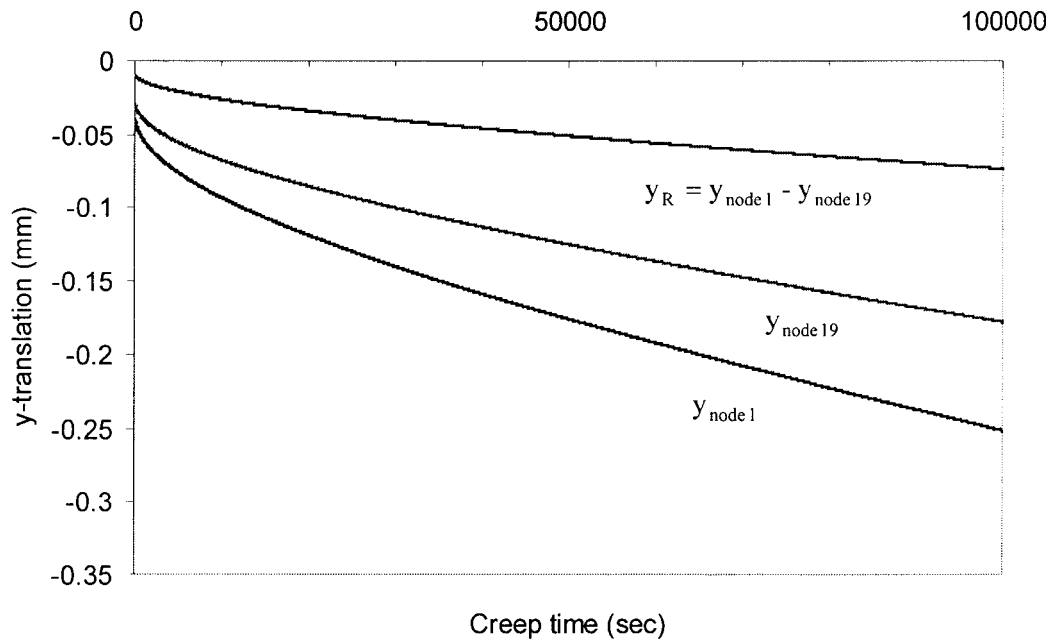


**Figure 5.31** Nodal displacement data from simulation ( $\sigma_e = 90$  MPa)

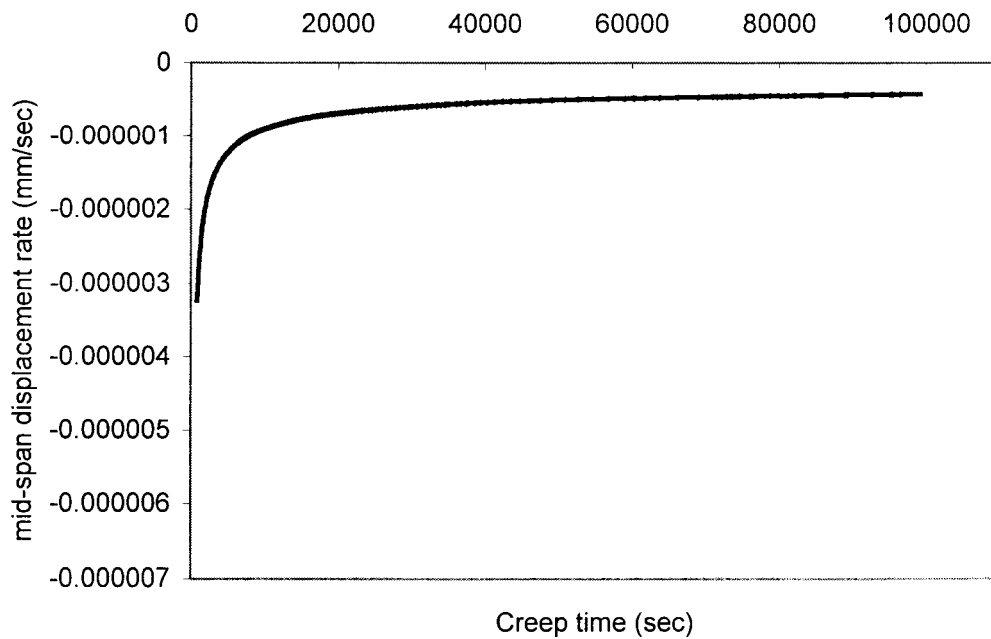


**Figure 5.32** Mid-span displacement rate ( $\dot{y}_R$ ) as a function of time ( $\sigma_e = 90$  MPa)

### 5.4.2 Evaluation of Chuang's Method

The Chuang's method to extract bend test data was already explained in section 2.3. The method has two highly non-linear coupled equations and a computer program to do numerical iterations and graphic solutions are required to estimate creep parameters. The two equations are shown below again.

$$R_1 [\dot{K}H / A_c]^{C_1} (H_c / H)^{C_2} + (H_c / H) = 1 \quad (2-20)$$

$$M / (BH^2) = [\dot{K}H / A_c]^{C_3} \left\{ [\dot{K}H / A_c]^{C_4} (R_3 / C_5) (1 - H_c / H)^{C_5} + (1 / C_6) (H_c / H)^{C_6} \right\} \quad (2-21)$$

In the current research, efforts were not given to compose the program and instead of following whole iteration steps of Chuang's method, curvature rates were estimated from the given creep parameters ( $A_t, A_c, n_t, n_c$ ) by using the above two equations. (see section 2.3.2 for details) And the estimated curvature rates were compared with the curvature rates obtained from simulations in section 5.6.1. The curvatures rates were calculated already by Chuang's equations (2-20) and (2-21) with the same creep parameters and specimen geometries. The result is given in the table 5.7.

The applied moments had been selected to match the same outer-fiber elastic stresses as in the simulations of section 5.4.1. Table 5.8 compares the curvature rates estimated from Chuang's equations and the curvature rates from simulations.

**Table 5.7** Curvature rate data from Chuang's equations

Specimen No.	Applied Moment $M$ (N mm)	Neutral Axis Location $H_c / H$	Curvature Rate $\dot{K}$
1	510	0.197	$8.00 \times 10^{-9}$
2	453	0.220	$4.88 \times 10^{-9}$
3	340	0.278	$1.57 \times 10^{-9}$
4	282	0.319	$7.82 \times 10^{-10}$
5	220	0.374	$3.28 \times 10^{-10}$

**Table 5.8** Curvature rates from Chuang's equations vs. simulations

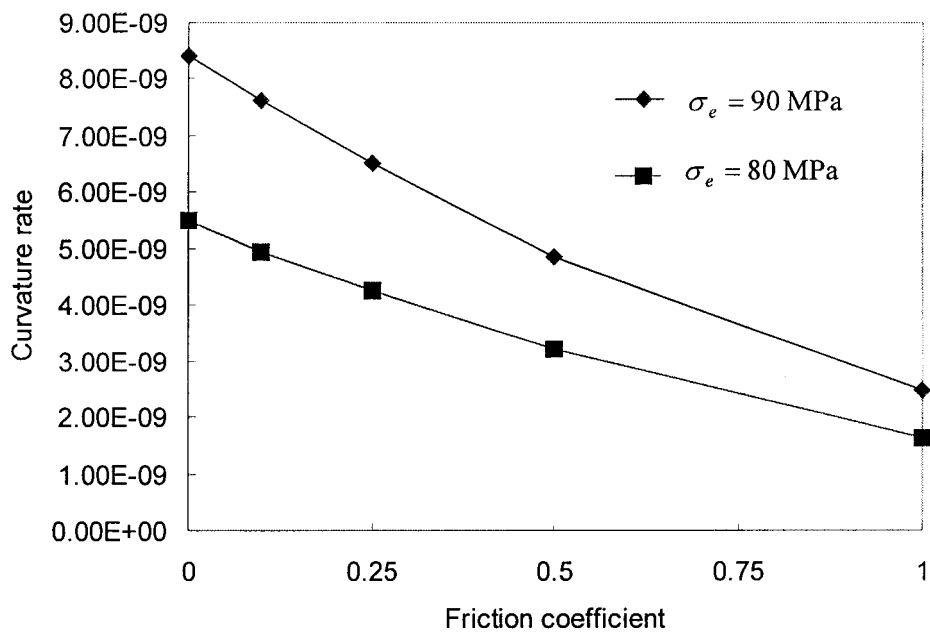
Outer-Fiber Elastic Stress $\sigma_e$ (MPa)	Curvature Rate (Chuang's Method) ( $\text{mm}^{-1}\text{sec}^{-1}$ )	Curvature Rate (Simulation) ( $\text{mm}^{-1}\text{sec}^{-1}$ )
90	$8.00 \times 10^{-9}$	$8.40 \times 10^{-9}$
80	$4.88 \times 10^{-9}$	$5.50 \times 10^{-9}$
60	$1.57 \times 10^{-9}$	$1.56 \times 10^{-9}$
50	$7.82 \times 10^{-9}$	$8.44 \times 10^{-10}$
39	$3.28 \times 10^{-10}$	$3.78 \times 10^{-10}$

### 5.4.3 Frictional Effect on Chuang's Method

Additional simulations were performed with various frictions between loading roller and specimen to see how friction affects the bending creep test and creep parameter estimation by Chuang's method. Table 5.9 and Figure 5.33 summarize the results.

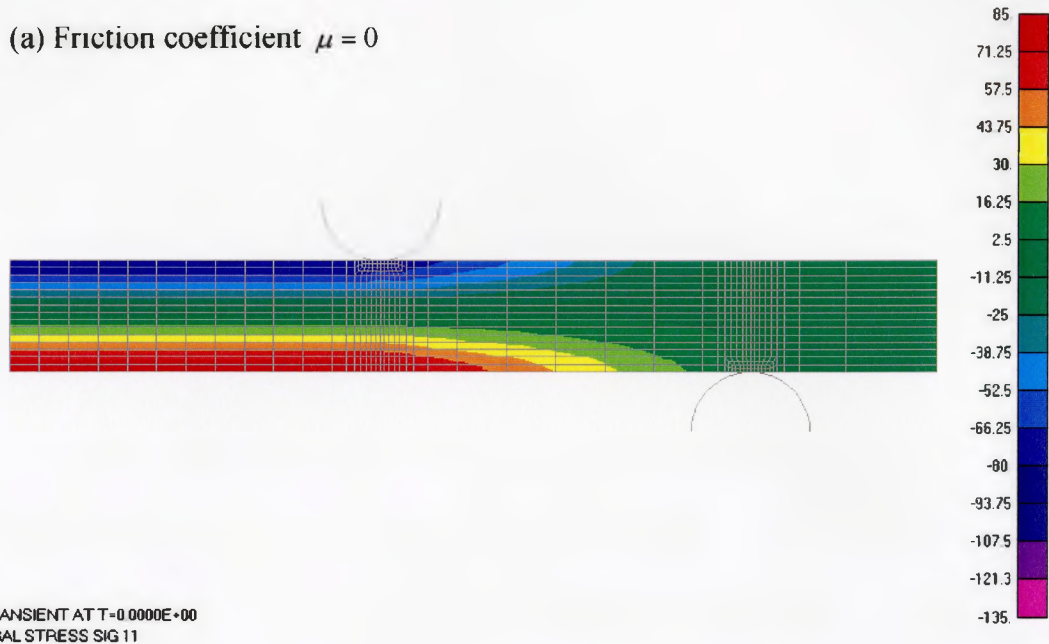
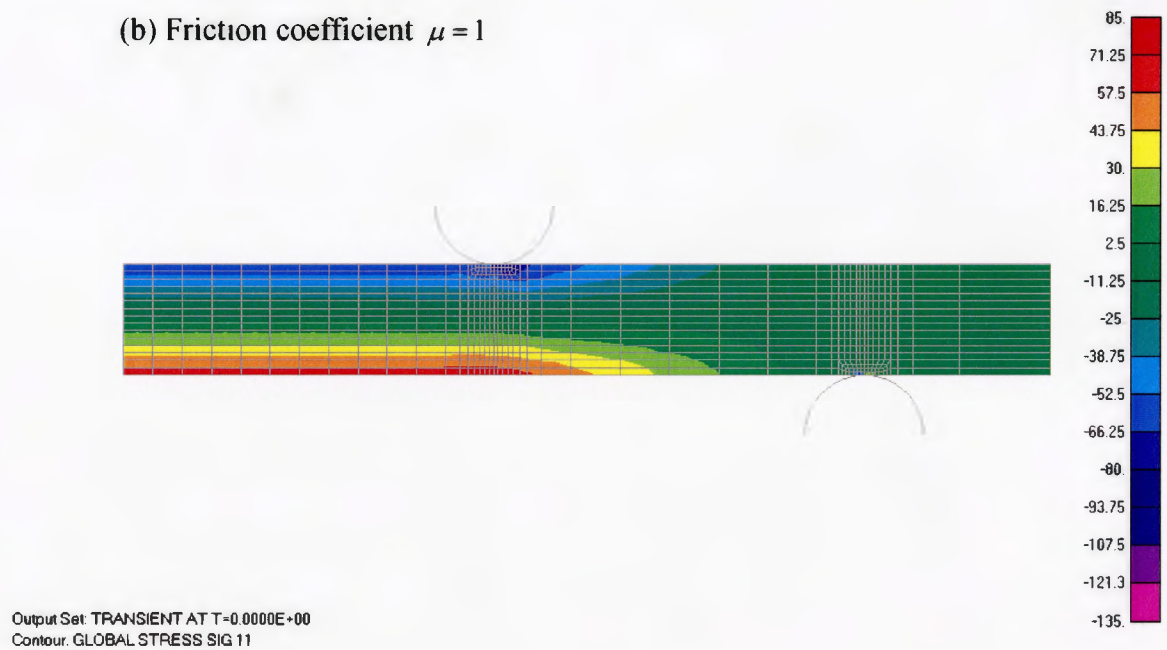
**Table 5.9** Curvature Rates from simulations depending on friction

$\sigma_e$ (Mpa)	$\dot{K}$ ( $\mu = 0$ )	$\dot{K}$ ( $\mu = 0.1$ )	$\dot{K}$ ( $\mu = 0.25$ )	$\dot{K}$ ( $\mu = 0.5$ )	$\dot{K}$ ( $\mu = 1$ )
90	$8.40 \times 10^{-9}$	$7.62 \times 10^{-9}$	$6.52 \times 10^{-9}$	$4.86 \times 10^{-9}$	$2.48 \times 10^{-9}$
80	$5.50 \times 10^{-9}$	$4.94 \times 10^{-9}$	$4.26 \times 10^{-9}$	$3.22 \times 10^{-9}$	$1.63 \times 10^{-9}$
60	$1.56 \times 10^{-9}$	-	$1.21 \times 10^{-9}$	$9.40 \times 10^{-10}$	$5.08 \times 10^{-10}$
50	$8.44 \times 10^{-10}$	-	$6.76 \times 10^{-10}$	$5.14 \times 10^{-10}$	$2.68 \times 10^{-10}$
39	$3.78 \times 10^{-10}$	-	$3.02 \times 10^{-10}$	$2.31 \times 10^{-10}$	$1.26 \times 10^{-10}$

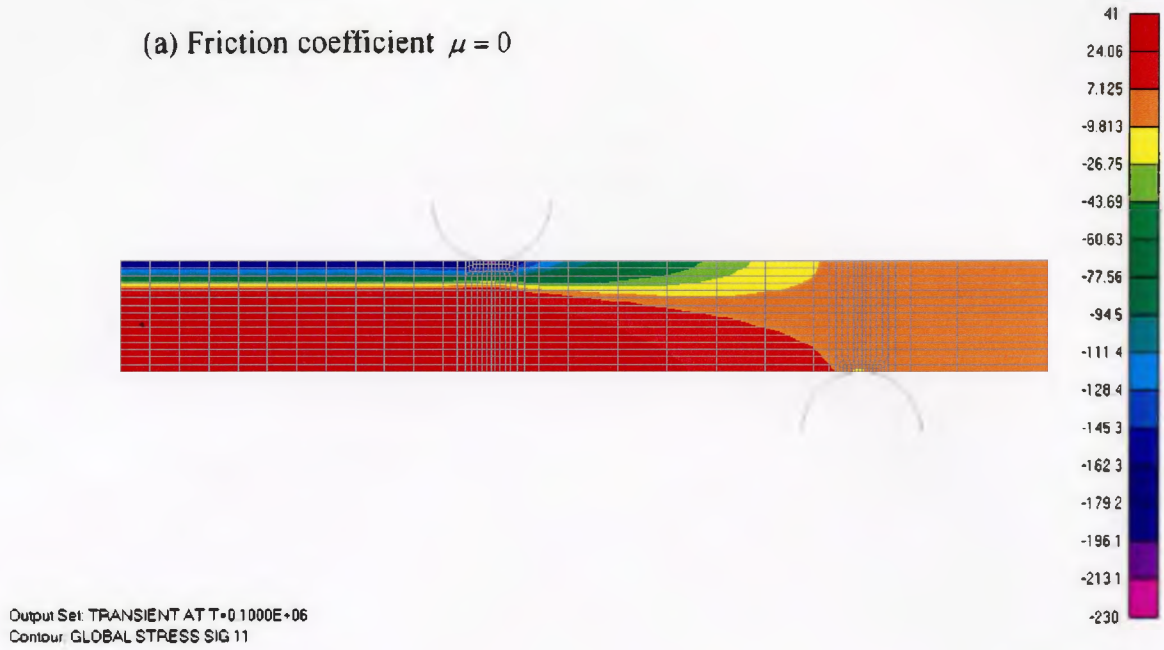
**Figure 5.33** Curvature rate changes depending on friction between loading roller and specimen

#### 5.4.4 Discussion

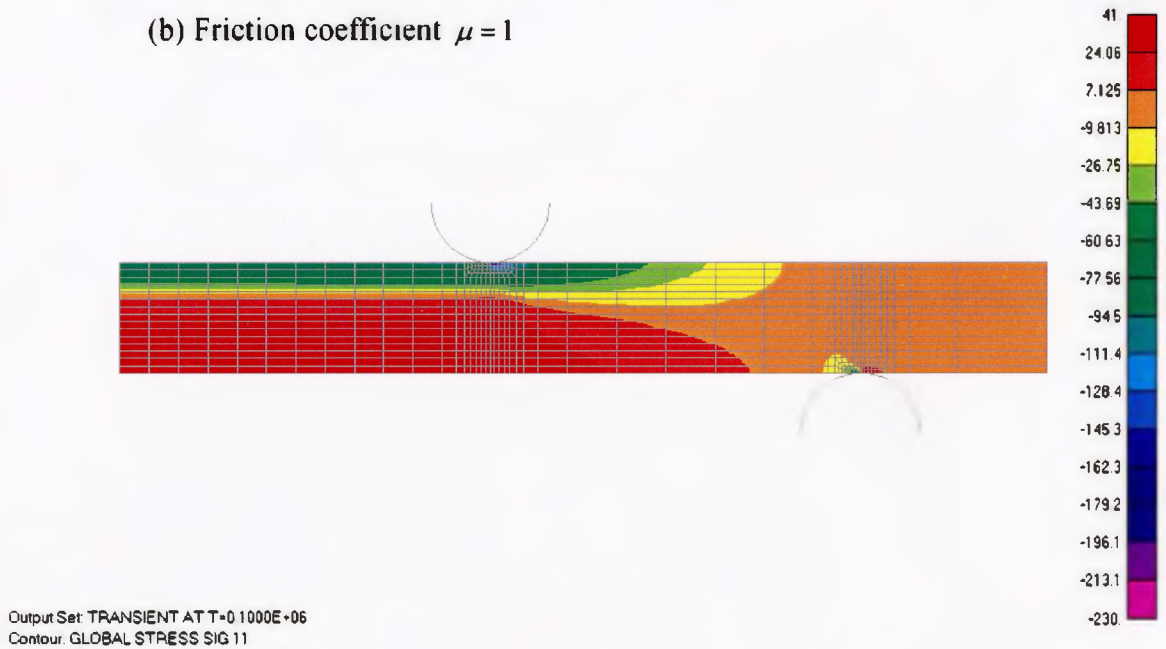
By comparing the curvature rates calculated by Chuang's equations with curvature rates from simulations, the Chuang's method was evaluated. The curvature rates from Chuang's equations were quite well matched with the curvature rates from simulations only when there was no friction between loading roller and specimen. Figures 5.34, 5.35 and 5.36 show how friction affects the stress distribution and creep deformation. One can see that friction lowered the outer-fiber elastic stresses and creep rates with friction defer from creep rates without friction. Therefore, the creep parameters estimated from bend creep data by Chuang's method are reliable only when the friction between loading rollers and specimen is maintained low enough during creep test.

(a) Friction coefficient  $\mu = 0$ (b) Friction coefficient  $\mu = 1$ **Figure 5.34** Stress ( $\sigma_x$ ) distribution at time = 0 ( $\sigma_e = 90$  MPa)

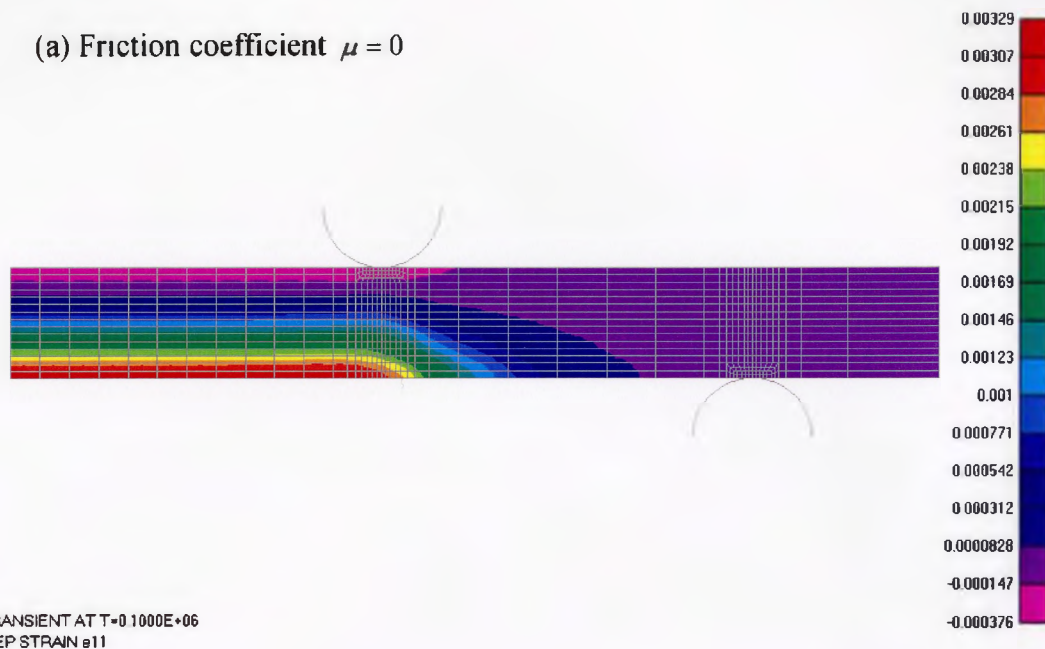
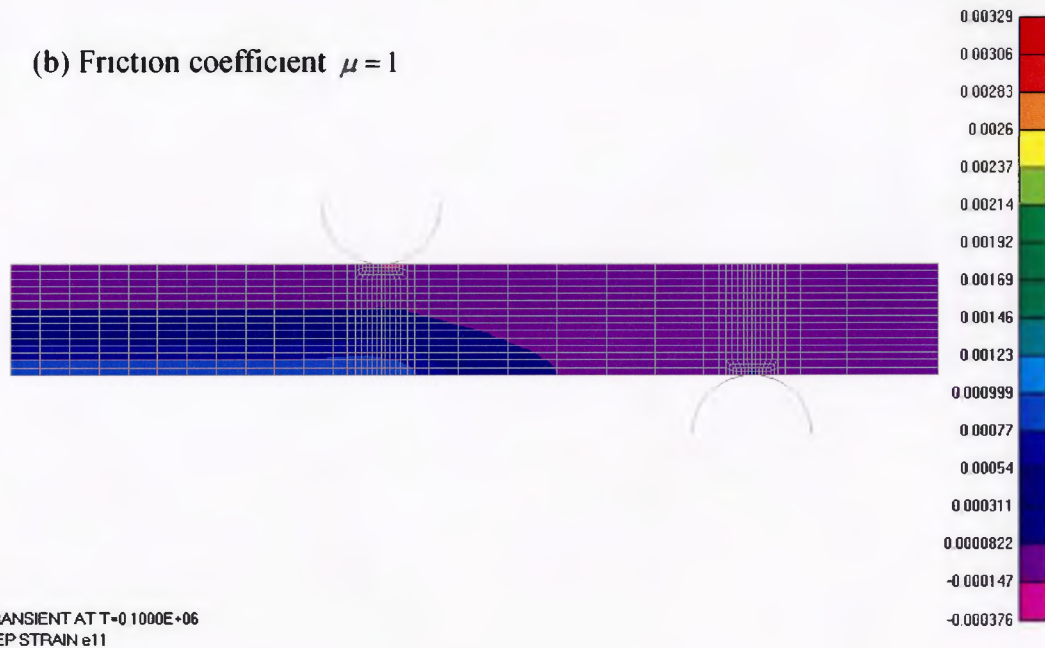
(a) Friction coefficient  $\mu = 0$



(b) Friction coefficient  $\mu = 1$



**Figure 5.35** Stress ( $\sigma_{xx}$ ) distribution at time = 27 hr ( $\sigma_e = 90$  MPa)

(a) Friction coefficient  $\mu = 0$ (b) Friction coefficient  $\mu = 1$ 

**Figure 5.36** Creep Strain ( $\epsilon_{xx}$ ) distribution at time = 27 hr  
( $\sigma_e = 90$  MPa)

## CHAPTER 6

### EVALUATION OF BEND TEST SET-UP

From finite element studies of four-point bending creep test in chapter 5, the methods of Hollenberg et al. (1971) and Chuang (1986) were verified that they can predict power-law creep parameters from bend test data when the friction between loading roller and specimen is low enough. In this chapter a bend creep test set-up is considered which might remove or reduce the friction between loading roller and specimen. Finite element simulations are performed to quantify the effect of friction.

#### 6.1 Recommended Bend Creep Test Set-up

The drawing in Figure 6.1 shows the frequently used four-point bending creep test set-up where the shallow grooves on the platens establish the positions of loading rollers.

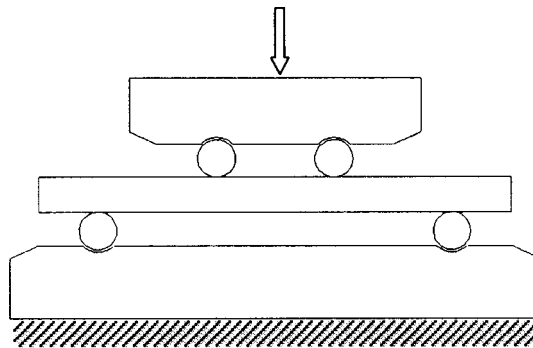


**Figure 6.1** Normal four-point bending creep test set-up

In this test set-up, the loading rollers may stick to the specimen and the platens during creep test because of high temperature, and the friction between loading roller and specimen is very high. Therefore the creep parameters measured from this set-up (especially pre-exponent  $A_t, A_c$ ) are inaccurate as proved in chapter 5 because of high friction.

Another creep test set-up which might remove the friction between loading roller and specimen is shown in Figure 6.2. ASTM C 1211 requires this test set-up to measure the ultimate strength of a advanced ceramics on the basis of researches of Hoagland et al. (1976) and Swank et al. (1990). Krause and Chuang (1991) showed that they used this set-up in creep test to get creep parameters from bend creep test data. In the creep test set-up shown in Figure 6.2, the loading rollers are expected to roll on the specimen and flat platens without applying significant friction forces on the specimen. The loading rollers are attached to platens temporarily with an organic cement which will melt away during creep testing. The vertical edges in the fixture facilitate accurate initial positioning of the rollers while not hindering rolling motions of rollers because they roll to opposite directions.

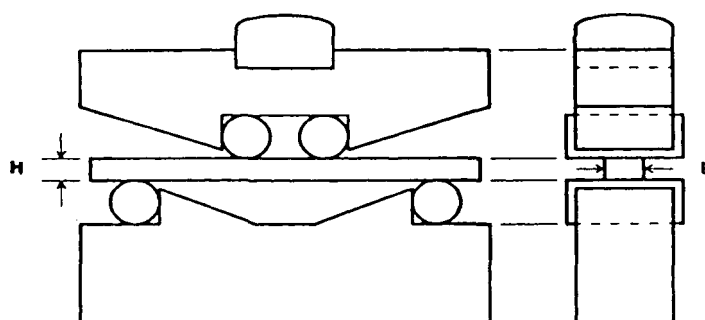


**Figure 6.2** Recommended four-point bending creep test set-up (Krause et al, 1991) (ASTM C 1211)

## 6.2 Simulation of the Recommended Bend Creep Test Set-up

The test set-up in ASTM C 1211 (Figure 6.2) was modeled with four contact surface sets as follows and simulation was performed with friction coefficient  $\mu = 1$  for them to depict the high friction condition during creep test. The rollers would roll between specimen and platens because of moment induced by friction forces.

The upper platen was modeled as rigid body using tied nodes, shell elements were used to model rollers and large thickness (16 mm) compared to element sizes was given to the shell elements so that the rollers behave like rigid body without significant elastic deformation.

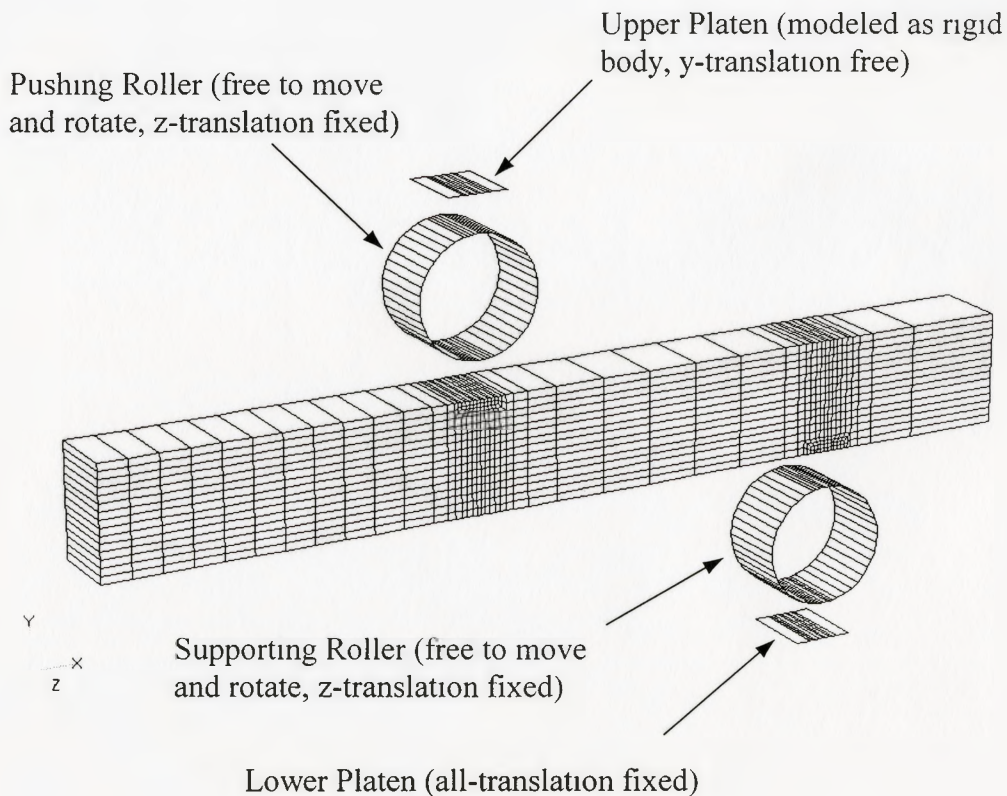
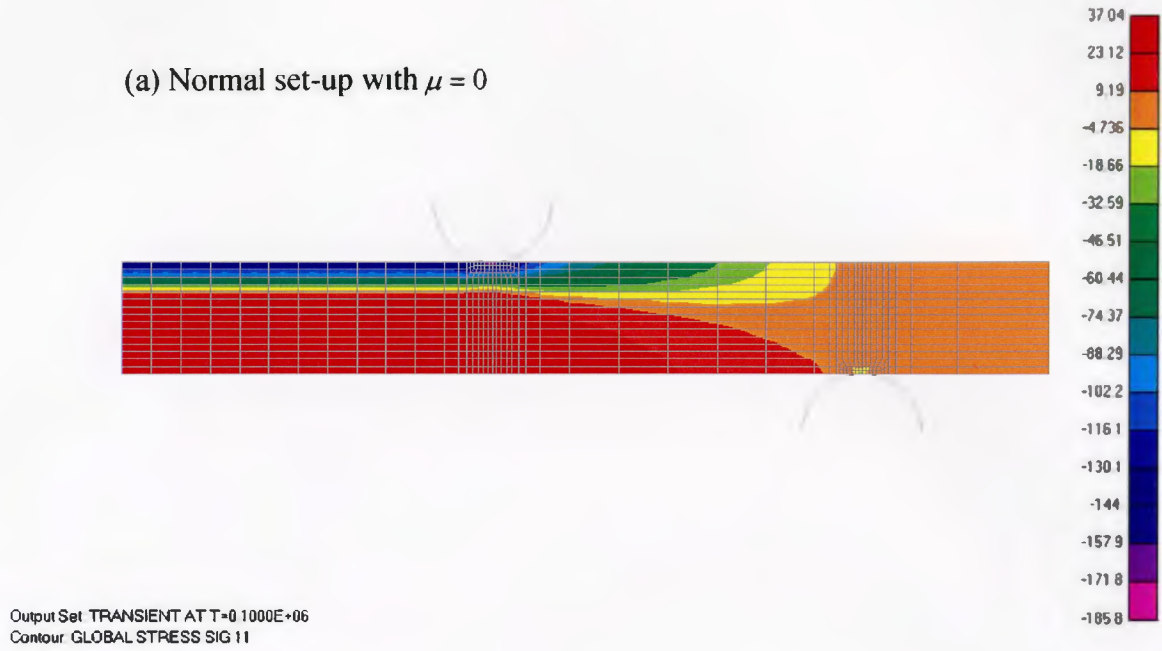
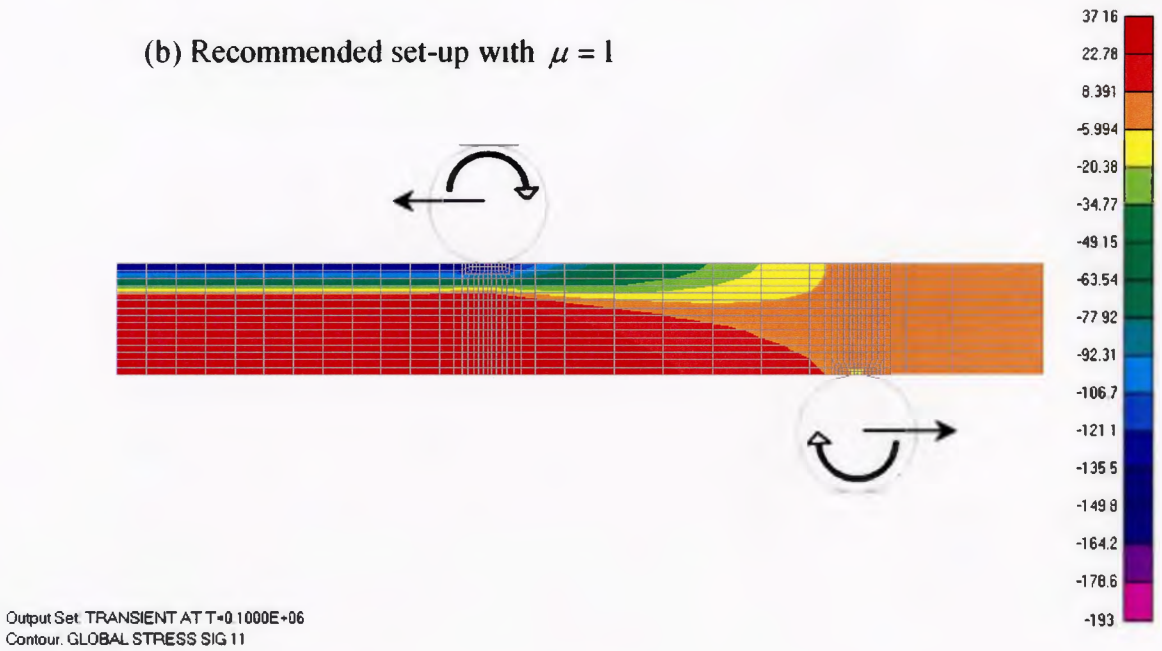


**Figure 6.3** Finite element model for recommended creep test set-up

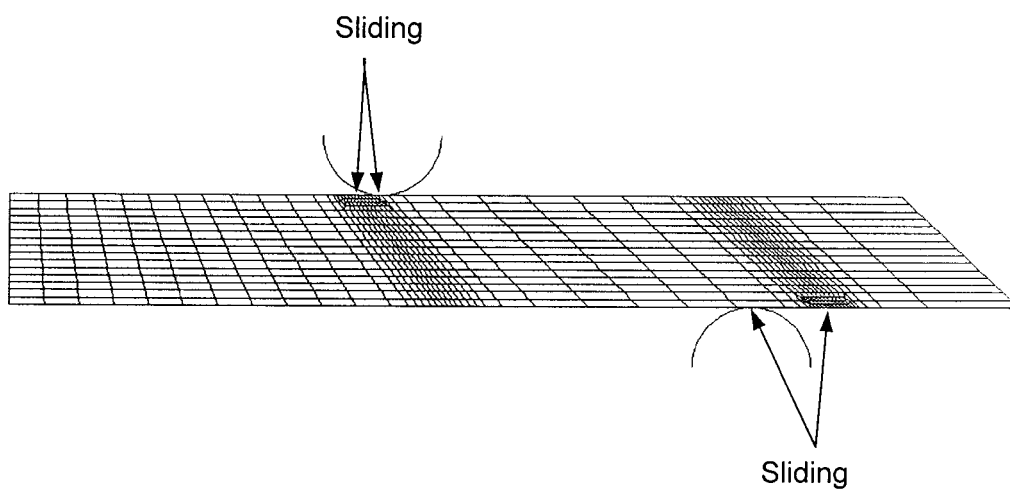
(a) Normal set-up with  $\mu = 0$



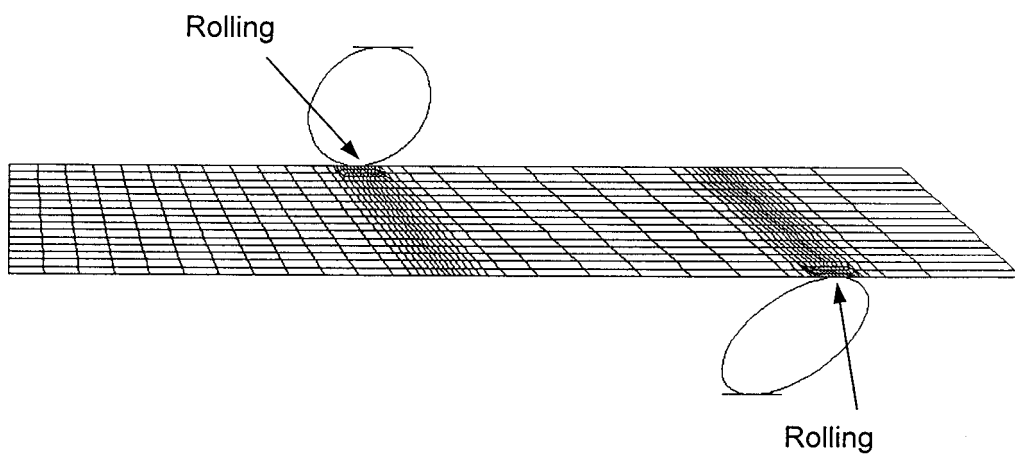
(b) Recommended set-up with  $\mu = 1$



**Figure 6.4** Stress ( $\sigma_x$ ) distribution at time = 27 hr ( $\sigma_y = 80$  MPa)  
(Legend was not scaled to show the max/min stress levels)

(a) Normal set-up with  $\mu = 0$ 

Output Set: TRANSIENT AT T=0.1000E+06  
 Deformed(0.0275): T1 TRANSLATION

(b) Recommended set-up with  $\mu = 1$ 

Output Set: TRANSIENT AT T=0.1000E+06  
 Deformed(0.0279): T1 TRANSLATION

**Figure 6.5** x-translation (exaggerated) visualized at time = 27 hr  
 ( $\sigma_e = 80$  MPa)

The same creep parameters and the first two loads used in simulations of section 5.4 were applied to the proof simulations. Then the curvature rates were obtained from the simulations as shown in Table 6.1.

Figure 6.4 compares the stress distribution between normal test set-up without friction and recommended test set-up with friction and shows how the recommended set-up removed the frictional effect on specimen. Figure 6.5 visualizes the x-translation of the model. In normal set-up without friction (Figure 6.5a), the contact points shifted due to the sliding between loading rollers and specimen. The rolling motion of rollers is apparent from the recommended set-up because the rollers rotated with initial contact points as rotation centers (Figure 6.5b). The rolling motion of rollers in simulation was quantified in Table 6.2. Rolling was bigger in supporting roller, which is discernable from Table 6.2 and Figure 6.5.

**Table 6.1** Curvature rates comparison between normal and recommended test set-up

$\sigma_e$	$\dot{K} (\mu = 0)$ (Simulation, Normal)	$\dot{K} (\mu = 1)$ (Simulation, Normal)	$\dot{K} (\mu = 1)$ (Simulation, Recommended)
90	$8.40 \times 10^{-9}$	$2.48 \times 10^{-9}$	$8.66 \times 10^{-9}$
80	$5.50 \times 10^{-9}$	$1.63 \times 10^{-9}$	$5.60 \times 10^{-9}$

**Table 6.2** Rolled angles of rollers at time=27 hr ( $\sigma_e = 90$ )

Total creep stain at outer-fiber in tension ( $\varepsilon_{11}$ )	Rotation (Upper roller, °)	Rotation (Bottom roller, °)
0.3 %	0.20	0.73

### 6.3 Discussion

The simulations showed that the bend test set-up in ASTM C 1211 effectively reduced the frictional effects between loading rollers and specimen in creep tests. The top rollers rolled on the upper platen toward the center and the bottom rollers rolled on the lower platen toward the outside because of the torque generated by contact friction forces. Due to this rolling, the distance between top roller and bottom increased and the bending moment increased. That is the reason why the curvature rates are slightly increased than the fixed roller simulation without friction. As one can see from Table 6.1, the effect of moment increase is minor. Therefore the bend test set-up in ASTM C 1211 was proved as a method to remove the frictional effects between loading rollers and specimen in bend creep tests.

## CHAPTER 7

### CONCLUSIONS AND RECOMMENDATIONS

#### 7.1 Conclusions

In this research, four-point bending creep test and methods to extract power-law creep parameters from bend test data were studied with finite element analysis. A material model for asymmetric creep behaviors of ceramics was developed and implemented in the non-linear finite element code H3DMAP. Ceramics C-ring compression creep test simulation was performed with asymmetric creep material model and benchmarking comparison with experimental data and simulation data proved its validity.

Jakus and Wiederhorn's observation of non-linear curvature distribution in the mid-span of four-point bend specimen was also proved in the simulations and it was shown from simulations that the non-linear curvature distribution is due to the asymmetric creep properties. The enhancement of curvature in the vicinity of loading points was observed from both symmetric and asymmetric creep simulations, whereas a constant curvature region was observed from symmetric creep simulations. Also, from simulations with symmetric creep ( $n=1$ ) where the stress distribution is linear at the specimen section during creep process, the total bending moment decrease was observed. This means that in four-point bending tests, the total bending moment keeps decreasing

as deformation goes and a wise decision of researchers for a quasi steady-state data is required in the creep tests.

The methods of Hollenberg et al. (1971) and Chuang (1986) were evaluated by comparison with simulation results. When friction between loading rollers and specimen was not applied in the simulations, both methods well predicted creep parameters from bend creep simulation data. But, when friction is high as in the real creep test, the pre-exponent ( $A$ ) was highly underestimated. Prediction of stress exponent ( $n$ ) was not affected much by friction. Measuring load-point displacement rates did not show much difference in creep parameter prediction than measuring curvature rates which is more difficult in real experiments.

The bend test set-up in ASTM C 1211 was recommended as a method to effectively reduce the friction between loading rollers and specimen in bend creep tests. Proof simulation showed that the test set-up in ASTM C 1211 effectively removed the frictional effect of normal creep test set-up.

Bending creep tests will never replace the uniaxial creep tests because of its apparent limitations such as assuming power-law creep law, but in spite of the doubts about four-point bending creep tests to get creep parameters of engineering ceramics, researchers are still performing bending creep tests at least to get reference data. From this research, the limitations and abilities of four-point bending creep tests and methods to predict creep parameters are more clearly understood. Errors and uncertainties are now more quantifiable so that researchers who are referring to four-point bending creep tests can be more confident in their results.

## 7.2 Recommendations for Future Work

In section 5.2 it was found that the non-uniform curvature in the mid-span of crept ceramics specimen is due to the asymmetric creep properties of ceramics material. It is evident that even with asymmetric creep properties, the shape of non-uniform curvature curve in the mid-span changes depending on the creep parameters ( $A_t, A_c, n_t, n_c$ ). For example, in the curvature curves of Figure 1.1 the maximum curvature enhancement locations are different. In Figure 1.1(a) the peaks moved inward from the inner loading locations but in Figure 1.1(b) the peaks are on the inner loading locations. This observation means that there is a possibility to be able to expect general tendency of creep parameters from the shape of curvature curves of crept bend specimen. Therefore finding the relationship between the shape of crept bend specimen and creep parameters is recommended for the further research.

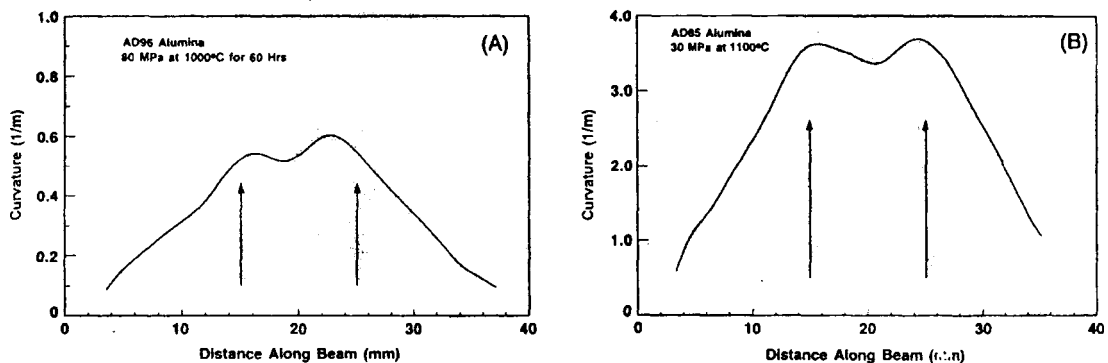


**Figure 1.1** Curvature as a function of distance along the bend bar (Jakus et al, 1988)

Wang et al. (1997) studied the optimum design of tensile creep specimen using a finite element method. They included the contact effects between pin and pinhole in the simulations, but symmetric creep properties were applied for the ease of computations. From the simulations they concluded that “creep symmetry seems to give rise to delayed head failure and creep asymmetry may play a beneficial role in preventing delayed head failure of the tensile creep specimens” (Wang et al., 1997). They suggested future research for the proof of this contention. In the research of this thesis, asymmetric creep material model was developed and successfully applied to four-point bending creep simulations where asymmetric creep and contact conditions were considered together. Therefore the tensile creep test simulations with asymmetric creep and contact are possible now and further research is recommended for the proof of the aforementioned contention that tensile specimens with asymmetry creep properties are more resistant to delayed head failure.

## REFERENCES

ASTM Standard C1211, 1988, "Standard Test Method for Flexural Strength of Advanced Ceramics at Elevated Temperatures," American Society for Testing and Materials, Philadelphia

Bailey, R. W., 1929, "Creep of Steel Under Simple and compound Stresses and the Use of High Initial Temperature in Steam Power Plants," Transactions, Tokyo Sectional Meeting of the World Power Conference, Tokyo, pp. 1089

Bathe, K.-J., 1982, "Finite Element Procedures in Engineering Analysis," Prentice-Hall Inc., Englewood Cliffs, New Jersey

Chen, C.-F., and T.-J. Chuang, 1990, "Improved Analysis for Flexural Creep with Application to Sialon Ceramics," Journal of the American Ceramics Society, Vol. 73, pp. 2366-2373

Chuang, T.-J., 1986, "Estimation of Power-Law Creep Parameters from Bend Test Data," Journal of Materials Science, Vol. 21, pp. 165-175

Chuang, T.-J., W.-J. Liu, and S. M. Wiederhorn, 1991, "Steady-State Creep Behavior of Si-SiC C-Rings," Journal of the American Ceramics Society, Vol. 74, pp. 2531-2537

Chuang, T.-J., Z.-D. Wang, and D. Wu, 1992, "Analysis of Creep in a Si-SiC C-Ring by Finite Element Method," Journal of Engineering Materials and Technology, Vol. 114, pp. 311-316

Cook, R. D., 1989, "Concepts and Applications of Finite Element Analysis," John Wiley & Sons, Inc., New York

Ferber, M. K., M. G. Jenkins, and V. J. Tennery, 1990, "Comparison of Tension, Compression, and Flexure Creep for Alumina and Silicon Nitride Ceramics," *Ceram. Eng. Sci. Proc.* Vol. 11, pp. 1028-1045

Fett, T., K. Keller, G. Martin, and O. Rosenfelder, 1991, "Direct Measurements of Displacements in the Inner Roller Span of Four-Point-Bending Creep Tests," *Journal of Testing and Evaluation*, Vol. 19, pp. 334-337

Hoagland, R., C. Marshall, and W. Duckworth, 1976, "Reduction of Errors in Ceramic Bend Strengths," *Journal of the American Ceramics Society*, Vol. 59, pp. 189-192

Hollenberg, G. W., G. R. Terwilliger, and R. S. Gordon, 1971, "Calculation of Stresses and Strains in Four-Point Bending Creep Tests," *Journal of the American Ceramics Society*, Vol. 54, pp. 196-199

Jakus, K., and S. M. Wiederhorn, 1988, "Creep Deformation of Ceramics in Four-Point Bending," *Journal of the American Ceramics Society*, Vol. 71, pp. 832-836

Krause, R. F. Jr., S. M. Wiederhorn, and J. J. Kubler, 2001, "Misalignment-Induced Bending in Pin-Loaded Tensile-Creep Specimens," *Journal of the American Ceramics Society*, Vol. 84, pp. 145-152

Lim, H. J., J. W. Jung, D. B. Han, and K. T. Kim, 1997, "A Finite Element Model for Asymmetric Creep Behavior of Ceramics," *Materials Science and Engineering A224*, pp. 125-130

Morrell, R., and K. H. G. Ashbee, 1973, "High Temperature Creep of Lithium Zinc Silicate Glass-Ceramics," *Journal of Materials Science*, Vol. 8, pp. 1253-1270

Norton, F. H., 1929, "The Creep of Steel at High Temperature," McGraw-Hill, New York

Quinn, G. D., and R. Morrell, 1991, "Design Data for Engineering Ceramics: A Review of the Flexure Test," *Journal of the American Ceramics Society*, Vol. 74, pp. 2037-2066

Sauve, R. G., and N. Badie, 1989, "Creep Response of Fuel Channels in Candu Nuclear Reactors," Ontario Hydro Research Division Report No. 89-2-K

Sauve, R. G., and N. Badie, 1992, "Non-Linear Three Dimensional Shell Formulation for Fuel Channel Creep," Ontario Hydro Research Division Report No. 92-97-P

Sauve, R. G., and D. R. Metzger, 1995, "Advances in Dynamic Relaxation Techniques for Nonlinear Finite Element Analysis," *Transactions of the ASME*, Vol. 117, pp. 170-176

Sauve, R. G., 1999, "H3DMAP Version 6.2-A General Three-Dimensional Finite Element Computer Code for Linear and Non-Linear Analyses of Structures," Ontario Hydro Research Division Report No. 181.1-H3DMAP-1998-RA-0001-R00

Seltzer, M. S., 1977, "High Temperature Creep of Silicon-Base Compounds," *American Ceramics Society Bulletin*, Vol. 56, pp. 418-423

Swank, L., J. C. Caverly, and R. L. Allor, 1990, "Experimental Errors in Modulus of Rupture Test Fixtures," *Ceramic Engineering and Science Proceedings*, Vol. 11, pp. 1329-1345

Underwood, P., 1983, "Dynamic Relaxation," Computational Methods for Transient Analysis, Vol. 1, pp. 245-265

Wang, Z.-D., C. K. Chiang, and T.-J. Chuang, 1997, "Optimum Design of a Ceramic Tensile Creep Specimen Using a Finite Element Method," Journal of Research of the National Institute of Standards and Technology, Vol. 102, pp. 15-28

Wiederhorn, S. M., and T.-J. Chuang, 1988, "Damage-Enhanced Creep in a Siliconized Silicon Carbide: Mechanics of Deformation," Journal of the American Ceramics Society, Vol. 71, pp. 595-601

Zienkiewicz, O. C., 1991, "The Finite Element Method," 4th edition, McGraw-Hill, London

Zhu, Z. G., and G. J. Weng, 1989, "Creep Deformation of Particle-Strengthened Metal Matrix Composites," ASME Journal of Engineering Materials and Technology, Vol. 111 pp. 99-105